

Boron nitride catalyst for partial oxidation of hydrocarbons

by

Leonardo David Garro Mena

B.S., University of Costa Rica, 2007

M.S., University of Costa Rica, 2014

AN ABSTRACT OF A DISSERTATION

submitted in partial fulfillment of the requirements for the degree

DOCTOR OF PHILOSOPHY

Tim Taylor Department of Chemical Engineering  
Carl R. Ice College of Engineering

KANSAS STATE UNIVERSITY  
Manhattan, Kansas

2021

## Abstract

The catalytic activity of hexagonal boron nitride (hBN) is not yet well understood but it seems to be related to hBN hydroxylated sites. A good understanding of those sites and how they are produced is a key step to reveal the true nature of hBN catalytic activity. Here, we report a set of thermal treatments to produce a diversity of hydroxylated sites, as well as a method to remove the boric acid produced by hBN decomposition. We found that some of the boric acid dehydrates on the surface of hBN to produce a borated hBN (hBNO) characterized by an FTIR peak at  $1090\text{ cm}^{-1}$  and an XRD shift due to the variation in the planar distance. When characterizing the thermally treated hBN, the storage of the sample changed the borate's hydration degree and modified both the XRD pattern and the FTIR spectrum. When stored in a humid environment, boric acid peaks are visible; but when stored in a dry place they are absent. The methods established here are a solid basis for the manufacture, purification and characterization of hBN by thermal treatments, showing how the process can be designed to generate various functional groups on its surface.

The thermally treated hBN was also evaluated as a support for Pt during partial oxidation of methane (POM) for the production of syngas. POM is a promising alternative to steam reforming of methane (SRM). POM is an exothermic reaction that requires lower temperatures and less energy than the endothermic SRM. The weaker interaction between Pt and hBN leads to a higher reducibility of Pt, which makes it more active than, for example, Pt/Al<sub>2</sub>O<sub>3</sub>. In this work we synthesized several Pt catalysts on thermally treated hBN and tested its activity for POM. We discovered that Pt/hBN is more active than Pt/Al<sub>2</sub>O<sub>3</sub>. The most active catalysts are those where boric acid is present on the surface of hBN before the Pt impregnation. The catalysts prepared this

way feature Pt particles on a borated hBN, which makes the Pt-support interaction even weaker, increasing its catalytic activity.

Finally, the oxidative dehydrogenation (ODH) of ethane was evaluated on thermally treated hBN. The catalytic activity of hBN using the ODH reaction was evaluated on hBN heated with an  $O_2/C_2H_6/N_2$  stream (activated hBN) vs a 100%  $N_2$  stream (non-activated hBN: hBN\*). hBN\* catalyzed the catalytic dehydrogenation (CDH) of ethane when the temperature was higher than 160 °C. At 160 °C or below, hBN\* was activated and the ODH reaction took place. The catalytic activity of hBN for the ODH reaction increased significantly when the thermal treatment was followed by a sonication step and a separation by centrifugation (labeled as hBNO). This sample showed a borated layer characterized by an FTIR vibration at  $\approx 1190\text{ cm}^{-1}$ . We concluded that there are several active sites on hBN catalyzing the ODH reaction, all of them involve oxygen and requires activation or preparation of the catalyst. Future work is needed to explore the nature of these active sites for the design of hBN based catalysts.

Boron nitride catalyst for partial oxidation of hydrocarbons

by

Leonardo David Garro Mena

B.S., University of Costa Rica, 2007  
M.S., University of Costa Rica, 2014

AN ABSTRACT OF A DISSERTATION

submitted in partial fulfillment of the requirements for the degree

DOCTOR OF PHILOSOPHY

Tim Taylor Department of Chemical Engineering  
Carl R. Ice College of Engineering

KANSAS STATE UNIVERSITY  
Manhattan, Kansas

2021

Approved by:

Major Professor  
Keith L. Hohn

# **Copyright**

© Leonardo David Garro Mena  
2021.

## Abstract

The catalytic activity of hexagonal boron nitride (hBN) is not yet well understood but it seems to be related to hBN hydroxylated sites. A good understanding of those sites and how they are produced is a key step to reveal the true nature of hBN catalytic activity. Here, we report a set of thermal treatments to produce a diversity of hydroxylated sites, as well as a method to remove the boric acid produced by hBN decomposition. We found that some of the boric acid dehydrates on the surface of hBN to produce a borated hBN (hBNO) characterized by an FTIR peak at  $1090\text{ cm}^{-1}$  and an XRD shift due to the variation in the planar distance. When characterizing the thermally treated hBN, the storage of the sample changed the borate's hydration degree and modified both the XRD pattern and the FTIR spectrum. When stored in a humid environment, boric acid peaks are visible; but when stored in a dry place they are absent. The methods established here are a solid basis for the manufacture, purification and characterization of hBN by thermal treatments, showing how the process can be designed to generate various functional groups on its surface.

The thermally treated hBN was also evaluated as a support for Pt during partial oxidation of methane (POM) for the production of syngas. POM is a promising alternative to steam reforming of methane (SRM). POM is an exothermic reaction that requires lower temperatures and less energy than the endothermic SRM. The weaker interaction between Pt and hBN leads to a higher reducibility of Pt, which makes it more active than, for example, Pt/Al<sub>2</sub>O<sub>3</sub>. In this work we synthesized several Pt catalysts on thermally treated hBN and tested its activity for POM. We discovered that Pt/hBN is more active than Pt/Al<sub>2</sub>O<sub>3</sub>. The most active catalysts are those where boric acid is present on the surface of hBN before the Pt impregnation. The catalysts prepared this

way feature Pt particles on a borated hBN, which makes the Pt-support interaction even weaker, increasing its catalytic activity.

Finally, the oxidative dehydrogenation (ODH) of ethane was evaluated on thermally treated hBN. The catalytic activity of hBN using the ODH reaction was evaluated on hBN heated with an  $O_2/C_2H_6/N_2$  stream (activated hBN) vs a 100%  $N_2$  stream (non-activated hBN: hBN\*). hBN\* catalyzed the catalytic dehydrogenation (CDH) of ethane when the temperature was higher than 160 °C. At 160 °C or below, hBN\* was activated and the ODH reaction took place. The catalytic activity of hBN for the ODH reaction increased significantly when the thermal treatment was followed by a sonication step and a separation by centrifugation (labeled as hBNO). This sample showed a borated layer characterized by an FTIR vibration at  $\approx 1190\text{ cm}^{-1}$ . We concluded that there are several active sites on hBN catalyzing the ODH reaction, all of them involve oxygen and requires activation or preparation of the catalyst. Future work is needed to explore the nature of these active sites for the design of hBN based catalysts.

# Table of Contents

Abstract .....	ii
Copyright .....	v
Abstract .....	vi
Table of Contents .....	viii
List of Figures .....	xi
List of Tables .....	xiv
Acknowledgements .....	xv
Dedication .....	xvi
Chapter 1 - Introduction .....	1
Oxidative dehydrogenation of hydrocarbons .....	1
Vanadium for ODH reactions .....	2
Hexagonal Boron Nitride for ODH reactions .....	4
Activation, intermediates and selectivity .....	8
Partial oxidation of methane, metallic catalysts and hBN .....	9
Hexagonal boron nitride functionalization .....	11
Thermal treatment .....	11
Sonication .....	11
Mechanical methods .....	12
Chapter 2 - Experimental setup .....	13
Pt catalyst preparation .....	15
Pt catalyst experiments .....	15
hBN thermal treatments .....	16
hBN experiments .....	16
Pt dispersion .....	17
Fourier-transform infrared spectroscopy .....	17
X-Ray powder diffraction .....	18
Scanning Electron Microscopy .....	18
Chapter 3 - Modification of Hexagonal Boron Nitride by Thermal Treatment .....	19
Experimental .....	21



Reagents .....	21
Thermal treatments .....	21
Sonication and centrifugation .....	21
Characterization .....	22
Thermal treatments .....	22
Results and Discussion .....	23
Heat Treatment of hBN.....	24
Boric acid removal .....	28
Post Treatment of Thermally Treated hBN.....	30
Boron nitride dehydration and borated hBN formation .....	32
Conclusions.....	35
Chapter 4 - Syngas production on a Pt/hBN catalyst: the role of the support .....	37
Experimental section.....	39
Reagents .....	39
Thermal treatments .....	39
Characterization .....	39
Catalyst preparation .....	40
Catalytic activity .....	40
Result and discussion.....	41
Catalytic activity .....	43
Conclusions.....	50
Chapter 5 - Details on hBN activity for ethane oxidative dehydrogenation.....	52
hBN active sites .....	53
Experimental Section.....	55
Reagents .....	55
Thermal treatments .....	55
Characterization .....	56
Catalytic activity .....	57
Result and discussion.....	57
Characterization .....	57
Catalytic activity for ODH.....	62

Catalyst stability.....	66
Conclusion .....	69
Chapter 6 - Conclusions and future work .....	70
References.....	74

## List of Figures

<b>Figure 1-1.</b> Monomeric (a) and polymeric (b) structure of vanadium deposited on a support.....	3
<b>Figure 1-2.</b> Proposed mechanism for hydrogen atom abstraction from propane by the active site (BO–ON) on the armchair edge of h-BN <sup>26</sup> .....	5
<b>Figure 1-3.</b> Production of ethene from ethane over h-BN in BOON sites on the armchair edge <sup>28</sup> . .....	6
<b>Figure 1-4.</b> Proposed mechanism for the production of ethene from ethane over h-BN in zig-zag BOOB sites <sup>31</sup> .....	7
<b>Figure 1-5.</b> Proposed mechanism for the production of ethene from ethane over h-BN in zig-zag BOOB sites formed in a modified B edge in h-BN <sup>29</sup> .....	7
<b>Figure 1-6.</b> FT-IR spectra of B–OH vibration over the BNOH catalyst (hydroxylated with a sodium nitrite solution) under C <sub>2</sub> H <sub>6</sub> /N <sub>2</sub> , C <sub>2</sub> H <sub>6</sub> /O <sub>2</sub> /N <sub>2</sub> and H <sub>2</sub> O/N <sub>2</sub> atmospheres at 590 °C <sup>25</sup> .	8
<b>Figure 2-1.</b> Experimental setup. Gases are feed at controlled rates using mass flow controllers (MFC). The furnace temperature is measured by a thermocouple (temperature transmitter: TT) and controlled by a PID controller. The temperature of the downstream gases from the reactor is controlled by a temperature controller (TC) connected to a thermocouple (TT)..	14
<b>Figure 3-1.</b> FTIR for thermally modified hBN and its chemical structure. ....	19
<b>Figure 3-2.</b> SEM images for thermally treated hBN. a) Untreated hBN; b) TTD950-3_PT:S18_C:D; c) TT:H900-3_PT:H310-10 S4_C:D; d) TT:H850-3_PT:H310-10 S4_C:D; e) TT:H850-3_PT:D600-5S4_C:D and f) TT:850H-6_C:D.....	25
<b>Figure 3-3.</b> FTIR spectra for thermally treated hBN at a) 950 °C, b) 900 °C, c) 850 °C and d) 650 °C.....	27
<b>Figure 3-4.</b> XRD patterns for thermally treated hBN. The same sample was measured dry and wet, giving different results due to the equilibrium between the hydrated and dehydrated borate species .....	28
<b>Figure 3-5.</b> XRD pattern of a thermal treated hBN sample at 850 °C plus a post treatment at 600 °C with humid air (TT:850-6_PT:TH600-t). The plot shows the evolution of boric acid content with time. a) Complete pattern. b) and c) zoom in on the boric acid signal. ....	29

<b>Figure 3-6.</b> Percent of remaining initial boric acid content (%IBA) during post treatment of a thermal treated hBN sample. Inset: hBN SEM images before (a) and after (b) post treatment .....	30
<b>Figure 3-7.</b> Borated hBN after boric acid dehydration on its surface. ....	31
<b>Figure 3-8.</b> Deconvoluted FTIR spectrum of <b>Figure 3.7</b> . The 3600 cm <sup>-1</sup> peak is assigned to OH groups attached to B <sub>2</sub> O <sub>3</sub> <sup>34</sup> . The 3400 cm <sup>-1</sup> is assigned to OH groups attached to hBN <sup>61,72</sup> . The 3000 cm <sup>-1</sup> peak is assigned to hydrogen bonding of B <sub>2</sub> O <sub>3</sub> species with the OH groups <sup>34</sup> . The 3200 cm <sup>-1</sup> could be boric acid or hBN concerted hydroxyl groups <sup>80</sup> .....	32
<b>Figure 3-9.</b> Borated hBN after boric acid dehydration on its surface .....	33
<b>Figure 3-10.</b> Suspensions of hBN and thermal treated hBN. The thermal treated suspension contains three times more solids due to the formation of hydrogen bonds with water .....	34
<b>Figure 3-11.</b> A left shift in the XRD pattern peak characteristic of the hBN 002 plane caused by an increase in the crystal plane spacing due to hBN oxidation (Inset: peaks normalized to equal height showing the left shift) .....	35
<b>Figure 4-1.</b> Production of syngas on a Pt/hBN catalysts. The hBN support was thermally treated before the Pt impregnation.....	37
<b>Figure 4-2.</b> XRPD patterns for hBN support, Pt catalysts right after calcination (Pt/hBN850) and after overnight exposure to a water saturated atmosphere (Pt/hBN850*). (Inset: Same catalysts after removing the boric acid). ....	42
<b>Figure 4-3.</b> SEM for Pt/hBN catalyst. <b>a:</b> General view; <b>b:</b> detailed view .....	43
<b>Figure 4-4.</b> Methane TOF for Pt deposited on hBN treated at 850 °C with humid air for 6 h (Pt/hBN850) and Pt/Al <sub>2</sub> O <sub>3</sub> . (a) Methane consumption. (b) CO production. (c) H <sub>2</sub> production. (d) H <sub>2</sub> /CO ratio. ....	45
<b>Figure 4-5.</b> TOF and H <sub>2</sub> production on Pt/Al <sub>2</sub> O <sub>3</sub> and Pt/hBN850 for the steam reforming of methane reaction compared to the partial oxidation of methane reaction. ....	46
<b>Figure 4-6.</b> Methane conversion on Pt catalysts for: <b>a.</b> Pt on thermally treated hBN at 650 °C for 60 h with humid air (Pt2%hBN-650: WI, Pt2%hBN-650-S: SWI); <b>b.</b> Pt on untreated hBN (Pt/hBN: WI, Pt/hBN-S: SWI); <b>c.</b> Pt on thermally treated hBN at 850 °C for 6 h with WI without boric acid removal (Pt2%/hBN-850) and with boric acid removal after the thermal treatment (Pt/hBN-850-P). <b>d.</b> Comparison of treatments. ....	48

<b>Figure 4-7.</b> Methane conversion on Pt catalysts for Pt on untreated hBN and hBN treated at 850 °C with humid air for 6 h. <b>a:</b> Sample used after calcination without purification (Pt2%/hBN-850-U) and with boric acid removal after the catalyst synthesis (Pt2%/hBN-850-); <b>b:</b> Pt on untreated hBN using wetness impregnation with water (Pt2%/hBN-WI) and incipient wetness impregnation with methanol (Pt2%/hBN-IWI).....	49
<b>Figure 4-8.</b> TOF for POM on Pt catalysts prepared with boric acid doped hBN (a) and Al <sub>2</sub> O <sub>3</sub> (b). .....	50
<b>Figure 5-1.</b> Oxidative dehydrogenation (ODH) of ethane on thermally treated hBN. ....	52
<b>Figure 5-2.</b> Percent of remaining initial boric acid content determined using the reference intensity ratio (RIR) method with the XRD patterns during post treatment with humid air at 600 °C. The initial sample was a thermally treated hBN sample. ....	56
<b>Figure 5-3.</b> SEM images for untreated hBN (a), thermally treated hBN sonicated and centrifuged: hBNO (b) and thermally purified hBNO (hBNO-P) (c). (d) shows the XRD patterns for the hBN materials. ....	59
<b>Figure 5-4.</b> FTIR for; a) hBNO, b) hBN, c) hBN850 and d) spent hBN and hBNO after a 50 h stability test. ....	60
<b>Figure 5-5.</b> Ethylene selectivity for the ODH of ethane on hBN* and the homogeneous reaction. The two different selectivity values at 570 °C for hBN* are the result of hBN* activation once a temperature lower than 570 °C is set.....	61
<b>Figure 5-6.</b> CO selectivity for the ODH of ethane on hBN* and the homogeneous reaction .....	61
<b>Figure 5-7.</b> CO <sub>2</sub> selectivity for the ODH of ethane on hBN* and the homogeneous reaction.....	62
<b>Figure 5-8.</b> Ethylene and CO selectivity for the ODH of ethane on hBN materials.....	64
<b>Figure 5-9.</b> CO <sub>2</sub> and H <sub>2</sub> selectivity for the ODH of ethane on hBN materials.....	65
<b>Figure 5-10.</b> Reaction rate for the ODH of ethane on hBN materials. ....	65
<b>Figure 5-11.</b> Stability test at 580 °C for hBN and hBNO during ethane ODH.....	67
<b>Figure 5-12.</b> Selectivity during the stability test at 580 °C for hBN and hBNO. ....	67
<b>Figure 5-13.</b> CO selectivity for the ODH of ethane on hBN* and the homogeneous reaction.....	68
<b>Figure 5-14.</b> Candidate active sites on hBN. a) Modified N edge <sup>29</sup> . b) Borated hBN. ....	68

## List of Tables

Table 1-1 Dehydrogenation and oxidative dehydrogenation (ODH) general reactions and thermodynamic comparison for propane. ....	2
Table 1-2 Activation steps and intermediates on metallic and hBN catalysts. ....	9
Table 3-1. Nomenclature for the hBN treatment protocols .....	23

## **Acknowledgements**

I want to thank all the Chemical Engineering faculty and staff. Since the first day, when I came to KSU for the first time and I get lost just trying to go from the Engineering Hall to the ISSS, the kindness of all of you people made me feel safe, welcome and comfortable.

This work was possible thanks to Dr. Hohn, my advisor, who helped me through the whole process. Thank you for your trust, your advice and all your kindness.

Dr. Edgar, you supported me all the time, not only in my research, but also with my personal challenges. Thank you.

I also want to thank Dr. Liu and Dr. Sues for their kindness and help.

And finally, to each person who shared his or her time with me and made me feel happy to be in Manhattan, far from home but so welcomed in this beautiful community.

## **Dedication**

A las dos personas más importantes de mi vida: Damaris Garro Mena, mi mamá, y Jenny Andrea Calderón Castro, mi compañera de vida.

To the most important people in my life: Damaris Garro Mena, my mom, and Jenny Calderón Castro, my life partner.



## Chapter 1 - Introduction

Hexagonal boron nitride (hBN) has been studied widely for its chemical, mechanical and electrical properties, but recently it has shown a surprising catalytic activity for the ODH of alkanes<sup>1-4</sup>. Some studies also have shown that hBN increases the Pt activity for certain reactions when used as a support due to its weaker Pt-support interaction. In this work we will explore hBN, its properties, its catalytic behavior and its active role when used as a catalyst support. To do that we will modify hBN by thermal treatments and characterize the product. Then we will use hBN to support Pt and evaluate the Pt activity on thermally treated hBN using the partial oxidation of methane reaction, so we can compare it to Pt/Al<sub>2</sub>O<sub>3</sub>. Finally, we will evaluate the hBN activity as a function of the thermal treatment to search for the nature of the hBN active sites using the oxidative dehydrogenation of ethane.

### Oxidative dehydrogenation of hydrocarbons

The market for olefins, especially propylene and ethylene, is growing<sup>5</sup>. The global ethylene market, for example, was valued at USD 146.3 billion in 2019 and the demand for these building block chemicals is expected to continue in the near future<sup>6,7</sup>. The production of olefins is currently done industrially by cracking and catalytic dehydrogenation<sup>8</sup>; however, these reactions present several problems such as coke formation and high temperature requirements<sup>9-11</sup>. The main problem is to activate the C–H bond and, using the same conditions, prevent further oxidation to CO<sub>x</sub><sup>12</sup>. Oxidative dehydrogenation (ODH) is an alternative to the traditional olefin production methods. ODH is exothermic, which is an advantage over dehydrogenation which is endothermic. Table 1-1 presents the details for the general reactions and a comparison of reaction enthalpies for the case of propane, showing that dehydrogenation of propane is endothermic ( $\Delta_r H_{298}^\circ =$

124.27 kJ/mol) and ODH is exothermic ( $\Delta_r H_{298}^\circ = -117.57$  kJ/mol). The formation of water in ODH, instead of hydrogen in dehydrogenation, favors the reaction<sup>13,14</sup>.

**Table 1-1** Dehydrogenation and oxidative dehydrogenation (ODH) general reactions and thermodynamic comparison for propane.

	Dehydrogenation	Oxidative dehydrogenation (ODH)
<b>General reaction</b>	$C_n H_{2n+2} \rightarrow C_n H_{2n} + H_2$ <b>1.1</b>	$C_n H_{2n+2} + \frac{1}{2} O_2 \rightarrow C_n H_{2n} + H_2 O$ <b>1.2</b>
<b>Example: Propane</b>	$C_3 H_8 \rightarrow C_3 H_6 + H_2$ <b>1.3</b>	$C_3 H_8 + \frac{1}{2} O_2 \rightarrow C_3 H_6 + H_2 O$ <b>1.4</b>
<b>Heat of reaction</b>	$\Delta_r H_{298}^\circ = 124.27$ kJ/mol	$\Delta_r H_{298}^\circ = -117.57$ kJ/mol

The exothermicity of ODH allows the use of lower temperatures compared with catalytic dehydrogenation, preventing the formation of coke. Amongst ODH catalysts, vanadium and molybdenum are the most prominent. Vanadium is more active than molybdenum<sup>15,16</sup>. However, the selectivity for this system is still low<sup>17</sup>. Recently a new catalytic system based in hexagonal boron nitride (hBN) was reported to show a selectivity as high as 70% at 52% conversion of propane to propene<sup>18</sup>.

In the following sections the role of vanadium, the most active metal oxide catalytic system, and boron nitride, a new promising alternative for highly selective ODH, will be analyzed and compared to understand the details of its activity, synthesis and reaction mechanism.

## Vanadium for ODH reactions

Understanding the active sites and reaction mechanisms for ODH is a key factor in the design of new catalysts. The role of the support, the vanadium coverage, vanadium phase structure

and many other factors affects the catalyst behavior. Supported vanadium oxide catalysts consists of a vanadia phase with isolated  $\text{VO}_x$  (**Figure 1-1a**) and polymerized  $\text{VO}_x$  (**Figure 1-1b**) on an oxide support. The polymerization degree is a function of vanadium loading. Above the monolayer coverage  $\text{V}_2\text{O}_5$  crystallites are formed <sup>19,20</sup>.

There are three different bond types in the two structures presented in Figure 1:  $\text{V}=\text{O}$ ,  $\text{V}-\text{O}-\text{V}$  and  $\text{V}-\text{O}-\text{Support}$ . The  $\text{V}=\text{O}$  bond is not involved in the rate determining step. The  $\text{V}-\text{O}-\text{V}$  bond is not critical for activation of the alkanes. The catalytic active site is associated with the  $\text{V}-\text{O}-\text{Support}$  bond. <sup>21</sup>.

The general mechanism of ODH reactions seems to involve only one active site<sup>21</sup> and four steps. The exact mechanism differs between studies, but the next four steps are generally accepted<sup>22</sup>:

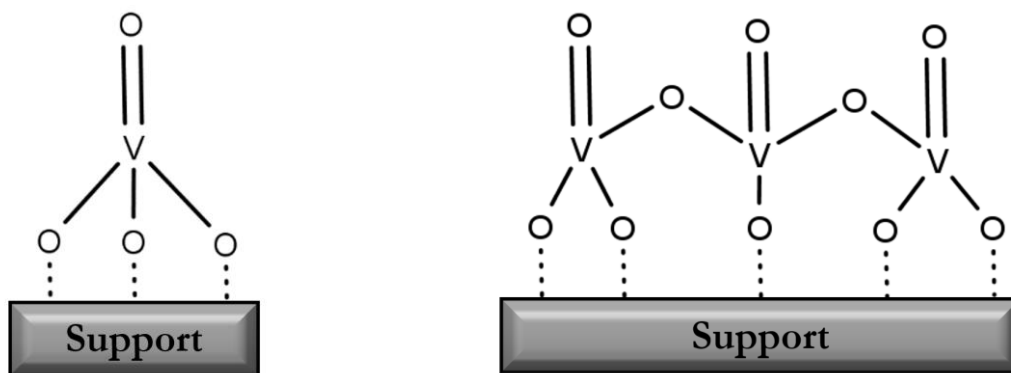
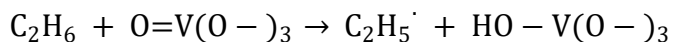


**Figure 1-1.** Monomeric (a) and polymeric (b) structure of vanadium deposited on a support.

- 1 Alkane absorption
- 2 C–H bond cleavage to produce the alkyl species
- 3 Reaction of the alkyl species with oxygen to produce the alkene
- 4 Cyclic reduction/oxidation of the catalyst

One of the key steps for the ODH reaction is the activation of the C–H bond (step 2 in the list above). When using a transition metal oxide catalyst, there is evidence that supports the

abstraction of a hydrogen by a metal oxo bond as the mechanism for the activation of the C–H bond<sup>23</sup>. For ethane, the reaction is as follows:



Then the  $\text{C}_2\text{H}_5\cdot$  radical is released to form ethylene by losing a hydrogen atom.

### Hexagonal Boron Nitride for ODH reactions

Hexagonal boron nitride (h-BN) was generally considered chemically inert, but it shows surprisingly high selectivity for the production of alkenes by the ODH reaction<sup>24</sup>. An ethylene selectivity of 95% at a 11% ethane conversion<sup>25</sup> or a propylene selectivity of 79% with a 12% propane conversion<sup>26</sup> have been reported, as well as other advantages as a more uniform temperature profile in a fixed bed reactor compared with  $\gamma\text{-Al}_2\text{O}_3$ , for example<sup>27</sup>.

The high selectivity of h-BN for the production of olefins by the ODH reaction could be explained by a reaction mechanism where O–O attached to the armchair side of the h-BN is the active site (BOON). In **Figure 1-2** propane is absorbed on the BOON site of h-BN. One of the hydrogens in propane is abstracted by the active site, breaking the O–O bond and forming a BOH species. Propane forms a bond with the other oxygen to give  $\text{NOCH}-(\text{CH}_3)_2$  species. The stability of the  $\text{NOCH}-(\text{CH}_3)_2$  intermediate could be the reason for the high selectivity compared, for example, with the metal oxide catalysts where the  $\text{C}_3\text{H}_7\cdot$  intermediate is not stable<sup>26</sup>. **Figure 1-3** presents the mechanism for the production of ethene from ethane using BOON sites in h-BN. After the formation of the intermediate (**Figure 1-3D**), the other carbon also loses a hydrogen (**Figure 1-3F**) and then the product desorbs and the catalyst is regenerated by oxygen<sup>28</sup>.

The previous mechanism is based on the BOON active sites, which are formed in the armchair edge in h-BN. However, the most frequently exposed edges in h-BN are zig-zag

terminations<sup>29,30</sup>. If this is the case, an alternative mechanism should be proposed to explain the catalytic activity of h-BN. An option is to allocate the active sites in the zig-zag B edge (**Figure 1-4**). If that edge is hydroxylated (BOH) it could be activated with oxygen to form BOOB and water. Next, the BOOB site will activate the C–H bond to produce  $\text{BCH}_2\text{CH}_3$  (if ethane is being reacted) and BOH. If there is oxygen present the formation of water and ethene is the next step. If oxygen is not present, hydrogen and ethane will be the products<sup>31</sup>.

A third alternative is a modified zig-zag B edge in h-BN with BOB and BOH groups (**Figure 1-5**). In this case the active site is a BOOB site in a zig-zag BOB edge. The dominantly exposed zig-zag B edge and the co-existence of BOB and B-OH groups was confirmed via multiple techniques (EELS, XPS, MAS NMR and IR)<sup>29</sup>.

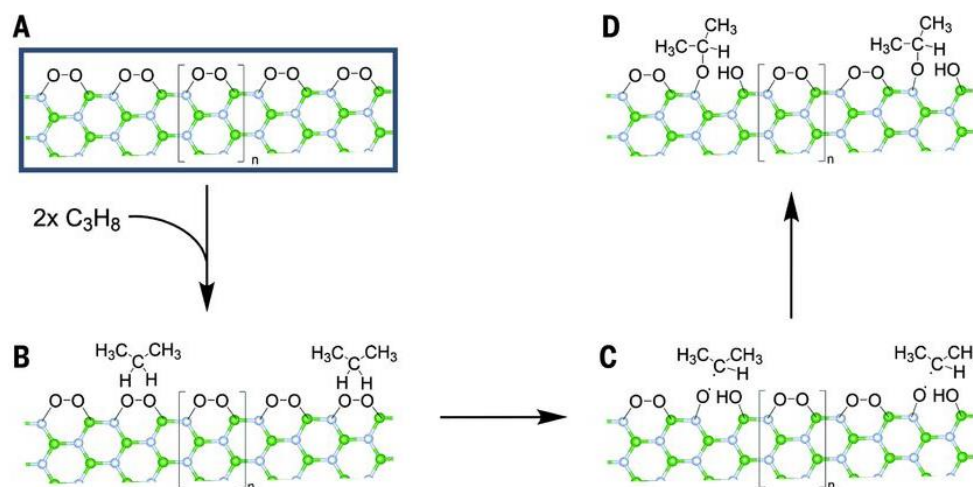


**Figure 1-2.** Proposed mechanism for hydrogen atom abstraction from propane by the active site (BO–ON) on the armchair edge of h-BN<sup>26</sup>.

Despite the lack of information about the exact mechanism and the nature of the active sites for h-BN catalytic activity, there is agreement in the role of oxygen and alkane in the

activation of h-BN. FTIR spectra show a typical OH vibration peak around  $3400\text{ cm}^{-1}$ . In **Figure 1-6** h-BN was hydroxylated using a 1 M sodium nitrite solution to impregnate h-BN and then calcinated at  $560\text{ }^{\circ}\text{C}$ . The product was then treated at  $530\text{ }^{\circ}\text{C}$  with 5 vol %  $\text{H}_2\text{O}/\text{N}_2$  to form hBOH (hydroxylated boron nitride). The obtained sample was exposed to  $\text{C}_2\text{H}_6/\text{N}_2$ ,  $\text{C}_2\text{H}_6/\text{O}_2/\text{N}_2$  and  $\text{H}_2\text{O}/\text{N}_2$  and FTIR was measured over time. When only ethane and nitrogen flow through hBOH there is no change in the OH peak and no ethene is produced. Under ethane, oxygen and nitrogen flow, the OH peak intensity decreases over time and ethene is produced, showing that there is an interaction of oxygen with the OH group in the reaction of ethane. Finally, when water and nitrogen is flowed through the catalyst, the intensity of the OH peaks are recovered. This means that the OH could be regenerated<sup>25</sup>. In other words, the active sites are structurally stable; they are not destroyed or changed irreversibly during the reaction.

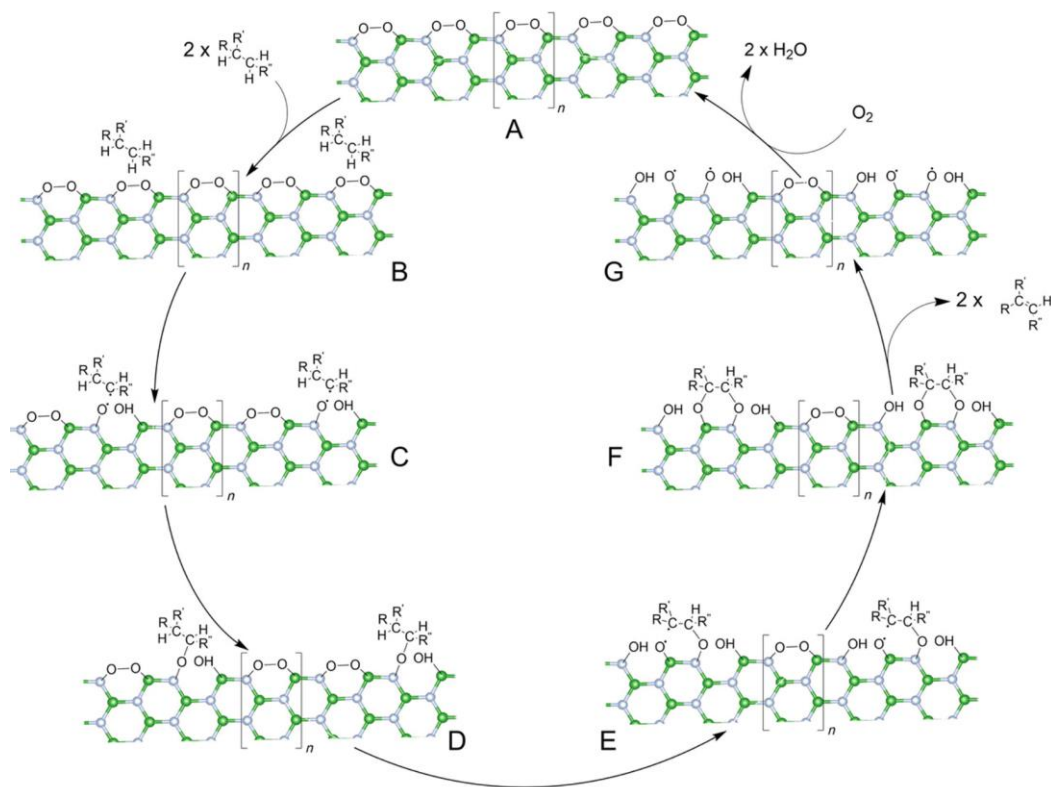


**Figure 1-3.** Production of ethene from ethane over h-BN in BOON sites on the armchair edge<sup>28</sup>.

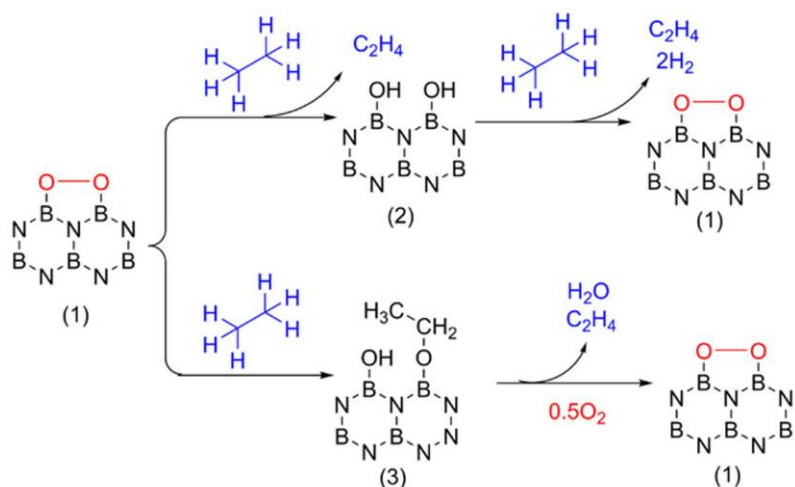


**Figure 1-4.** Proposed mechanism for the production of ethene from ethane over h-BN in zig-zag BOOB sites<sup>31</sup>.

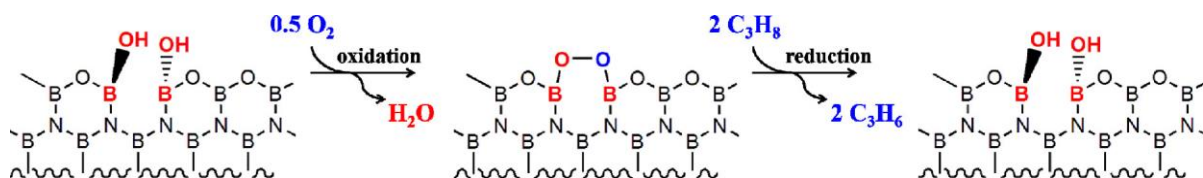


**Figure 1-5.** Proposed mechanism for the production of ethene from ethane over h-BN in zig-zag BOOB sites formed in a modified B edge in h-BN<sup>29</sup>.

In summary

- Boron nitride is functionalized and the OH groups are detected using FTIR<sup>25</sup>.
- Ethane does not react with functionalized boron nitride unless oxygen is present<sup>25</sup>.
- During the reaction of ethane using hydroxylated boron nitride in the presence of oxygen, the OH peak weakens over time<sup>25</sup>.
- The peaks are quickly recovered by flowing water/N<sub>2</sub> at 590 °C<sup>25</sup>.

- Boron nitride cannot be hydroxylated quickly using water vapor at 590 °C<sup>32-34</sup>.

Conclusion: The ethane reaction does not destroy the active sites (OH groups) because the OH peaks are easily recovered when water vapor is flowed through the spent material. What is happening, apparently, is a change in the structure of the active sites; that change makes the OH peak disappear, but the active site is there and its original structure can be recovered with water vapor.

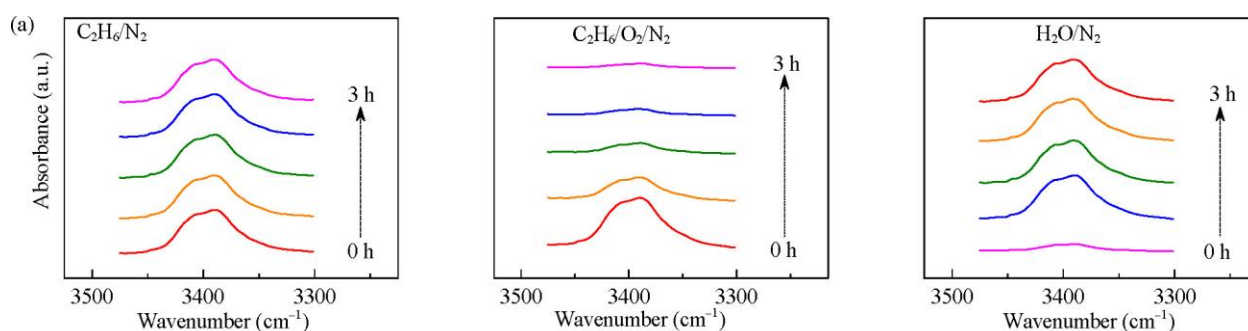


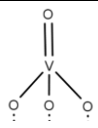
**Figure 1-6.** FT-IR spectra of B–OH vibration over the BNOH catalyst (hydroxylated with a sodium nitrite solution) under C<sub>2</sub>H<sub>6</sub>/N<sub>2</sub>, C<sub>2</sub>H<sub>6</sub>/O<sub>2</sub>/N<sub>2</sub> and H<sub>2</sub>O/N<sub>2</sub> atmospheres at 590 °C<sup>25</sup>.

### Activation, intermediates and selectivity

Even though the structure of the active sites on hBN is not yet well understood, the higher alkene selectivity shown by hBN during ODH reactions, compared to vanadium, could be explained by a more stable intermediate (Table 1-2). The intermediate formed during the ODH on hBN is an hBN-alkane intermediate, similar to the one formed in the alkane dehydrogenation reaction on metallic catalysts (metal-alkane). These intermediates are more stable than the radical formed when vanadium is used to catalyze the ODH reaction (Table 1-2)<sup>21,22,26,28</sup>.



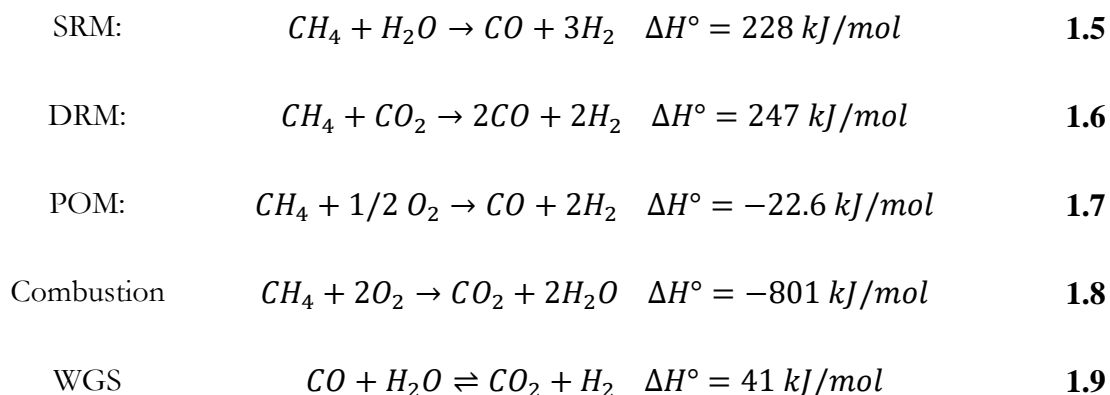
**Table 1-2** Activation steps and intermediates on metallic and hBN catalysts.

	Dehydrogenation	ODH / vanadium	ODH / h-BN
Activation	Adsorption of propane and activation of the C-H bond	Hydrogen abstraction by metal oxo bond	Adsorption of propane and activation of the C-H bond
	$C_2H_6S + S \rightarrow C_2H_5S$	$C_2H_6 + OV(O^-)_3 \rightarrow C_2H_5\cdot + HOV(O^-)_3$	$C_2H_6 + hBNO + hBNO \rightarrow C_2H_5hBNO + HhBNO$
Intermediate	Metal-alkane	Radical intermediate	hBN-Alkane
	$C_2H_5S$	$C_2H_5\cdot$	$C_2H_5hBNO$
			<b>S:</b> Active sites on metal-based catalyst <b>hBNO:</b> Active site on hBN

### Partial oxidation of methane, metallic catalysts and hBN

The catalytic activity shown by hBN for the ODH of alkanes is well known, but there are other properties of hBN (and hBN related, such as B<sub>2</sub>O<sub>3</sub>) that are worthy of further study, such as its behavior as a catalyst support<sup>35-38</sup>. An important reaction for this study is partial oxidation of methane (POM). The natural gas production in the US increased more than 50% in the last 10 years<sup>39</sup>. Converting methane, the main component in natural gas, to syngas is a key step in its exploitation chain<sup>40</sup>. There are several reaction pathways to achieve this, such as: Steam reforming of methane (SRM, Eq. 1.5), Dry reforming of methane (DRM, Eq. 1.6) and Partial oxidation of methane (POM, Eq. 1.7)<sup>41</sup>. SRM is the most widely used method to produce syngas industrially. Both SRM and DRM are endothermic reactions that require high temperatures. This causes some undesirable effects such as coke formation in DRM. POM is an exothermic reaction, which makes

it energetic favorable requiring lower temperatures and reduced energy costs<sup>42,43</sup>. In addition, the H<sub>2</sub>/CO ratio produced by POM is about 2, which makes it ideal for the further production of methanol or Fischer–Tropsch synthesis<sup>44</sup>. Other details of POM for syngas production have been reviewed in detail<sup>40,45–47</sup>.



POM does not take place directly through Eq. 1.7, but through a first complete combustion step (Eq. 1.8) followed by steam (Eq. 1.5) and dry (Eq. 1.6) reforming. The water-gas shift reaction (WGS) (Eq. 1.9) is also involved<sup>48–52</sup>. For Pt catalysts on Al<sub>2</sub>O<sub>3</sub> the H<sub>2</sub>/CO ratio decreases with temperature<sup>49</sup>, but if hBN is used to support Pt, the weaker Pt-hBN interaction<sup>53</sup> could play a key role in this behavior because the Pt activity is increased by a higher Pt reducibility on hBN compared to Al<sub>2</sub>O<sub>3</sub><sup>54,55</sup>.

This is in keeping with past studies that demonstrated that reduced sites are required when Ni is used for POM<sup>56,57</sup> and for Pt when used for hydrocarbon oxidation<sup>58,59</sup>. The hydrophobicity of the hBN support, opposed to the widely used hydrophilic oxide supports, could also be a key factor affecting the Pt activity towards a higher CO production<sup>60</sup>.

## Hexagonal boron nitride functionalization

Several methods had been developed to hydroxylate h-BN. Once hBN is hydroxylated its catalytic activity changes. In the next sections some of the most common methods are described.

### Thermal treatment

Cui et al.<sup>32</sup> treated hBN with air at 1000 °C and hydroxyl groups were detected using FTIR spectroscopy. They suggested that the hydroxyl groups formed in the boron zigzag edge, but there is no evidence to support it. Xiao et al.<sup>61</sup> used humid air at 850 °C to produce hydroxylated boron nitride. In this case hBN reacts with water to produce hydroxylated boron nitride, boric acid and ammonia. Jin et al.<sup>62</sup> treated hBN at 600 °C with dry air. Previous work found that h-BN is stable below 800 °C in the presence of air up to 8 h<sup>32</sup>, but when treated at 600 °C for 144 h a layer of oxidized hBN (hBNO) formed on the surface of the material. The presence of hydroxyl groups was confirmed by a 3200 cm<sup>-1</sup> peak in the FTIR spectra. Raman shifts and XRD patterns also confirmed the oxidation of the hBN<sup>62</sup>.

It is important to point out the differences between the edge hydroxylated boron nitride produced by Xiao et al.<sup>61</sup> (confirmed by EELS) using humid air at 850 °C and the surface hydroxylation (confirmed by HRTEM) produced by Jin et al.<sup>62</sup> at 600 °C in air. These results suggest that the hydroxylation of hBN can be tuned by choosing an appropriate method to obtain edge or surface functionalization.

### Sonication

Sonication is an easy process to hydroxylate h-BN. The simplest method is to sonicate hBN with water. In this case the defects in boron nitride are susceptible to hydrolysis, causing the defect

to propagate and generating a “cutting” of large hBN sheets into smaller ones. This process ends up with the hydroxylation of the edges and the exfoliation of the h-BN to produced boron nitride nanosheets (hBNNS). The exfoliation is attributed to the hydrolytic cutting of hBN sheets, on one hand, and the polarity of the solvent, which interacts with the surface of h-BN and facilitates the peeling of the sheets, on the other <sup>63</sup>. Wu et al.<sup>64</sup> used a similar approach but instead of water, they used nitric acid to sonicate h-BN and produced hydroxylate boron nitride.

### **Mechanical methods**

Ball milling is used to generate shear stress on the surface of the h-BN particles, leading to peeling of h-BNNS. When milling is assisted by a solution of NaOH, the hBN is hydroxylated during the cutting that takes place when hBN reacts with OH<sup>-</sup> ions. Edge hydroxylated hBNNS are obtained with this process<sup>65</sup>.

Another mechanical method used to exfoliate hBN is quenching. In this method hBN at 800 °C is immersed into liquid nitrogen until liquid nitrogen gasifies completely. The heated hBN is thermal expanded, and this expansion causes the van der Waals forces between layers to weaken. When h-BN is immersed into liquid nitrogen (-196 °C) the exfoliation occurs due to a dual effect: a curling process and an exfoliation triggered by nitrogen expansion<sup>66</sup>.

## Chapter 2 - Experimental setup

The experimental setup described in this section was design to study the catalytic activity of hBN based materials. Pt/hBN for partial oxidation of methane and hBN for oxidative dehydrogenation of ethane were used. The activity was evaluated in terms of reacted moles of reagent per mole of active site (for POM on Pt/hBN) or per gram of catalyst (for ODH on hBN).

All catalytic experiments were evaluated in a quartz tubular reactor (internal diameter = 12 mm) with a continuous flow operating at near atmospheric pressure. The catalyst was packed into the reactor between quartz wool. The reactor tube was encased in an electrically heated tube furnace with a PID temperature controller connected to a coaxial thermocouple (**Figure 2-1**). Before each run, the metallic catalysts (Pt/Al<sub>2</sub>O<sub>3</sub> and Pt/hBN) were activated by reduction in H<sub>2</sub> flow during 30 min at 550 °C. Then, the catalyst was purged with N<sub>2</sub> and heated to the reaction temperature. The reactor effluent gases were analyzed by an on-line gas chromatograph (SRI 8610C GC) equipped with a silica gel column connected in series with a Molsieve MS13x 6 column and two detectors, TCD and FID. A methanizer converted carbon monoxide and carbon dioxide to methane to give greater sensitivity. The conversion and selectivity were calculated on a carbon basis, except for H<sub>2</sub> selectivity, which was calculated on a hydrogen basis (Equations 2.1, 2.2 and 2.3).

$$\text{Conversion (\%)} \quad X_i = \frac{\dot{n}_{i,in} - \dot{n}_{i,out}}{\dot{n}_{i,in}} \times 100\% \quad 2.1$$

$$\text{Carbon Atom} \\ \text{Selectivity (\%)} \quad S_i = \frac{\dot{n}_{i,out}}{n_{alkane,in} - n_{alkane,out}} \times \frac{z_i}{z_{alkane}} 100\% \quad 2.2$$

Hydrogen Atom  
Selectivity (%)

$$S_i = \frac{\dot{n}_{i,out}}{n_{alkane,in} - n_{alkane,out}} \times \frac{h_i}{h_{alkane}} 100\%$$

2.3

In equations 2.1, 2.2 and 2.3:

$X_i$ : Conversion of  $i$

$\dot{n}_i$ : Molar flow rate of  $i$

$S_i$ : Selectivity of  $i$

$z_i$ : Number of carbon atoms in  $i$

$h_i$ : Number of hydrogen atoms in  $i$

The subscript *alkane* refers to the feeding hydrocarbon (methane or ethane)

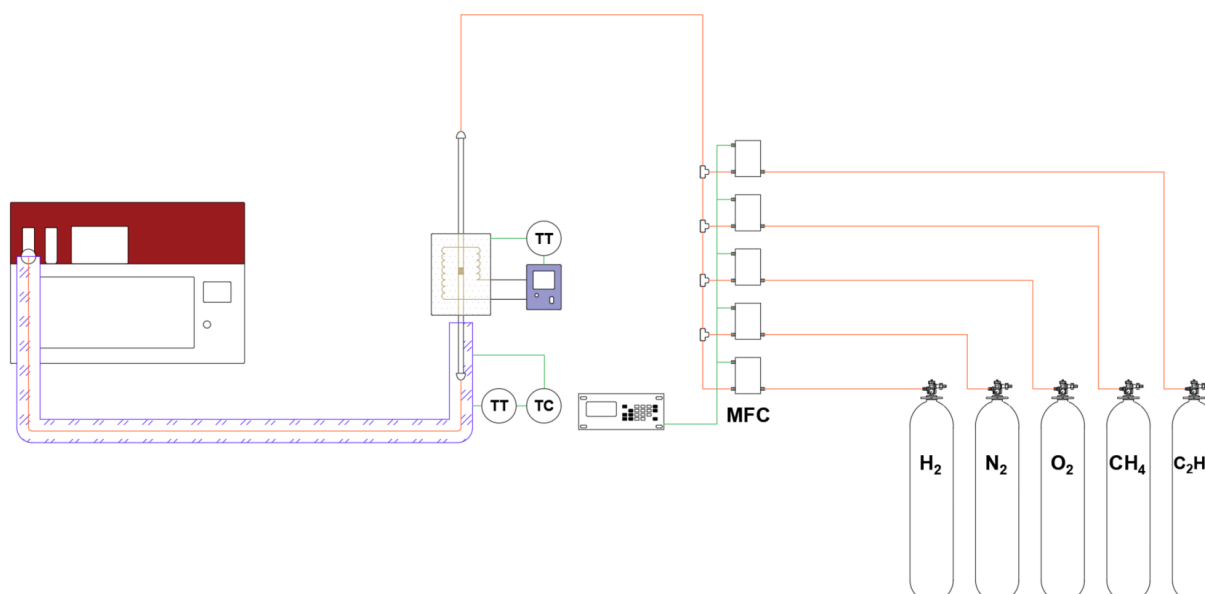


**Figure 2-1.** Experimental setup. Gases are feed at controlled rates using mass flow controllers (MFC). The furnace temperature is measured by a thermocouple (temperature transmitter: TT) and controlled by a PID controller. The temperature of the downstream gases from the reactor is controlled by a temperature controller (TC) connected to a thermocouple (TT).

## **Pt catalyst preparation**

The Pt/hBN catalysts were prepared using the wet impregnation (WI) method with an aqueous solution of chloroplatinic acid hexahydrate ( $\text{H}_2\text{PtCl}_6 \cdot 6\text{H}_2\text{O}$ ) from Sigma-Aldrich. The hBN support (Alfa Aesar, 325-mesh powder 99.5% purity) was suspended in water (1 g/100 mL) for 1 h using an ultrasonic bath sonicator. Then the Pt precursor solution was added and stirred for 2 h without sonication (wet impregnation samples) or with sonication (sonochemical wet impregnation samples). The mixture was dried overnight at 110 °C followed by calcination in a tubular furnace for 4 h with a heating ramp of 5 °C/min.

The incipient wetness impregnation method (IWI) was also tested with a solution of  $\text{H}_2\text{PtCl}_6 \cdot 6\text{H}_2\text{O}$  in methanol, but the Pt dispersion was much lower than the dispersion obtained with WI in water. Due to the lower dispersion the water WI was used for all the samples.

## **Pt catalyst experiments**

The experiments using the Pt catalysts were performed using Pt pellets. Pellets were prepared applying a 1000 psi pressure to a catalyst sample for 60 seconds. Then pellets were crushed and sieved to a size between 300  $\mu\text{m}$  and 500  $\mu\text{m}$ .

After the  $\text{H}_2$  reduction for 30 minutes and the  $\text{N}_2$  purge, the reactor was heated to the reaction temperature. Once that temperature was reached, the  $\text{N}_2$  stream was switched to  $\text{N}_2/\text{CH}_4/\text{O}_2$ . After 10 minutes of reaction at the reaction temperature the first sample was injected to the GC and then one injection was made every 30 minutes. After each injection, the temperature was changed between 500 °C and 900 °C in 100 °C steps. Each temperature was chosen randomly to prevent any effects associated to a linear temperature increase. For each experiment we repeated the sampling for each temperature 3 times.

## **hBN thermal treatments**

Thermal treatments took place in a Lindberg Blue M tubular furnace. For the humid air treatments, a water bubbler at room temperature with a diffuser was used to saturate the air stream before the furnace inlet. hBN850 was treated at temperatures from 600 °C to 950 °C with humid air. For the samples treated at 600 °C the thermal treatment did not change hBN significantly in short periods of time (less than 10 h), so we tried 60 h and 144 h.

The samples treated at 850 °C or higher were treated for 3 h, 6 h or 9 h. The thermal treatments at temperatures equal or higher than 850 °C for periods longer than 6 h produced a significant decomposition of hBN. We measured the decomposition by looking at the FTIR spectrum and at the XRD patterns. All samples were heated from room temperature at 10 °C/minute. After the treatments, with the objective of removing some products of the partial decomposition of hBN, samples were purified with humid air for 24 h at 600 °C.

hBNO was produced using humid air at 850 °C for 3 h, dry air at 850 °C for 2 h and dry air at 600 °C for 5 h. After the thermal treatments hBNO was suspended in deionized water (100 mL of water/g of hBN), sonicated for 4 h in a bath sonicator and centrifuged at 1000 rpm for 30 min. After the centrifugation the liquid phase was dried at 110 °C overnight and thermally purified using humid air at 600 °C in the furnace for 24 h.

## **hBN experiments**

The experiments with thermally treated hBN were carried out at temperatures from 560 °C to 610 °C in steps of 10 °C. The catalysts were used in their powder form. The reactor was heated up to 580 °C with a stream of N<sub>2</sub>/C<sub>2</sub>H<sub>6</sub>/O<sub>2</sub>, then the reactor was kept at that temperature for 10 minutes before the first injection to the GC. After the first injection the temperature was kept at



580 °C for the next 5 injections (one every 30 minutes). This “activation period” was necessary for some hBN samples to reach their full activity. After the activation period the temperature was changed randomly to one of the values established for the experiment (560, 570, 580, 590, 600 or 610 °C) to cover the whole range. Each experiment was repeated 2 more times.

For the stability tests we used a temperature of 580 °C. The injections to the GC were made every 30 minutes and the temperature and all other variables were constant during the whole experiment.

### **Pt dispersion**

The Pt dispersion was evaluated in a AMI-200 Catalyst Characterization System using an oxygen pulse chemisorption technique. The chemisorbed oxygen was determined by adding the difference between each oxygen peak area and the area of the peak once the sample was saturated (the consecutive pulses did not change). The sum of the areas was then transformed in oxygen molecules by a comparison with an oxygen pulse calibration (repeated 10 times) at the end of the experiment using a known amount of oxygen.

### **Fourier-transform infrared spectroscopy**

Fourier-transform infrared (FTIR) spectroscopy was performed to identify the functional groups attached to thermally treated hBN. FTIR spectra were collected using a Thermo Nicolet Nexus 670 operating in diffuse reflectance mode with a DTGS detector. The samples were diluted in FTIR grade KBr supplied by Alfa Aesar. The amount of sample used was 0.1 g diluted in 0.3 g of KBr. This ratio was tuned to prevent the saturation of the detector, which happens if too much

sample is used, and also prevent the signal to become weak, which happen if the sample is diluted too much.

All samples were collected in the  $500\text{ cm}^{-1}$  to  $4000\text{ cm}^{-1}$  range with a resolution of 1 data point /  $2\text{ cm}^{-1}$ . For the “Details on hBN activity for ethane oxidative dehydrogenation” section (Chapter 5) all fourier-transform infrared (FTIR) spectra were collected using a Cary 630 FTIR operating in ATR mode with an MCT detector. All samples were collected in the  $500\text{ cm}^{-1}$  to  $4000\text{ cm}^{-1}$  range with a resolution of 2 data points /  $\text{cm}^{-1}$ .

### **X-Ray powder diffraction**

X-ray powder diffraction (XRPD) patterns were collected with a Rigaku MiniFlex II at 30 kV, 15 mA and  $10^\circ < 2\theta < 60^\circ$ . Prior to the measurements of the XRPD patterns, the samples were dehydrated overnight at  $110\text{ }^\circ\text{C}$  in an oven. For some samples a “wet” spectrum was obtained by exposing them to a water saturated atmosphere overnight at room temperature before the measurement. Those samples were labeled as “wet”. All the samples were crushed with a pestle and mortar before each measurement.

### **Scanning Electron Microscopy**

Scanning Electron Microscopy (SEM) was used to evaluate the microstructure detail on the materials surface. The main goal with this technique was to determine if the morphology of hBN was preserved after the treatments and catalyst synthesis. SEM performed with a SEM-FID ZEISS Crossbeam 340 equipped with energy dispersive X-ray spectroscopy microprobe EDS Oxford Aztec, Silicon drift  $80\text{ mm}^2$ . Three images were taken for each sample at magnifications of 500x, 1000x and 5000x.

## Chapter 3 - Modification of Hexagonal Boron Nitride by Thermal Treatment<sup>1</sup>

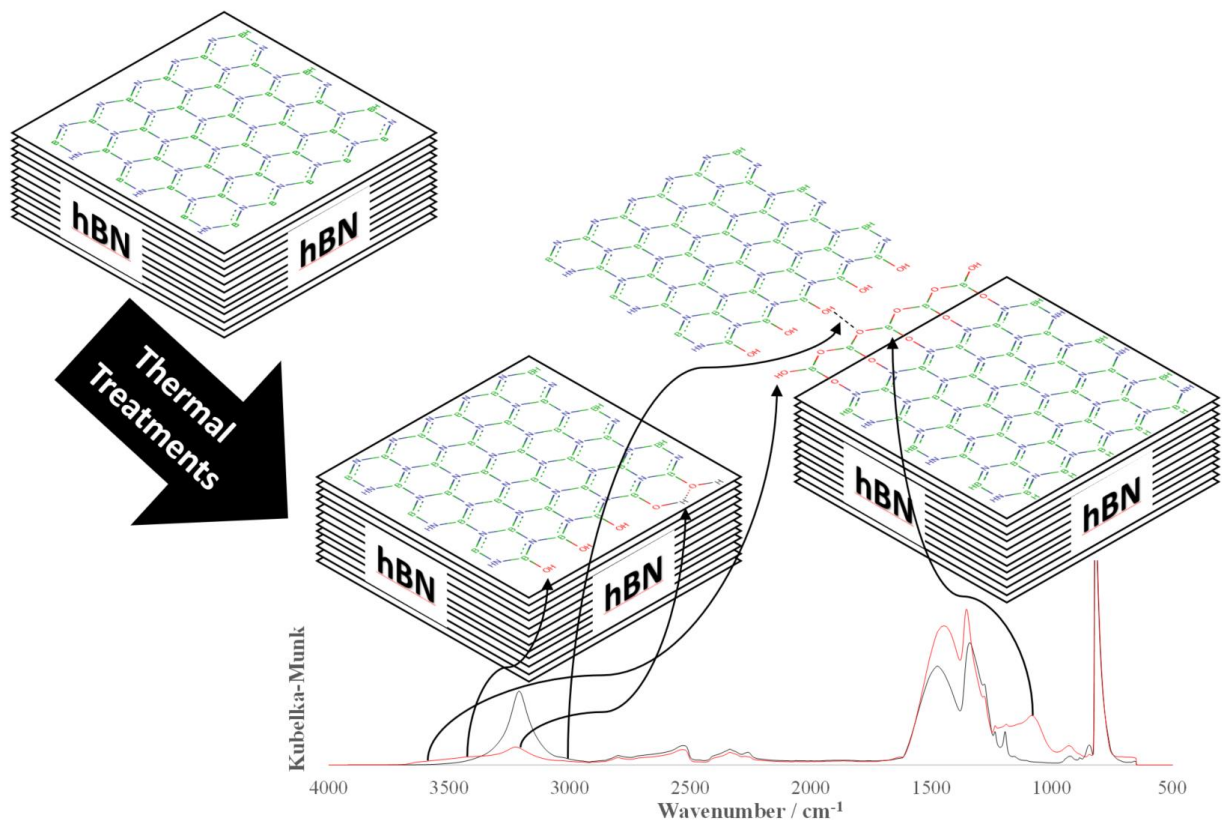


**Figure 3-1.** FTIR for thermally modified hBN and its chemical structure.

Hexagonal boron nitride (hBN) is attracting a lot of attention in the catalysis field due to its activity and selectivity in the oxidative dehydrogenation (ODH) of hydrocarbons<sup>1-4</sup>. The superior thermal and mechanical properties of hBN make this material suitable for many applications<sup>67-69</sup>, but at the same time make it difficult to modify it to introduce active catalytic sites. Thermal treatments (heating hBN at a given temperature for a given time in a controlled

<sup>1</sup> This chapter is based on a manuscript submitted to the Journal of Materials Science

atmosphere) are known to be a feasible way of functionalizing hBN<sup>32,61,62</sup> and previous studies claim this method adds hydroxyl groups to the edges<sup>32</sup> and surface<sup>62</sup> of hBN. Thermal treatments are preferred to other methods that require adding exogenous compounds which contaminate the sample<sup>70,71</sup>. Thermal treatments are also much simpler compared to synthesis methods which, instead of modifying hBN, use a synthesis method to produce a hydroxylated hBN from, for example, graphitic carbon nitrides and boric acid<sup>72</sup>.

Boron nitride hydroxylation also occurs during the induction period of ODH reactions. When a mixture of ethane and oxygen reacts on pristine boron nitride, the ethane conversion increases over time, as does the B-OH FTIR signal at 3200 cm<sup>-1</sup> peak<sup>2</sup>. However, selectivity to ethylene is generally higher if hBN has previously been hydroxylated<sup>1</sup>. Curiously, the FTIR peak for B-OH is present at 3400 cm<sup>-1</sup> in this case. The discrepancy in the wavenumber of the FTIR peaks for B-OH has been noted in other studies. Some assign the 3200 cm<sup>-1</sup> peak to hydroxylated hBN (hBNOH)<sup>32,62,73,74</sup> and others assign a 3400 cm<sup>-1</sup> peak to hBNOH and the one at 3200 cm<sup>-1</sup> to boric acid<sup>61,72</sup>. Unlike metal-based catalysts, the active sites of hBN are not clearly identified and cannot be measured yet, but in terms of reactivity, both OH groups, the one at 3200 cm<sup>-1</sup> and the one at 3400 cm<sup>-1</sup>) appear to be catalytically active<sup>1,28</sup>. In some cases, an additional signal shows up in the FTIR spectra after a thermal treatment due to oxygen doping of hBN. This peak is around 1100 cm<sup>-1</sup> due to N-B-O vibrations<sup>75-78</sup>.

Here, several thermal treatments are used to produce a variety of functionalized hBN materials with hydroxyl groups and oxidized surfaces. Boric acid is produced as a byproduct due to hBN decomposition during the treatments. Those materials are characterized using FTIR and XRD spectroscopy to reveal the nature of the functional groups added to hBN. In order to increase the reactivity of hBN, humid air is used<sup>34</sup>. This allows for functionalization at shorter times and

lower temperatures than those required in the absence of water. Additionally, a purification method is developed to remove the boric acid produced during the treatment due to the decomposition of hBN. As a final step, a sonication method to disperse the particles, followed by centrifugation, allowed us to separate the most stable water suspended particles, which showed a FTIR peak at  $1090\text{ cm}^{-1}$ , assigned to the B-N-O vibration. This suggests the formation of a borated hBN by the dehydration of boric acid on the surface of hBN. The goal of this study is to show that hBN can be functionalized in a variety of ways by changing the thermal treatment temperature, time and humidity.

## **Experimental**

### **Reagents**

Hexagonal boron nitride was supplied by Alfa Aesar as a 325-mesh powder 99.5% purity. Boric acid was supplied by Acros Organics with a 99.99% purity. All reagents were used as supplied for all the thermal treatments.

### **Thermal treatments**

Thermal treatments took place in a Lindberg Blue M tubular furnace. For the humid air treatments, a water bubbler with a diffuser was used to saturate the air stream before the furnace inlet.

### **Sonication and centrifugation**

In a typical procedure, the sample was sonicated in a bath sonicator using deionized water (100 mL of water per gram of sample). After the sonication time the samples were transferred to

50 mL conical-bottom centrifuge tubes and centrifuged for 30 minutes at 1000 rpm. After centrifugation the upper 35 mL of liquid were collected and dried overnight at 110 °C.

## **Characterization**

Fourier-transform infrared (FTIR) spectra were collected using a Thermo Nicolet Nexus 670 operating in diffuse reflectance mode. The samples were diluted in FTIR-grade KBr supplied by Alfa Aesar. The FTIR results presented here are representative of multiple repeat trials: at least two samples for each treatment.

SEM images were obtained using a Hitachi S-3500N with Pd sputter coating on all samples.

X-ray powder diffraction (XRD) patterns were collected on a Rigaku MiniFlex II at 30 kV, 15 mA and  $10^\circ < 2\theta < 60^\circ$ .

Prior to the measurements for the FTIR spectra and XRD patterns, the samples were dehydrated overnight at 110 °C in an oven with ambient air. For some samples a “wet” spectrum was obtained by exposing them to a water saturated atmosphere overnight at room temperature before the measurement. Those samples were labelled as “wet”. For both techniques, all the samples were crushed with a pestle and mortar before each measurement.

## **Thermal treatments**

Samples were thermally treated at temperatures ranging from 650 °C through 950 °C. After studying the effect of different temperatures and the humid or dry atmosphere, a set of temperatures were chosen to run the complete set of experiments presented here (650 °C, 850 °C, 900 °C and 950 °C). Temperatures lower than 800 °C are not effective to change the material in a short period

of time. A temperature of 600 °C was used to evaluate the effect of a long thermal treatment at low temperatures.

## Results and Discussion

In this study, we applied several thermal treatment protocols to hBN. Each protocol consisted on a series of steps grouped in 3 categories: Treatment, Post treatment and Storage. The first one is the thermal treatment itself. Its objective is to introduce hydroxyl groups to hBN, as well as cause other changes that will be discussed later. The second one is the post treatment. Its objective is to remove impurities generated during the thermal treatment, especially boric acid. It consists of a lower temperature thermal treatment followed by sonication and centrifugation. The third one is the storage of the samples after synthesis. Storage is not part of the hBN modification process, but samples stored in different environments gave different results, so this step was included as part of the protocol.

Treatment and storage are always present in every protocol, but some samples were not subjected to post treatment. Table 3-1 summarizes the available steps with a nomenclature and examples to name the protocol.

Table 3-1. Nomenclature for the hBN treatment protocols

Treatment (TT)	Post treatments (PT)	Characterization
<b>D:</b> Dry air	<b>T:</b> Thermal <b>D:</b> Dry air	<b>D:</b> Dried overnight at 110 °C
<b>H:</b> Humid air	<b>H:</b> Humid air <b>Y:</b> Time in h	<b>W:</b> Overnight exposure to a
<b>X:</b> Temperature in °C	<b>X:</b> Temperature in °C	water saturated atmosphere at
<b>Y:</b> Time in h	<b>S:</b> Sonication and centrifugation	room temperature
	<b>N:</b> Sonication time in h	

Table 3 1. Nomenclature for the hBN treatment protocols, Continued

<b>Nomenclature</b>		
TT:(D/H)X-Y	PT(T/S)(D/H)-Y·SN	C:(D/W)
<b>Example</b>		
First TT with H air at 850 °C for 6 h. Second TT with D air at 950 °C for 3 h.	PT with H air at 550 °C for 24 h followed by S for 4 h and centrifugation.	Characterization after overnight drying at 110 °C.
TT:H850-6	PT:TH550-24·S4	C:D
TT:H850-6_PT:TH550-24·S4_C:D		

### Heat Treatment of hBN

The morphology of the materials was evaluated using SEM images (**Figure 3-2**). Most of the samples did not show any morphological change after the treatment compared with the starting material (hBN shown in **Figure 3-2a**). The only exception was hBN treated at 950 °C with humid air and sonicated for 18 hours (**Figure 3-2b**) which is showing a morphology similar to the one in **Figure 3-6** (Inset a) due to the presence of a boron oxide phase.

The first sample evaluated was hBN treated at 950 °C in dry air for three hours with a 18 h sonication post treatment (

**Figure 3-3a**). There is a peak in 3213 cm<sup>-1</sup> in the FTIR spectrum. This peak is assigned to an OH vibration, probably from boric acid produced during hBN decomposition<sup>61,72</sup> ( $hBN + 3H_2O \rightarrow NH_3 + B(OH)_3$ ). A relatively wide peak also appears at 1090 cm<sup>-1</sup>. This peak is assigned to oxidized hBN (hBNO). Additional experiments later in this work will support this assignment.

Next, pristine hBN was treated at 900 °C with water-saturated air (



**Figure 3-3b)** followed by a post treatment at 310 °C and sonication. The goal of the low temperature post treatment is to remove some of the boric acid from the sample by a displacement of the equilibrium between the dehydrated form of boric acid,  $B_2O_3$ , which has a high boiling point, to a hydrated species with a lower boiling point (Reactions 3.1 and 3.2)<sup>79</sup>. By keeping a humid atmosphere, the hydration of the boron compounds is promoted, while the low temperature prevents decomposition of hBN, resulting in a net reduction of the boric acid content in the sample. After sonication, the 1090  $cm^{-1}$  peak appears even bigger than in the treatment at 950 °C.

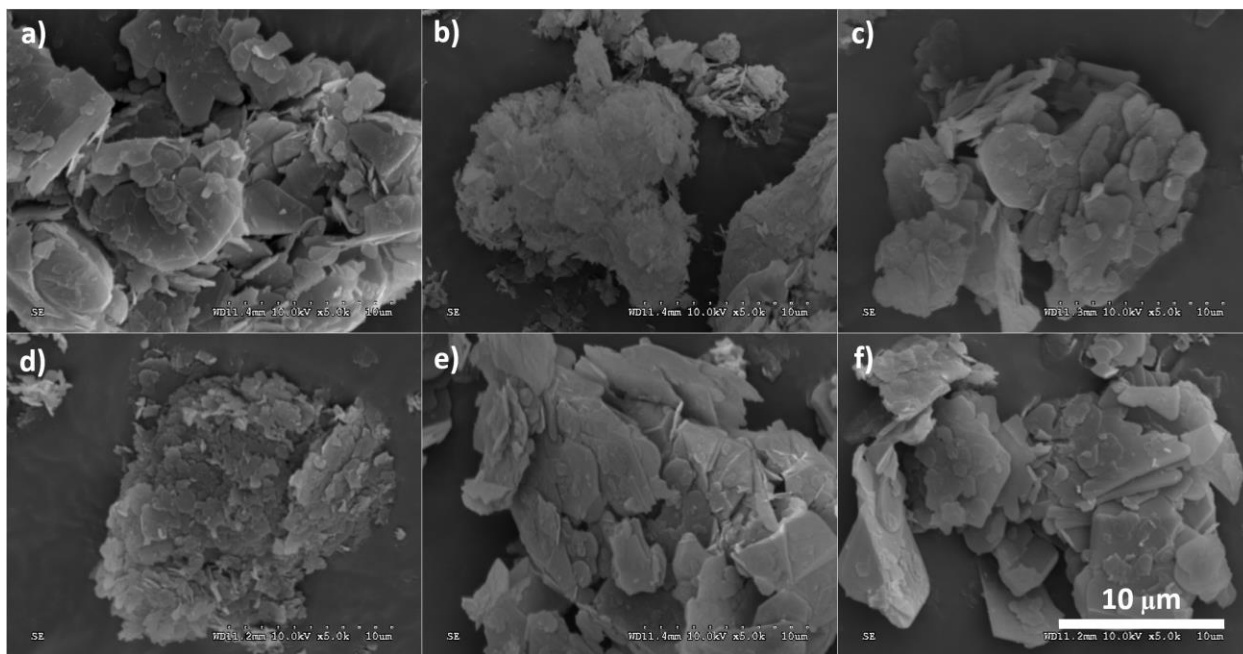


**Figure 3-2.** SEM images for thermally treated hBN. a) Untreated hBN; b) TTD950-3\_PT:S18\_C:D; c) TT:H900-3\_PT:H310-10 S4\_C:D; d) TT:H850-3\_PT:H310-10 S4\_C:D; e) TT:H850-3\_PT:D600-5S4\_C:D and f) TT:850H-6\_C:D

If there is an equilibrium between hydrated and dehydrated boron species in the thermal treated hBN samples, it means that XRD patterns for a sample with dehydrated boron species (stored at 110 °C after the treatment) will not exhibit boric acid peaks. On the other hand, the XRD pattern for a sample with hydrated boron species (stored in a water-saturated atmosphere at room temperature) will show the boric acid peaks. To test the impact of these storing methods, the XRD patterns were measured for a hBN sample treated at 850 °C for 6 h under humid air (TT:850H-6) when the sample was stored in a dry environment (TT:850H-6\_C:D) and when it was stored in a humid environment (TT:850H-6\_C:W) (**Figure 3-4**). As expected, the dry sample appears almost boric acid-free in **Figure 3-4** because the boron species are dehydrated and the XRD pattern for B<sub>2</sub>O<sub>3</sub> is not visible in the presence of hBN. On the other hand, the wet sample clearly shows the boric acid pattern (PDF No: 01-072-3608) mixed with the one for hBN. These data demonstrate that a simple change in the sample preparation could hide the presence of boric acid and lead to erroneous conclusions.

The FTIR peaks at 2213 cm<sup>-1</sup> appeared when hBN was treated at 850 °C for 3 h with humid air (**Figure 3-3c**), but there was no significant change in the FTIR spectra when hBN was treated with humid air at 650 °C (

**Figure 3-3d**) even after 60 hours of treatment.

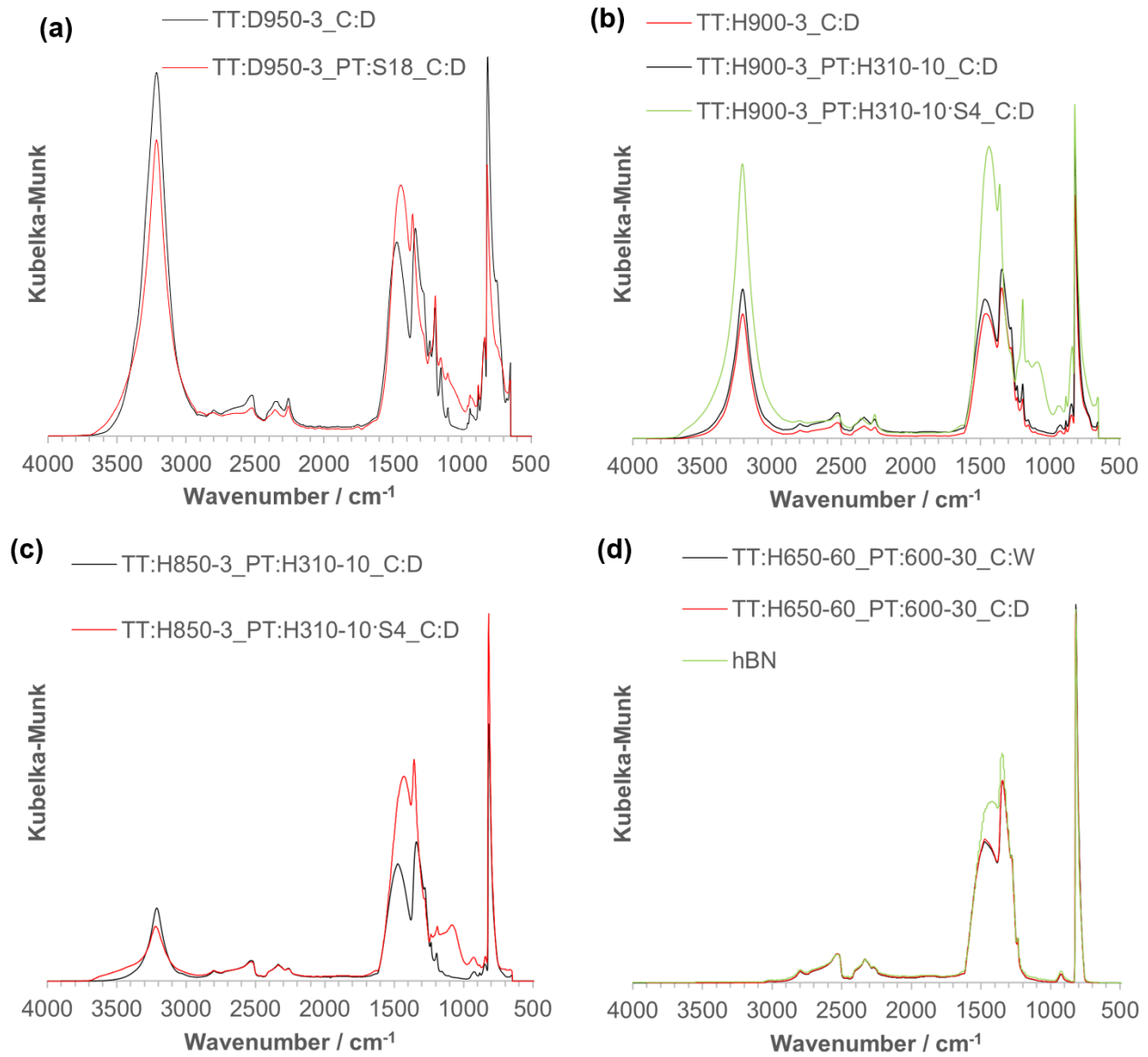


**Figure 3-3.** FTIR spectra for thermally treated hBN at a) 950 °C, b) 900 °C, c) 850 °C and d) 650 °C

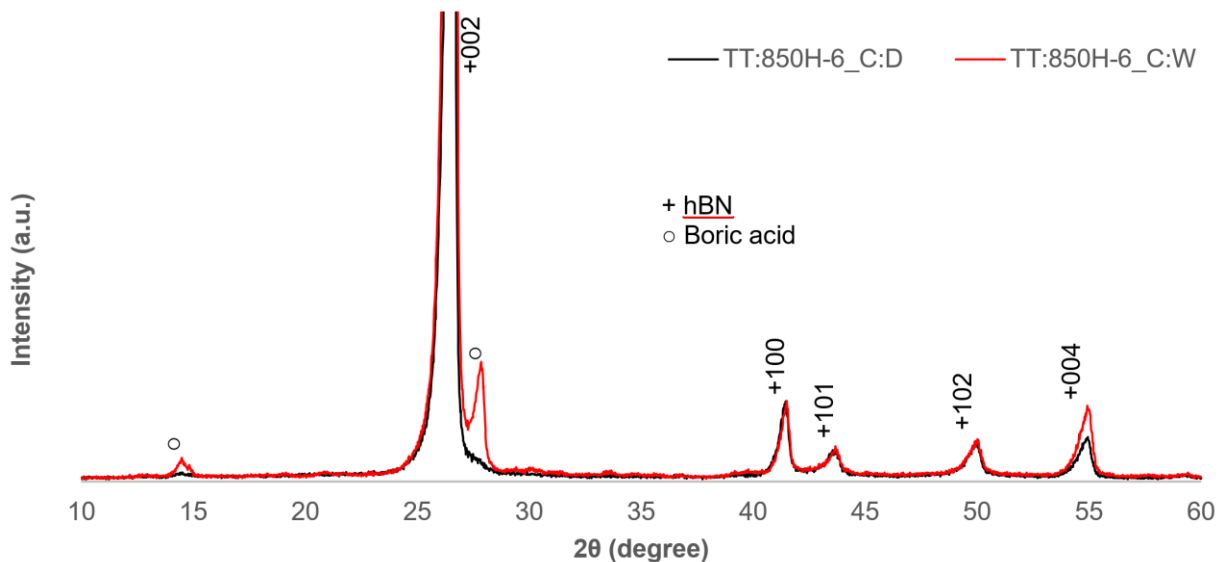


**Figure 3-4.** XRD patterns for thermally treated hBN. The same sample was measured dry and wet, giving different results due to the equilibrium between the hydrated and dehydrated borate species

### Boric acid removal

As described above, thermal treatment in air at temperatures above 850°C with humid air led to formation of boric acid, as identified in both FTIR and XRD spectra. To further understand the role of boric acid in thermally treated hBN samples, boric acid removal was studied by treating an hBN sample at 850 °C for 6 h in humid air. XRD patterns were measured for the sample at different times during the boric acid removal treatment at 600 °C for several hours. **Figure 3-5a** shows the XRD patterns along with identified peaks for hBN (PDF No: 01-085-1068) and boric acid (PDF No: 01-072-3608). Both boric acid peaks are expanded in **Figure 3-5b** and **Figure 3-5c**. As seen in **Figure 3-5b** and **Figure 3-5c**, the boric acid peaks diminish over time, indicating that there is a reduction of the boric acid content with post treatment time. The XRD data was used to estimate the boric acid content of each stage of the post treatment using the reference intensity ratio (RIR) method and the trend is typical for a first order dynamics ( $dC_{BA}/dt = aC_{BA}$ , where  $a$  is

a rate constant and  $C_{BA}$  is the boric acid concentration in the sample). Setting the initial concentration of boric acid equal to  $C_{BA0}$ , the dynamic equation can be solved to give:  $C_{BA}/C_{BA0} = e^{-0.124t}$ . If a 24 h treatment is used, this equation predicts that 95% of boric acid will be eliminated from the sample.

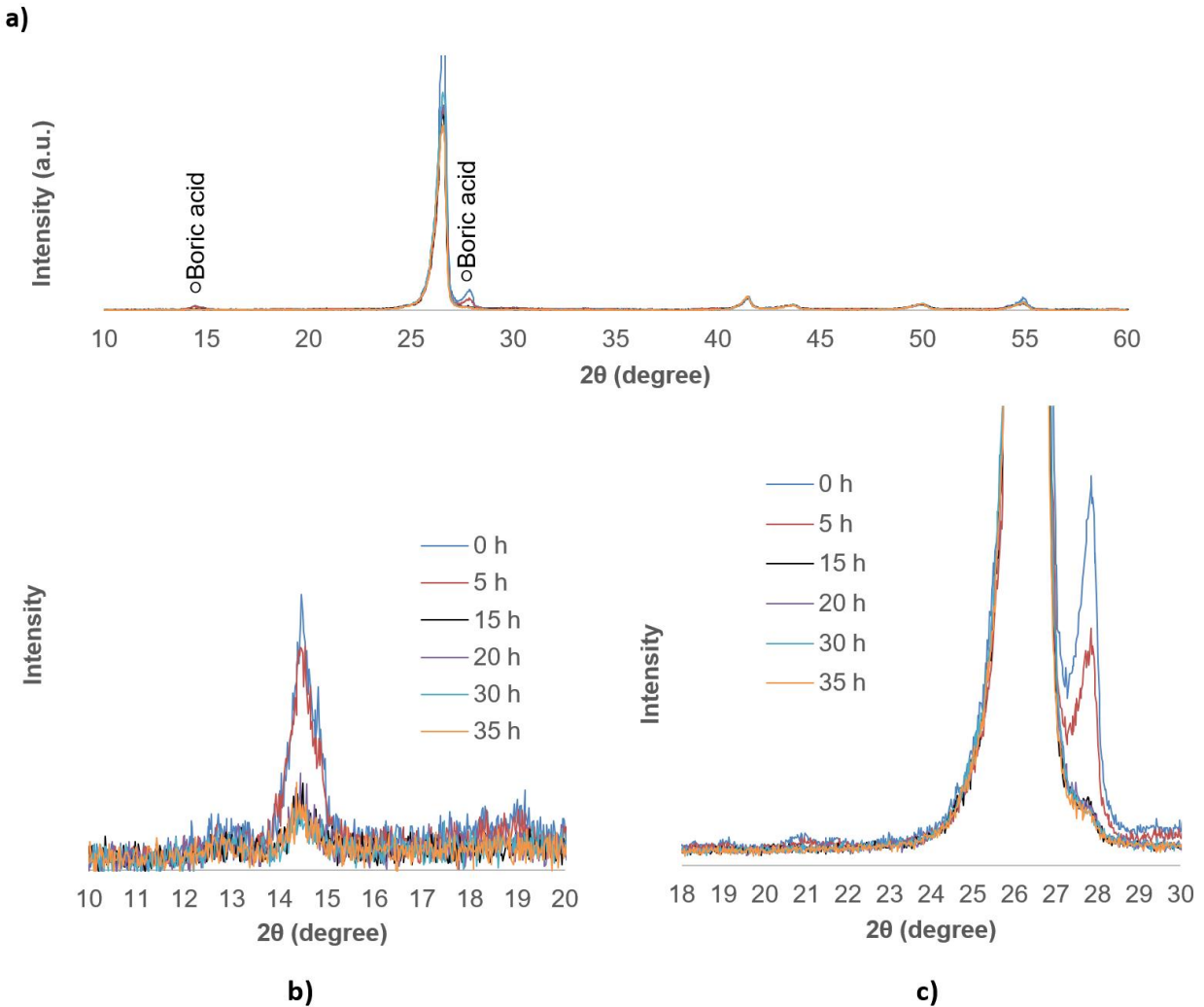


**Figure 3-5.** XRD pattern of a thermal treated hBN sample at 850 °C plus a post treatment at 600 °C with humid air (TT:850-6\_PT:TH600-t). The plot shows the evolution of boric acid content with time. a) Complete pattern. b) and c) zoom in on the boric acid signal.

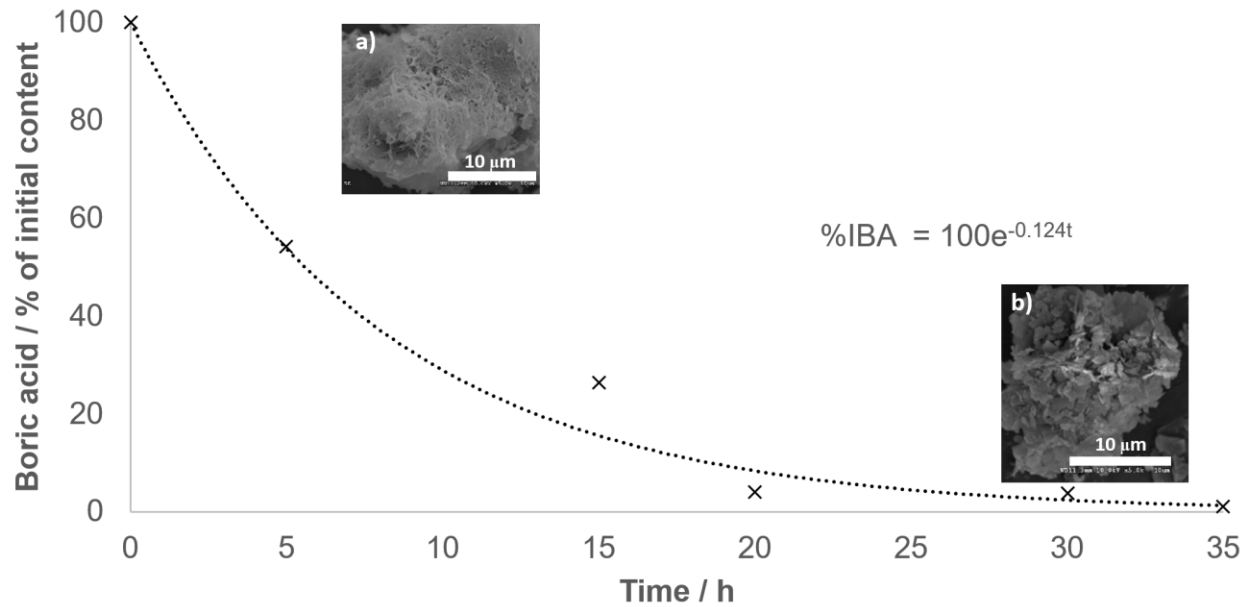


**Figure 3-6.** Percent of remaining initial boric acid content (%IBA) during post treatment of a thermal treated hBN sample. Inset: hBN SEM images before (a) and after (b) post treatment

### Post Treatment of Thermally Treated hBN

The impact of post treatment of the thermally-treated hBN samples was studied by subjecting a sample that had been thermally treated at 850 °C for 3 h with humid air to post treatment at 600 °C with dry air for 5 h. The FTIR spectra were measured before and after a 4 hours sonication final step as shown in **Figure 3-7**. An FTIR spectrum was measured with a dry sample to minimize the boric acid peak at 3200  $\text{cm}^{-1}$  and better show other peaks between 3000  $\text{cm}^{-1}$  and 4000  $\text{cm}^{-1}$ . The peaks for this sample show a variety of boron species on treated hBN. The peak at 1090  $\text{cm}^{-1}$  is much stronger after the sonication-centrifugation step and there are overlapping peaks near 3300  $\text{cm}^{-1}$  (**Figure 3-7**).

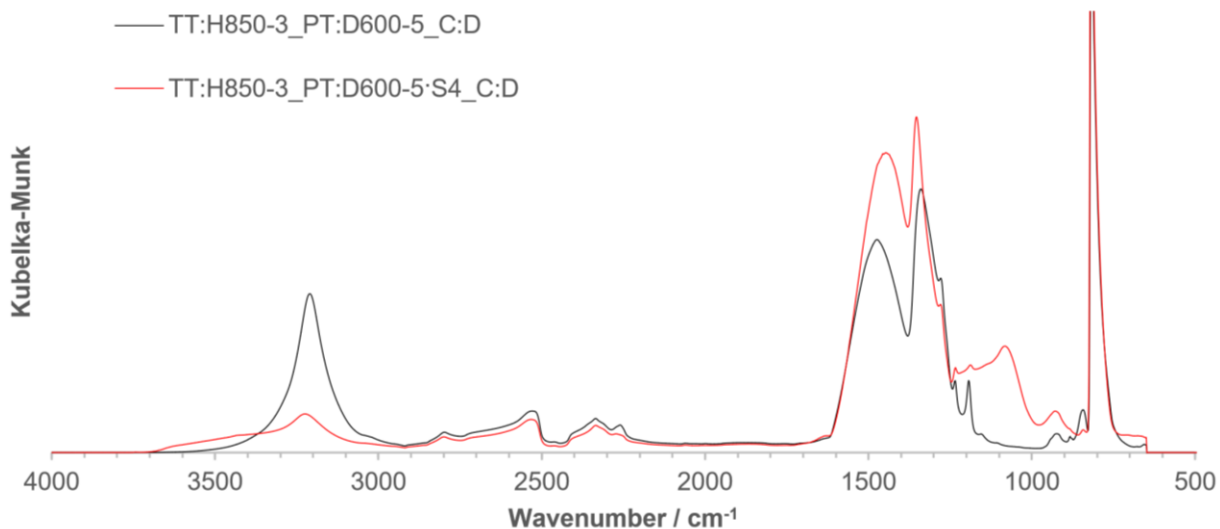


**Figure 3-7.** Borated hBN after boric acid dehydration on its surface.

To understand these results a deconvolution of the FTIR spectra between  $2900\text{ cm}^{-1}$  and  $3800\text{ cm}^{-1}$  is presented in **Figure 3-8**. The deconvolution unveiled four peaks:  $3600\text{ cm}^{-1}$ , assigned to OH groups attached to  $\text{B}_2\text{O}_3$ <sup>34</sup>;  $3400\text{ cm}^{-1}$ , assigned to OH groups attached to hBN<sup>61,72</sup>;  $3000\text{ cm}^{-1}$ , assigned to hydrogen bonding of  $\text{B}_2\text{O}_3$  species with the OH groups<sup>34</sup> and  $3200\text{ cm}^{-1}$  assigned to boric acid and hBN concerted hydroxyl groups<sup>80</sup>. The  $1090\text{ cm}^{-1}$  peak is assigned to N-B-O vibrations<sup>75-78</sup>. The simplest explanation that we can give to fit all these results involves a partial decomposition of hBN to boric acid followed by dehydration of boric acid on the surface of hBN and the formation of a borated hBN species. The details are presented below.

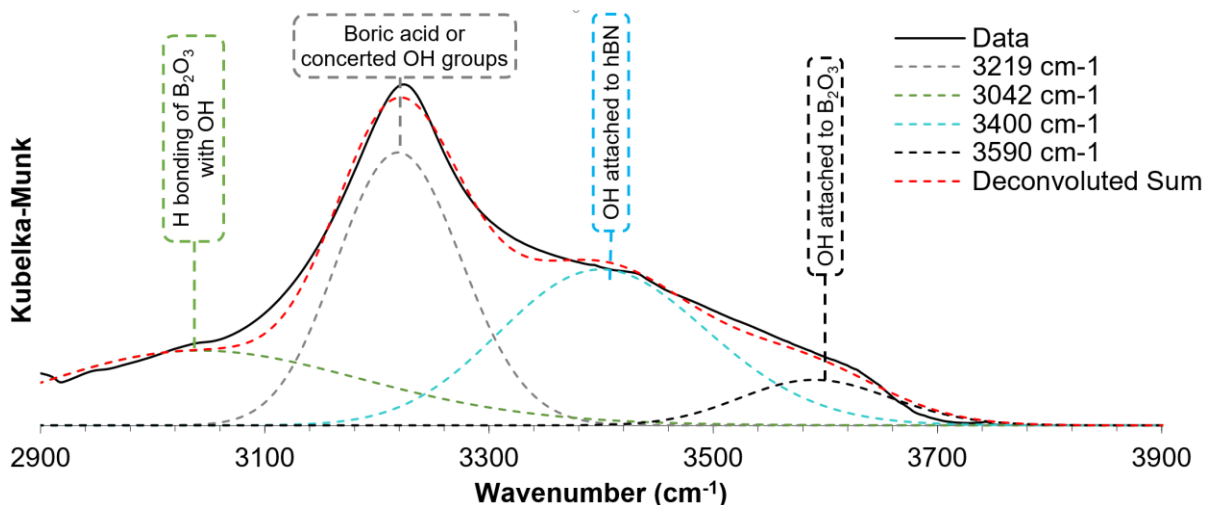
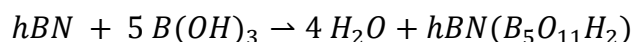


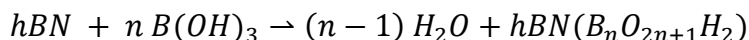
**Figure 3-8.** Deconvoluted FTIR spectrum of **Figure 3-7**. The 3600 cm<sup>-1</sup> peak is assigned to OH groups attached to B<sub>2</sub>O<sub>3</sub><sup>34</sup>. The 3400 cm<sup>-1</sup> is assigned to OH groups attached to hBN<sup>61,72</sup>. The 3000 cm<sup>-1</sup> peak is assigned to hydrogen bonding of B<sub>2</sub>O<sub>3</sub> species with the OH groups<sup>34</sup>. The 3200 cm<sup>-1</sup> could be boric acid or hBN concerted hydroxyl groups<sup>80</sup>.

### Boron nitride dehydration and borated hBN formation

When hBN is decomposed into boric acid and ammonia, the boric acid could dehydrate on the surface of hBN to form borated hBN. For example, if 5 molecules of boric acid lose 4 molecules of water on the surface of hBN, the reaction will be:



where  $hBN(B_5O_{11}H_2)$  is borated hBN (**Figure 3-9**). A similar result was obtained before for borated alumina<sup>81</sup>. In general, for any given amount of boric acid molecules (n) being dehydrated on the surface of hBN, the resulting product will be:





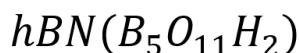
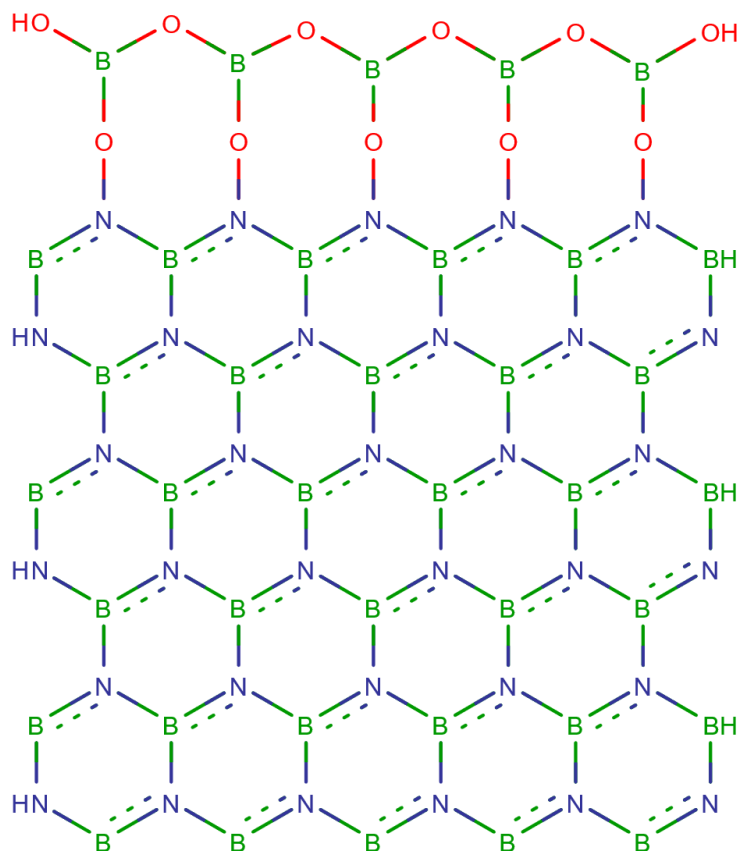


**Figure 3-9.** Borated hBN after boric acid dehydration on its surface

This borated hBN explains all the peaks present in **Figure 3-7** and **Figure 3-8** and its structure is similar to the borated alumina found in another study<sup>36</sup>. In addition, the presence of borated hBN explains why in **Figure 3-7** the peak at  $1090\text{ cm}^{-1}$  is much stronger after the sonication-centrifugation. Borated hBN will be more stable in water than hBN due to hydrogen bonding between its framework oxygen and water. When borated hBN is centrifuged, the resulting centrifuged liquid sample is richer in borated species than the original sample that contained both borate and non-borated hBN. To prove this point, two suspensions of the same mass of hBN and thermal treated hBN (hBN850-6h) were made by sonicating the suspensions and then spinning

them in a centrifuge for 30 min. The thermal treated hBN suspension contains 3 times more solids than the pristine hBN (

**Figure 3-10).**

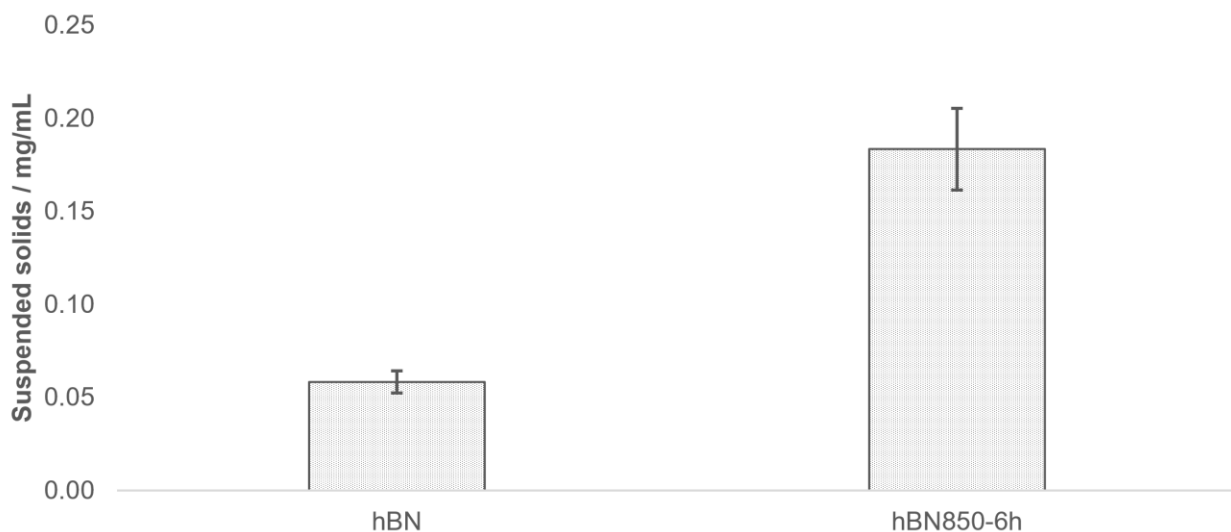


**Figure 3-10.** Suspensions of hBN and thermal treated hBN. The thermal treated suspension contains three times more solids due to the formation of hydrogen bonds with water

Additional support for the hypothesis that borated hBN is formed is shown in **Figure 3-11**. A shift to a smaller  $2\theta$  angle in the hBN [002] plane suggests that the hBN surface is oxidized, causing an increase in the crystal plane spacing (Inset of **Figure 3-11** shows the peaks normalized to equal height showing the left shift).

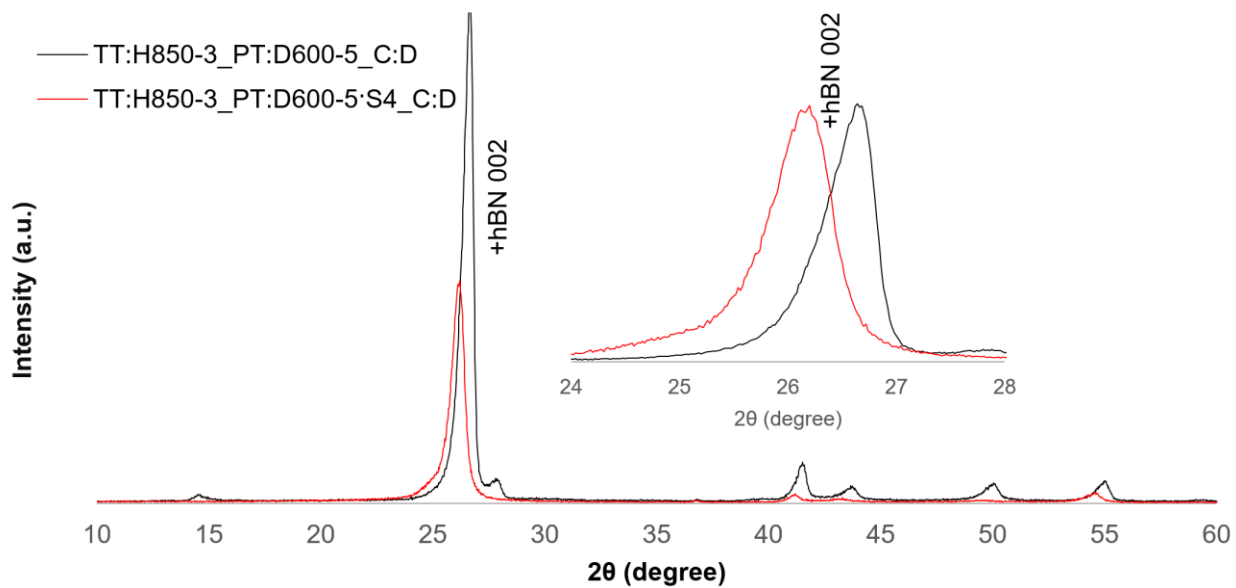


**Figure 3-11.** A left shift in the XRD pattern peak characteristic of the hBN 002 plane caused by an increase in the crystal plane spacing due to hBN oxidation (Inset: peaks normalized to equal height showing the left shift)

## Conclusions

This work shows how different thermal treatments can be used to hydroxylate hBN and how the final material can be tuned by changing the treatment temperature, time, atmosphere and post treatment. Boric acid is extensively formed when hBN is treated in humid air at high temperatures, but it can be removed by a thermal post treatment at low temperature using air saturated with water. This prevents hBN particles reaggregation or loss of material, which can plague alternative methods such as filtration. Furthermore, boric acid can dehydrate to  $B_2O_3$  at high temperatures, ultimately forming hBNO. These materials form more stable suspensions in water than pristine hBN. Finally, XRD and FTIR analysis can be complicated by the formation of boric acid if thermal treated hBN samples are stored in a humid environment. Analysis of samples

stored in a dry environment demonstrate the absence of boric acid and the presence of  $B_2O_3$ . This is an important consideration to take into account when characterizing thermally treated samples.

## Chapter 4 - Syngas production on a Pt/hBN catalyst: the role of the support

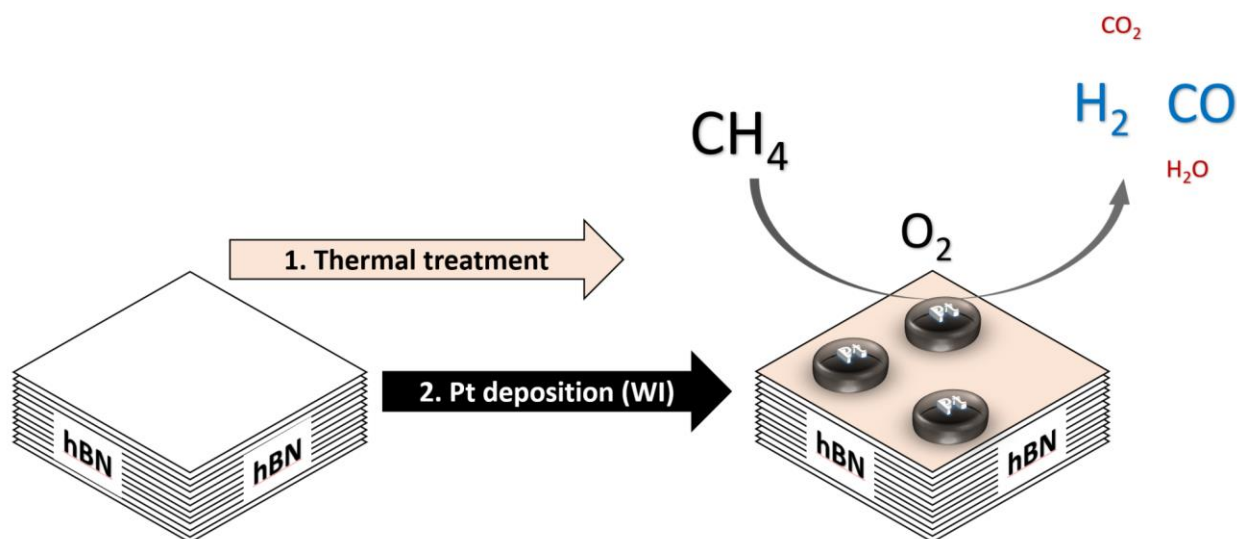
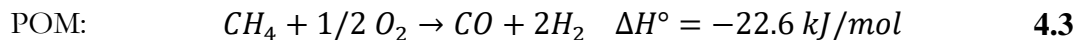
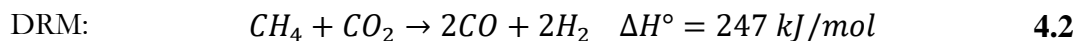
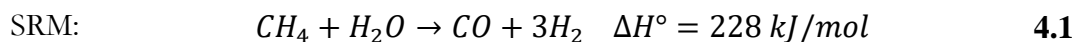


**Figure 4-1.** Production of syngas on a Pt/hBN catalysts. The hBN support was thermally treated before the Pt impregnation.

Natural gas production in the US has increased more than 50% in the last 10 years<sup>39</sup>. Converting methane, the main component in natural gas, to syngas is a key step in its exploitation chain<sup>40</sup>. There are several reaction pathways to achieve this, such as: Steam reforming of methane (SRM, Eq. 4.1), Dry reforming of methane (DRM, Eq. 4.2) and Partial oxidation of methane (POM, Eq. 4.3)<sup>41</sup>. SRM is the most widely used method to produce syngas industrially. Both SRM and DRM are endothermic reactions that require high temperatures. This causes some undesirable effects such as coke formation in DRM. POM is an exothermic reaction, which makes it energetic favorable requiring lower temperatures and reduced energy costs<sup>42,43</sup>. In addition, the H<sub>2</sub>/CO ratio produced by POM is about 2, which makes it ideal for the further production of methanol or

Fischer–Tropsch synthesis<sup>44</sup>. Other details of POM for syngas production have been reviewed in detail<sup>40,45–47</sup>.



POM, however, has some disadvantages. The reaction mechanism is proposed to be a two-step reaction<sup>48</sup>: a total combustion first step and then dry and steam reforming to produce syngas in addition to the water gas shift reaction<sup>44</sup>. Such mechanism causes a temperature gradient in the catalyst bed because combustion is highly exothermic and the subsequent reactions are endothermic, leading to a difficult temperature regulation due to the formation of hot spots, especially when low thermal conductivity supports are used (i.e. Al<sub>2</sub>O<sub>3</sub>) causing catalyst deactivation<sup>49</sup>. The higher conductivity of hBN (125 W/m/K) will distribute the energy better than Al<sub>2</sub>O<sub>3</sub> (23 W/m/K), reducing the hot spots<sup>82–84</sup>. Moreover, the weaker interaction between Pt and hBN could improve the catalytic activity of Pt, such it does with other metals<sup>36</sup>, because the metal–support interaction is generally negative for the catalyst activity<sup>36,83,85</sup> and also affects the metal particles shape<sup>86</sup>.

In this work Pt/hBN catalysts are prepared using a variety of thermal treated hBN supports. The goal of the thermal treatments is to change the interaction between Pt and hBN, which strongly affects the Pt activity. Most of the thermal treatments applied produce boric acid due to the decomposition of hBN. This boric acid interacts with the Pt precursor during the catalyst synthesis, so removal of boric acid in different stages of the catalyst synthesis is evaluated and compared with untreated hBN or untreated hBN doped with boric acid. Catalytic tests evaluate the effect of

such treatments on catalysts activity, selectivity and H<sub>2</sub>/CO ratio compared with a regular Al<sub>2</sub>O<sub>3</sub> catalyst. We focus our attention on the Pt/support interaction, how this interaction can be modified by changing the synthesis method, and how the interaction affects the activity of the catalyst.

## **Experimental section**

### **Reagents**

Hexagonal boron nitride was supplied by Alfa Aesar as a 325-mesh powder 99.5% purity. Boric acid was supplied by Acros Organics with a 99.99% purity. All reagents were used as supplied for all the thermal treatments.

### **Thermal treatments**

Thermal treatments took place in a Lindberg Blue M tubular furnace. For the humid air treatments, a water bubbler with a diffuser at room temperature was used to saturate the air stream before the furnace inlet.

### **Characterization**

Fourier-transform infrared (FTIR) spectra were collected using a Thermo Nicolet Nexus 670 operating in diffuse reflectance mode. The samples were diluted in FTIR grade KBr supplied by Alfa Aesar.

X-ray powder diffraction (XRPD) patterns were collected with a Rigaku MiniFlex II at 30 kV, 15 mA and  $10^\circ < 2\theta < 60^\circ$  using a copper source with a wavelength of 1,54 Å.

Prior to the measurements for the FTIR spectra and XRD patterns, the samples were dehydrated overnight at 110 °C in an oven. For some samples a “wet” spectrum was obtained by

exposing them to a water saturated atmosphere overnight at room temperature before the measurement. Those samples were labeled as “wet”. For both techniques all the samples were crushed with a pestle and mortar before each measurement.

Scanning electron microscopy was performed with a SEM-FID ZEISS Crossbeam 340 equipped with energy dispersive X-ray spectroscopy microprobe EDS Oxford Aztec, Silicon drift 80 mm<sup>2</sup>. All samples were coated with Pd.

The Pt dispersion was evaluated in a AMI-200 Catalyst Characterization System using an oxygen pulse chemisorption technique. The chemisorbed oxygen was determined by adding the missing oxygen in each pulse before reaching the saturation stage characterized by constant consecutive pulse areas.

### **Catalyst preparation**

The Pt/hBN catalysts were prepared using the wet impregnation method with an aqueous solution of chloroplatinic acid hexahydrate ( $\text{H}_2\text{PtCl}_6 \cdot 6\text{H}_2\text{O}$ ) from Sigma-Aldrich. The hBN support (Alfa Aesar, 325-mesh powder 99.5% purity) was suspended in water (1 g/100 mL) for 1 h using an ultrasonic bath sonicator. Then the Pt precursor solution was added and stirred for 2 h without sonication (wet impregnation samples) or with sonication (sonochemical wet impregnation samples). The mixture was dried overnight at 110 °C followed by calcination at 375 °C in air using a tubular furnace for 4 h with a heating ramp of 5 °C/min.

### **Catalytic activity**

The catalytic activity was evaluated in a quartz tubular reactor (internal diameter = 12 mm) with a continuous flow operating at near atmospheric pressure. The catalyst was pelletized and



packed into the reactor between quartz wool. The reactor tube was encased in an electrically heated tube furnace with a PID temperature controller connected to a coaxial thermocouple. Before each run, the catalysts were activated by reduction in H<sub>2</sub> flow during 30 min at 550 °C. Then, the catalyst was purged with N<sub>2</sub> and heated to the reaction temperature. The reactor effluent gases were analyzed by an on-line gas chromatograph (SRI 8610C GC) equipped with a silica gel column connected in series with a Molsieve MS13x 6 column and two detectors, TCD and FID. A methanizer converted carbon monoxide and carbon dioxide to methane to give greater sensitivity. The conversion and selectivity were calculated on a carbon basis, except for H<sub>2</sub> selectivity, which was calculated on a hydrogen basis.

## Result and discussion

The Pt/hBN catalysts and their support, hBN, were characterized by XRPD (**Figure 4-2**). The diffraction pattern of the support confirms the presence of the hexagonal phase of BN (reference pattern 01-085-1068). The impregnation of Pt (reference pattern 01-087-0642) and the thermal treatment did not change the support significantly. However, there is boric acid present in the thermal treated catalyst hBN850\* (reference pattern 01-072-3608). Both catalysts, Pt/hBN850 and hBN850\* are the same sample but the XRPD pattern for the first one was measured after the calcination step, while the second one was exposed to a water saturated atmosphere overnight before the measurement. By doing this, the presence of boric acid was revealed because the calcination process dehydrates it to boron trioxide<sup>87</sup> (which is not visible with XRPD). This explains why there is no evidence of boric acid in Pt/hBN850. But if Pt/hBN850 is exposed to humid air the boron trioxide rehydrates to boric acid<sup>79</sup> (Pt/hBN850P\*), which is visible in the XRPD pattern. We also developed a method to remove boric acid from the samples by heating

them at 600 °C with humid air. There is no presence of boric acid in Pt/hBN850\* after the purification step. This sample is denoted as Pt/hBN850P\* and is shown in the inset in **Figure 4-2**.

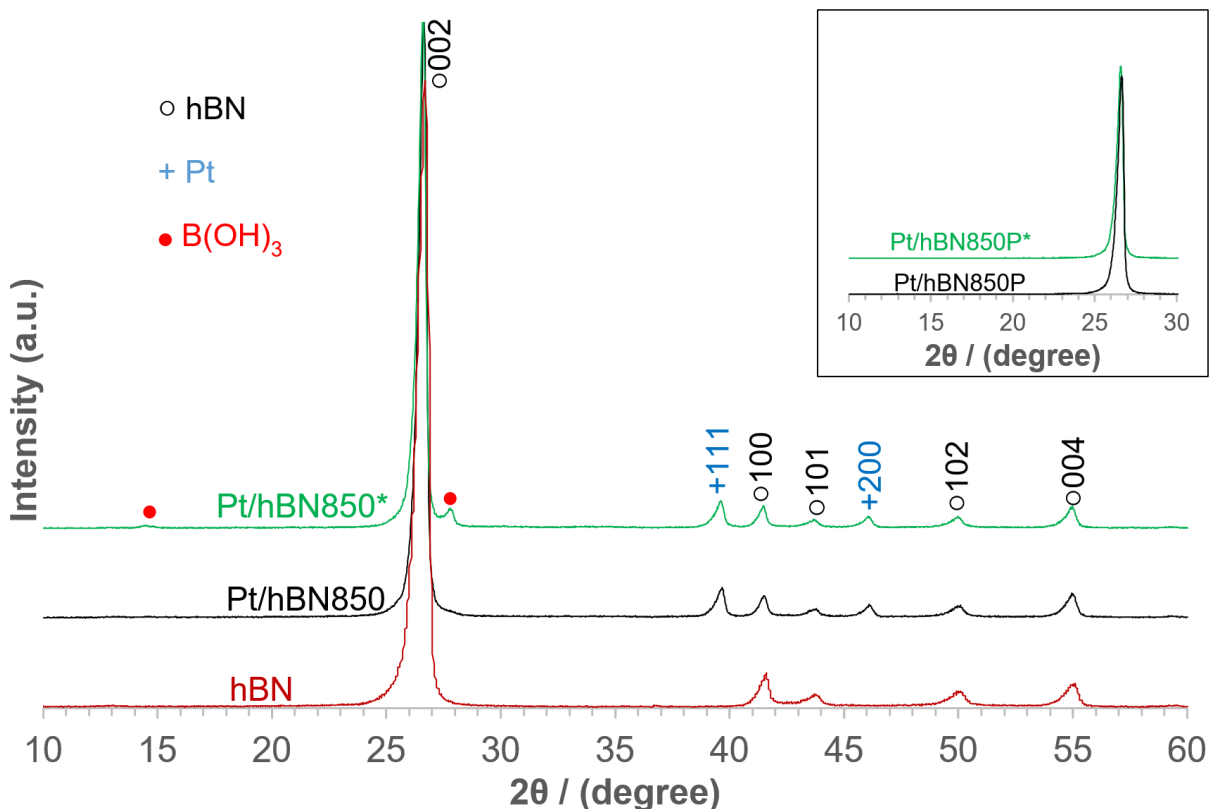
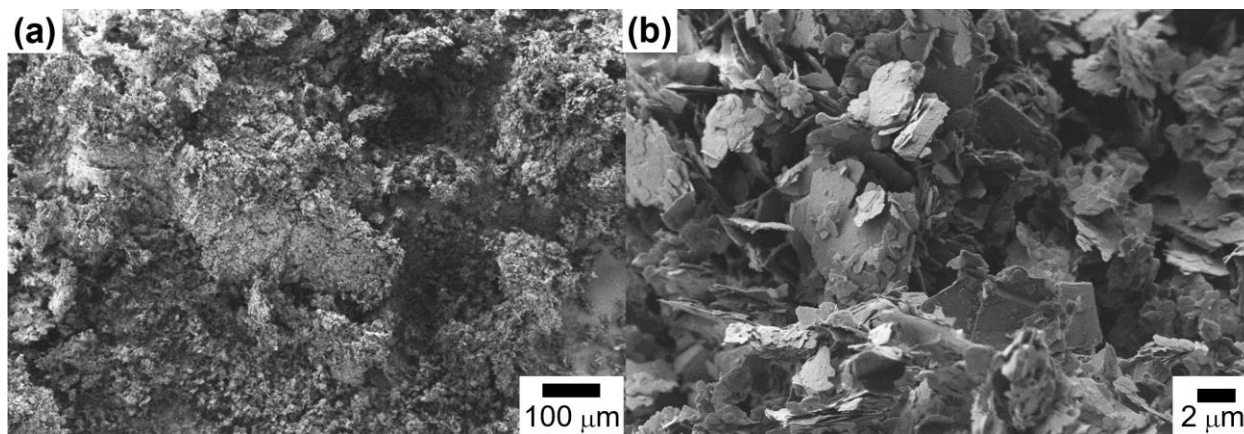


**Figure 4-2.** XRPD patterns for hBN support, Pt catalysts right after calcination (Pt/hBN850) and after overnight exposure to a water saturated atmosphere (Pt/hBN850\*). (Inset: Same catalysts after removing the boric acid).

Morphological analysis of the samples was performed by Scanning Electron Microscopy **Figure 4-3a** is a general view of the material. Due to the layered structure of hBN, most of the particles are thinner along the [002] direction. The thickness of the particles is between 50 nm and 1 μm, as shown in **Figure 4-3b**.

## Catalytic activity

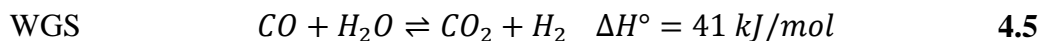
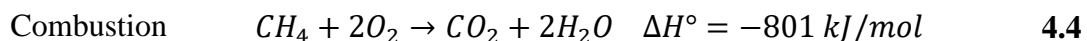
The activity of various Pt/hBN materials was tested for POM. As a comparison, 1% Pt/Al<sub>2</sub>O<sub>3</sub> from Alfa Aesar was also tested under the same conditions. **Figure 4-4** shows the turnover frequency (TOF=molar flowrate/active sites, the active sites were calculated using the dispersion determined by oxygen chemisorption and the catalyst loading. For the products, the molar flowrate is the flow rate out of the reactor, for methane, the flowrate is the consumed methane) results for the Pt/Al<sub>2</sub>O<sub>3</sub> reference and Pt on thermal treated hBN at 850 °C for 6 h (Pt/hBN850). The Pt dispersion determined by O<sub>2</sub> pulse chemisorption was 22 % for Pt/Al<sub>2</sub>O<sub>3</sub> and 16 % for Pt/hBN850. As shown in **Figure 4-4a**, methane TOF is on average 60% higher for Pt/hBN850: at 700 °C the difference is the highest with a 73% higher TOF for Pt/hBN850.



**Figure 4-3.** SEM for Pt/hBN catalyst. **a:** General view; **b:** detailed view

The CO and H<sub>2</sub> production are shown in **Figure 4-4b** and **Figure 4-4c**. The CO selectivity is 90% for Pt/Al<sub>2</sub>O<sub>3</sub> and 87% for Pt/hBN850 at 700 °C. The expected H<sub>2</sub>/CO ratio for POM is ≈2 (Eq. 4.3). At all temperatures, the production of H<sub>2</sub> is favored by Pt/Al<sub>2</sub>O<sub>3</sub> keeping the ratio higher than 2, especially at low temperatures (**Figure 4-4d**). For Pt/hBN850 the ratio is 1.8 at 500 °C and

$\approx 2.1$  after 700 °C. At low temperatures there is a lot CO<sub>2</sub> being produced,  $\approx 60\%$  CO<sub>2</sub> selectivity at 500 °C and  $\approx 25\%$  at 600 °C for both materials. It is generally believed that POM does not take place directly through Eq. 4.3, but through a first complete combustion step (Eq. 4.4) and steam (Eq. 4.1) and dry (Eq. 4.2) reforming. The water-gas shift reaction is also involved<sup>48–52</sup>. At reaction temperatures below 700 °C the H<sub>2</sub>/CO ratio is higher than that above 700 °C for Pt/Al<sub>2</sub>O<sub>3</sub> (**Figure 4-4d**), similar to previous results obtained by other researchers<sup>48</sup>. But for Pt/hBN850 the opposite is true. This is a clear indication that the hBN support is changing the Pt activity to favor the reactions producing more CO and less H<sub>2</sub> by, for example, pushing the water gas shift (WGS, Eq. 4.5) reaction towards the production of CO or favoring the DRM reaction (Eq. 4.2). The weaker Pt-hBN interaction plays a key role in this behavior. The Pt activity is increased by a higher Pt reducibility on hBN compared to Al<sub>2</sub>O<sub>3</sub><sup>54,55</sup>. This is in keeping with past studies that demonstrated that reduced sites are required when Ni is used for POM<sup>56,57</sup> and for Pt when used for hydrocarbon oxidation<sup>58,59</sup>. The hydrophobicity of the hBN support, opposed to the widely used hydrophilic oxide supports, could also be a key factor affecting the Pt activity towards a higher CO production<sup>60</sup>. This was confirmed in a separated experiment where we used Pt1%/Al<sub>2</sub>O<sub>3</sub> and Pt1%/hBN850 to catalyze the SRM reaction (**Figure 4-5**). Even though the Pt/hBN catalysts was more active for the POM reaction than the Pt/Al<sub>2</sub>O<sub>3</sub> catalyst, for the SRM reaction the most active catalyst was Pt/Al<sub>2</sub>O<sub>3</sub> (in terms of methane consumption and hydrogen production). Probably the water dissociation step during the SRM reaction<sup>88–90</sup> was slowed down by the hBN hydrophobicity, causing the lower activity.



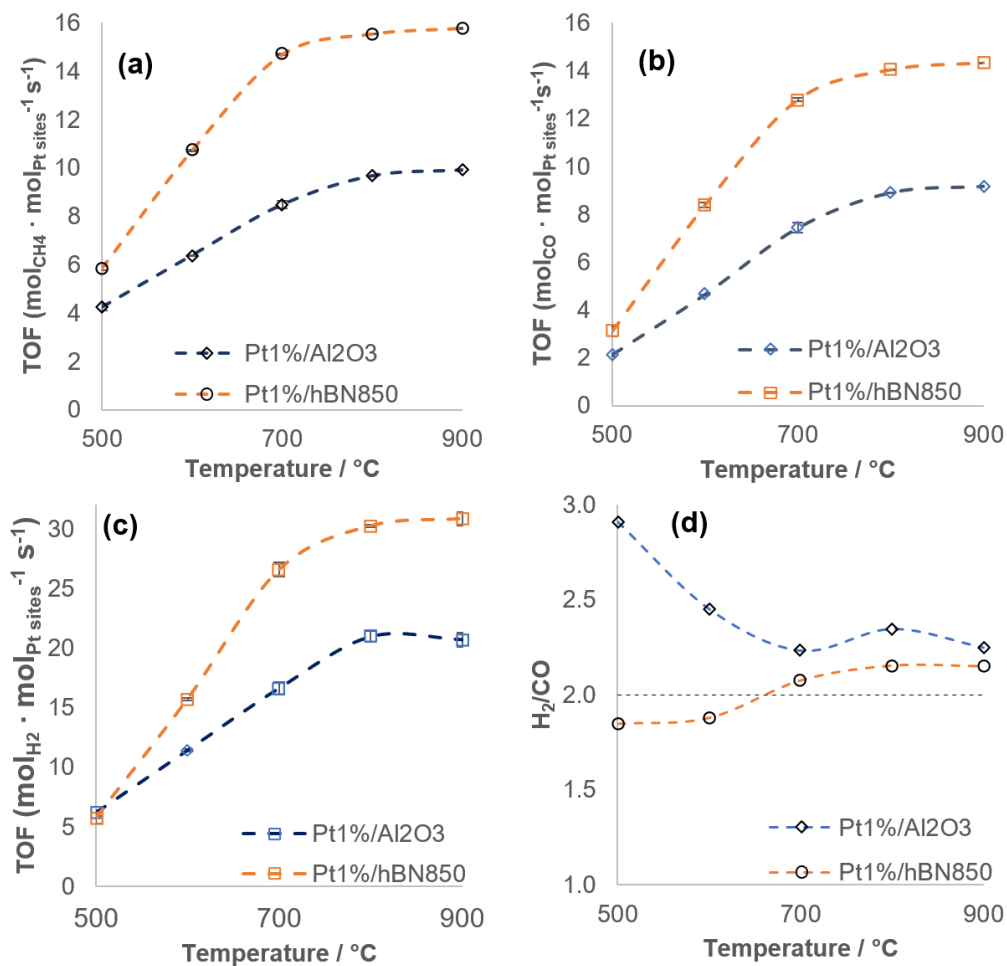


**Figure 4-4.** Methane TOF for Pt deposited on hBN treated at 850 °C with humid air for 6 h (Pt/hBN850) and Pt/Al<sub>2</sub>O<sub>3</sub>. (a) Methane consumption. (b) CO production. (c) H<sub>2</sub> production. (d) H<sub>2</sub>/CO ratio.

In a search for a higher Pt dispersion a sonochemical wetness impregnation method (SWI)<sup>91–93</sup> was used. But, when using thermal treated samples with SWI the conversion for those catalysts was significantly lower (

**Figure 4-6a**). The sonication of hBN in water have shown to cause its hydrolysis. An oxygen atom from water attacks a B-N bond near to a defect site and propagates from there<sup>63</sup>. The binding energies of Pt clusters on hBN defects, such as B or N monovacancies or BN divacancies, are 4 –

5 times higher than those in the defect free surface of hBN<sup>94</sup>. We first thought this to be the cause for the lower activity of the materials produced by the sonochemical method: more defects will produce stronger Pt-hBN interactions, lowering the catalytic activity. But sonication itself does not cause our catalysts to be less active, as noted in

**Figure 4-6b.** Lower activities are the result of having boric acid and the Pt precursor together during the sonication stage in the sonochemical method.

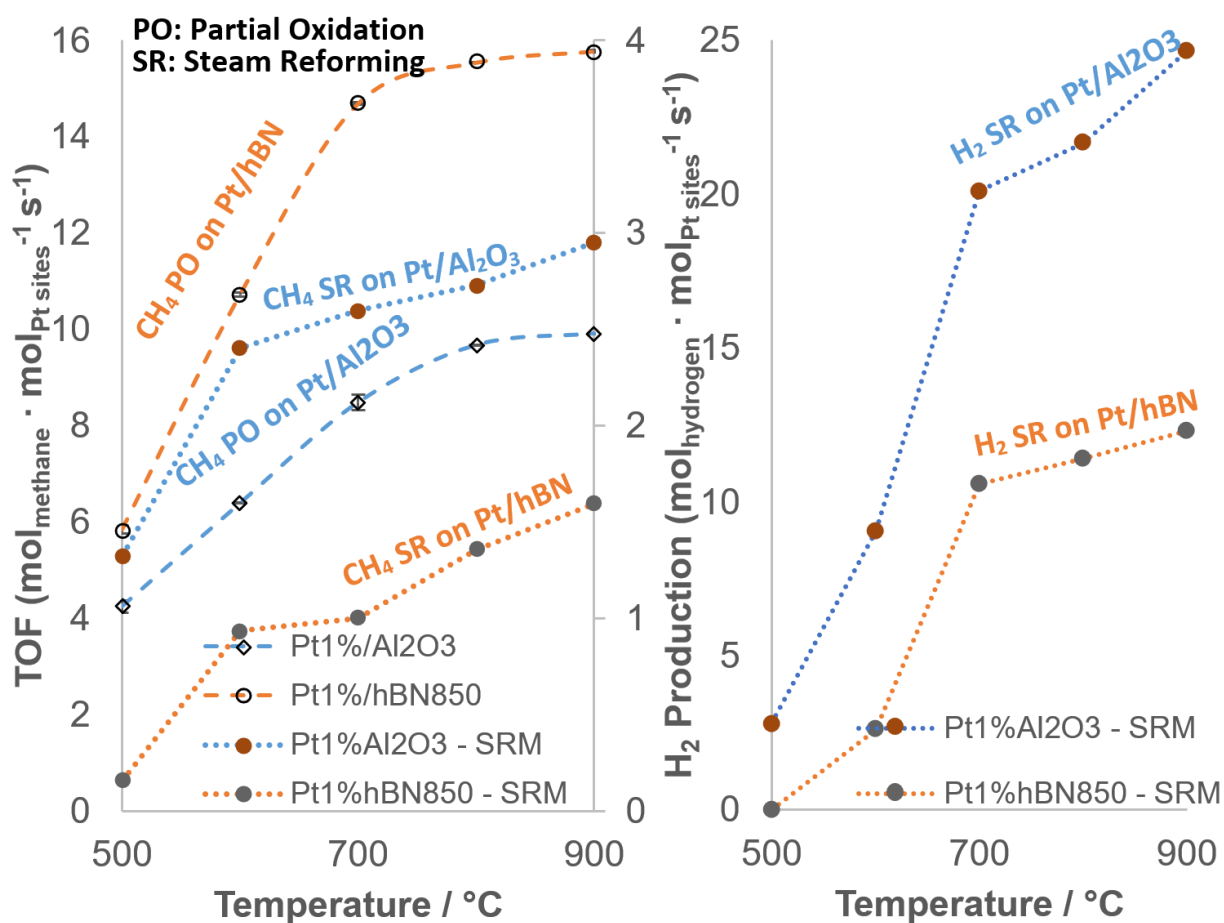


**Figure 4-5.** TOF and H<sub>2</sub> production on Pt/Al<sub>2</sub>O<sub>3</sub> and Pt/hBN850 for the steam reforming of methane reaction compared to the partial oxidation of methane reaction.

When using untreated hBN to synthesize Pt/hBN catalysts, WI and SWI produced catalysts with similar activity (

**Figure 4-6b**). This lower activity for sonicated samples was the result for every thermal treatment we tried. The cause of this phenomenon remains undetermined but the key factor affecting the sonicated samples is the remaining boric acid on the samples after the thermal treatment.

The role of boric acid in the catalyst behavior was further investigated. We developed a method to remove the boric acid present in the thermal treated samples by heating them at 600 °C for 24 h with flowing humid air. When the boric acid is removed after the thermal treatment and before the catalyst synthesis (Pt2%/850-P in

**Figure 4-6c**) the conversion is lower. From this, we conclude that when boric acid is added to the support before the catalyst synthesis, it plays an active role in the catalytic activity of Pt/hBN<sup>36</sup>. A similar effect was reported before for Pt/Al<sub>2</sub>O<sub>3</sub>. When boric acid was added to the catalyst before Pt the activity increased, when boric acid was added after the Pt (after the catalyst synthesis), the activity decreased<sup>95</sup>.

**Figure 4-6d** is a summary of the activity of Pt catalysts as a function of the temperature of the thermal treatment. A temperature of 850 °C for 6 h improve the catalyst activity compared with untreated hBN, but a 650 °C treatment for a 60 h results in a less active catalyst. Additional details related to the role of boric acid in the catalytic activity of Pt was discovered by removing boric acid after the catalyst synthesis using humid air at 600 °C for 24 h. By doing this the conversion increased respect to the same sample without boric acid removal (**Figure 4-7a**). This shows that the presence of free boric acid (boric acid that can be removed by the thermal treatment with humid

air) is detrimental for Pt activity, but the boric acid taking part in the Pt/hBN structure (Pt on a borated hBN surface<sup>36</sup>), increases the catalytic activity. It is not the boric acid itself interacting with Pt that increase the activity, but the Pt deposited on a borated hBN surface<sup>95</sup>.

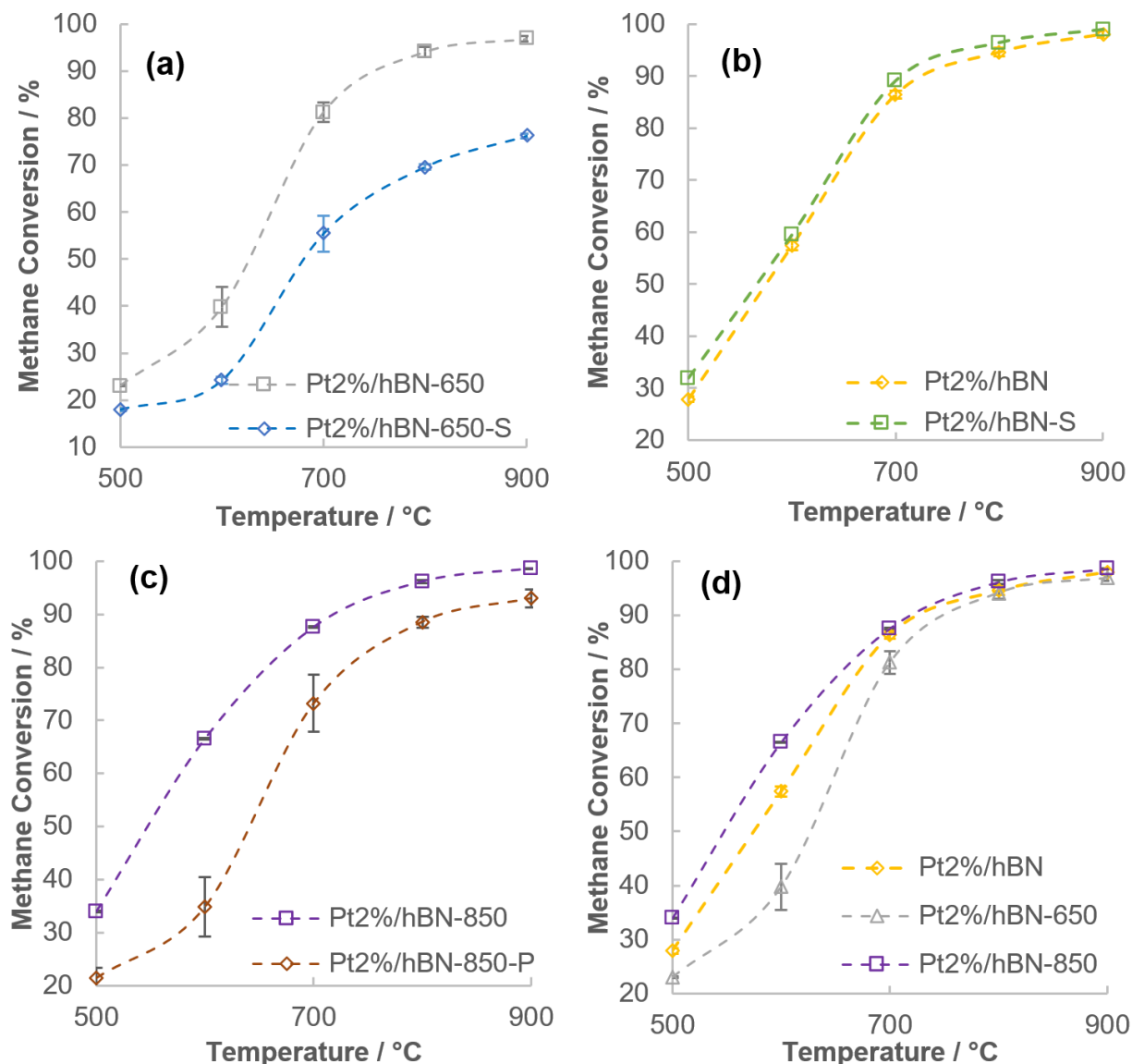


**Figure 4-6.** Methane conversion on Pt catalysts for: **a.** Pt on thermally treated hBN at 650 °C for 60 h with humid air (Pt2%hBN-650: WI, Pt2%hBN-650-S: SWI); **b.** Pt on untreated hBN (Pt/hBN: WI, Pt/hBN-S: SWI); **c.** Pt on thermally treated hBN at 850 °C for 6 h with WI without boric acid



removal (Pt2%/hBN-850) and with boric acid removal after the thermal treatment (Pt/hBN-850-P). **d.** Comparison of treatments.

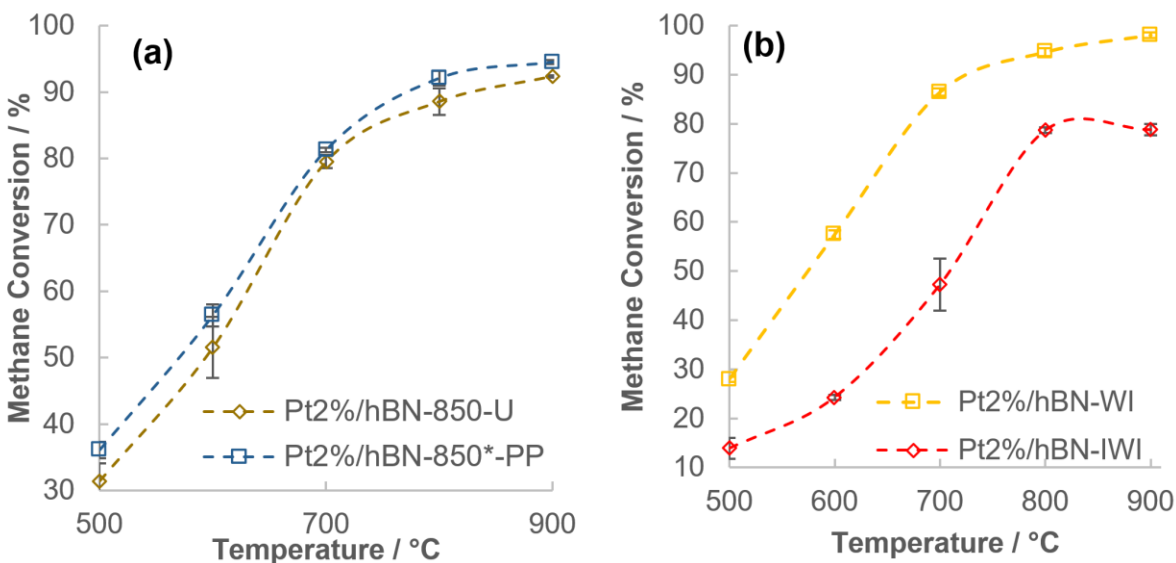


**Figure 4-7.** Methane conversion on Pt catalysts for Pt on untreated hBN and hBN treated at 850 °C with humid air for 6 h. **a:** Sample used after calcination without purification (Pt2%/hBN-850-U) and with boric acid removal after the catalyst synthesis (Pt2%/hBN-850-); **b:** Pt on untreated hBN using wetness impregnation with water (Pt2%/hBN-WI) and incipient wetness impregnation with methanol (Pt2%/hBN-IWI).

For all the Pt/hBN samples, wetness impregnation with water as a solvent was preferred to synthesize the catalysts because using incipient wetness impregnation with methanol produced poor catalysts (**Figure 4-7b**) due to the aggregation of Pt particles on the surface of hBN caused by the absence of mesoporosity. Other studies found that the dispersion of some metals is better inside the pores<sup>96</sup>.

For a deeper understanding of the role of boric acid we prepared a sample with 10% weight boric acid and 90% untreated hBN. The two compounds were mixed and crushed in a pestle and mortar and heated overnight at 180 °C. After that, the same procedure was followed as before to produce a Pt/hBN catalyst. These samples confirmed that the presence of boric acid during SWI (Pt2%/hBN+B(OH)3-S in **Figure 4-8a**) is causing the catalyst to be less active compared to WI (Pt2%/hBN+B(OH)3 in **Figure 4-8a**). Additionally, those samples had a much lower Pt dispersion ( $\approx 6\%$ ) compared to Pt on a thermal treated hBN (16%).

Finally, we added boric acid (10% weight) to a sample of  $\gamma$ -alumina and synthesized a Pt catalyst by IWI. The Pt/Al<sub>2</sub>O<sub>3</sub>+B(OH)<sub>3</sub> catalyst showed a higher conversion (**Figure 4-8b**), in agreement with previous results<sup>36,95</sup>. This confirms the active role of the Pt-support bond in the catalytic activity of Pt.

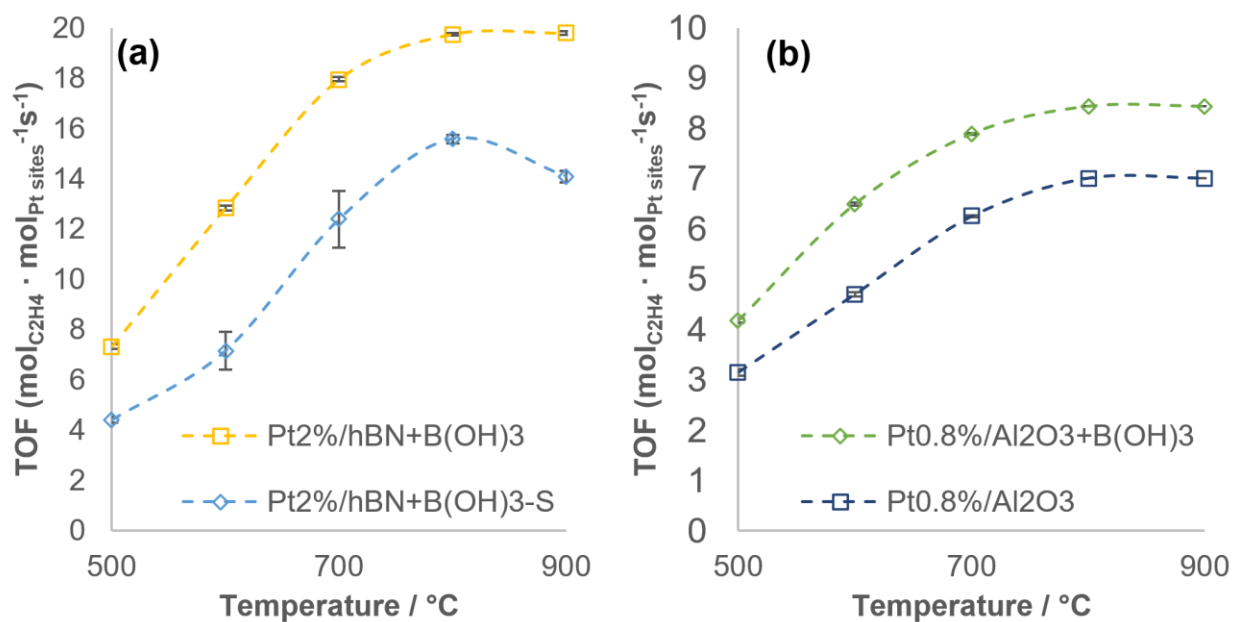


**Figure 4-8.** TOF for POM on Pt catalysts prepared with boric acid doped hBN (a) and Al<sub>2</sub>O<sub>3</sub> (b).

## Conclusions

Highly active catalysts for partial oxidation of methane (POM) can be produced using hBN to support Pt. The higher activity of this catalyst, compared to Pt/Al<sub>2</sub>O<sub>3</sub>, relies on the weaker Pt-support interaction, which increase the Pt reducibility. This higher reducibility also affects the variation of the H<sub>2</sub>/CO ratio with temperature. The hBN supported Pt produces a stream with a H<sub>2</sub>/CO ratio that is relatively constant ( $\approx 2$ ) with temperature, probably due to alterations in the POM pathway: complete combustion followed by steam and dry reforming.

Thermal treating hBN at 850 °C with humid air before the Pt impregnation generates even more active catalysts. When hBN is thermal treated, boric acid is formed. During the catalysts synthesis this boric acid forms a borated surface and Pt is deposited on it, creating an even weaker interaction with the support (Pt/Borated hBN). This result cannot be completely reproduced by adding boric acid to hBN and then using it to synthesize the catalyst, even though the catalysts created this way are more active than those produced only with hBN because the Pt dispersion is much lower (around a third) compared with the thermal treated hBN.

Boric acid itself is detrimental for Pt activity. Borated hBN increases the activity of Pt, but if there is “free” boric acid after the catalyst synthesis, it lowers the activity. This was determined by removing the “free” boric acid after the catalyst synthesis using a purification step with humid air at 600 °C.

## Chapter 5 - Details on hBN activity for ethane oxidative dehydrogenation

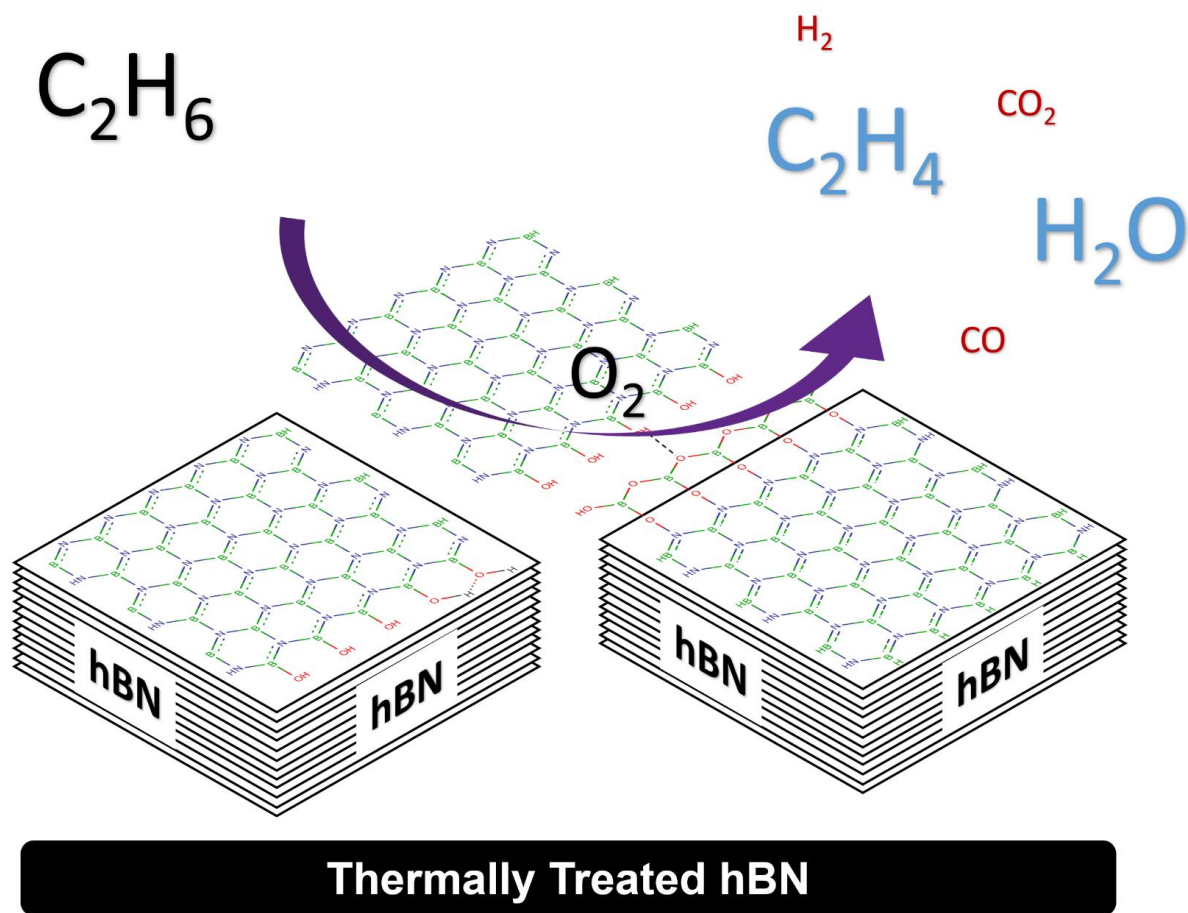


**Figure 5-1.** Oxidative dehydrogenation (ODH) of ethane on thermally treated hBN.

The market for olefins, especially propylene and ethylene, is growing<sup>5</sup>. The global ethylene market, for example, was valued at USD 146.3 billion in 2019 and the demand for these building block chemicals is expected to continue in the near future<sup>6,7</sup>. The production of olefins is currently done industrially by cracking and catalytic dehydrogenation<sup>8</sup>, however, these reactions presents several problems such as coke formation and high temperature requirements<sup>9-11</sup>. The main problem

is to activate the C–H bond and, at the same time, using the same conditions, prevent further oxidation to  $\text{CO}_x$ <sup>12</sup>. Oxidative dehydrogenation (ODH) is an alternative to the traditional olefin production methods. ODH is exothermic, which is an advantage over endothermic dehydrogenation<sup>13,14</sup>.

Recently a completely new metal-free catalyst was reported as active for ODH reactions. Hexagonal boron nitride (hBN) is chemically inert, but it shows surprisingly high selectivity for the production of alkenes by the ODH reaction<sup>24</sup>. An ethylene selectivity of 95% at a 11% ethane conversion<sup>25</sup> or a propylene selectivity of 79% with a 12% propane conversion<sup>26</sup> have been reported, as well as other advantages such as a more uniform temperature profile in a fixed bed reactor compared with  $\gamma\text{-Al}_2\text{O}_3$ , for example<sup>27</sup>.

### **hBN active sites**

The high selectivity of hBN to produce olefins by the ODH reaction could be explained by a reaction mechanism where O–O attached to the armchair side of the h-BN is the active site (BOON). The alkane is absorbed in BOON site of h-BN. One of the hydrogens is subtracted by the active site, breaking the O–O bond and forming a BOH species. The alkane forms a bond with the other oxygen to give  $\text{NOCH}-(\text{CH}_3)_n$  species. The stability of the  $\text{NOCH}-(\text{CH}_3)_n$  intermediate could be the reason for the high selectivity compared, for example, with the metal oxide catalysts where the  $\text{C}_n\text{H}_{2n+1}$  intermediate is not stable<sup>26</sup>. Finally, the product desorbs and the catalyst is regenerated by oxygen<sup>25,28</sup>.

The previous mechanism is based on the BOON active sites, which are formed in the armchair edge in hBN. However, the most frequently exposed edges in h-BN are zig-zag terminations<sup>29,30</sup>. If this is the case, an alternative mechanism should be proposed to explain the

catalytic activity of hBN. An option is to allocate the active sites in the zig-zag B edge. If that edge is hydroxylated (BOH) it could be activated with oxygen to form BOOB and water, then the BOOB site will activate the C–H bond to produce  $\text{BCH}_2\text{CH}_3$  (if ethane is being reacted) and BOH. If there is oxygen present the formation of water and ethene is the next step. If oxygen is not present, hydrogen and ethylene will be the products<sup>31</sup>. A third alternative is a modified zig-zag B edge in h-BN with BOB and BOH groups. In this case the active site is a BOOB site in a zig-zag BOB edge<sup>29</sup>. Even nitrogen mono vacancies have been suggested as active sites for propane ODH<sup>97</sup>.

There is also evidence suggesting that a  $\text{BO}_x$  layer formed over boron containing materials (B,  $\text{B}_4\text{C}$ ,  $\text{TiB}_2$ ,  $\text{NiB}$ ...) during ODH contains the active sites for this reaction<sup>73</sup>. Some borated supports such as  $\text{B}_2\text{O}_3/\text{Al}_2\text{O}_3$  are selective for oxidation of alkanes<sup>35,37,38</sup>, as well as boron oxides on silica<sup>98</sup>. The active role of boron oxides in the catalysis field was also proved using a metallic catalyst ( $\text{Re}_2\text{O}_7$ ) deposited on  $\text{B}_2\text{O}_3/\text{Al}_2\text{O}_3$ , the catalytic activity of the catalyst was improved by reducing the strength of the Metal-Support bond<sup>36</sup>. All these details, even though they are not directly related to alkanes ODH, are valuable inputs due to the lack of more information related to the catalytic nature of hBN.

The understanding of the active sites and reaction mechanisms for ODH is a key factor in the design of new catalysts. Despite the lack of information about the exact mechanism and the nature of the active sites for hBN catalytic activity, there is agreement about the role of oxygen in the activation of hBN. Moreover, the active sites, once formed, appear to be structurally stable, they are not destroyed or changed irreversibly during the reaction<sup>25,99</sup>.

The aim of this work was the study of different hBN materials for the oxidative dehydrogenation of ethane. We wanted to show that there are different active sites on hBN catalyzing the ODH of ethane reaction. We focused our attention on the catalytic activity of those

materials, how that activity change as a function of the thermal treatments and how the catalysts behave along time. With that, we described the catalytic activity as a function of the active sites generated with the different treatments with the goal of discovering new details related with the active sites present on hBN.

## Experimental Section

### Reagents

Hexagonal boron nitride was supplied by Alfa Aesar as a 325-mesh powder 99.5% purity. All reagents were used as supplied for all the thermal treatments.

### Thermal treatments

Thermal treatments took place in a Lindberg Blue M tubular furnace. For the humid air treatments, a water bubbler with a diffuser was used to saturate the air stream before the furnace inlet. hBN850 was treated at 850 °C with humid air for 3 h and then purified with humid air for 24 h at 600 °C. hBNO was produced using humid air at 850 °C for 3 h, dry air at 850 °C for 2 h and dry air at 600 °C for 5 h, after the thermal treatments hBNO was suspended in deionized water (100 mL of water/g), sonicated for 4 h and centrifuged at 1000 rpm for 30 min. After the centrifugation the liquid phase was dried at 110 °C overnight and thermally purified using humid air at 600 °C in the furnace for 24 h (see details in **Figure 5-2**). For the reactions with hBN and hBN\* the materials were used without any treatment. The difference between hBN and hBN\* is that hBN\* is heated up in the reactor with a N<sub>2</sub> stream, this prevents its activation. hBN is heated up in the presence of O<sub>2</sub>/N<sub>2</sub>/C<sub>2</sub>H<sub>6</sub> and it is activated during the heating period.

## Characterization

Fourier-transform infrared (FTIR) spectra were collected using a Cary 630 FTIR operating in ATR mode. The purpose of the FTIR was to reveal the active sites present on the hBN materials at each stage of the experiments (before and after treatment and before and after the reaction).

X-ray powder diffraction (XRPD) patterns were collected with a Rigaku MiniFlex II at 30 kV, 15 mA and  $10^\circ < 2\theta < 60^\circ$  with a copper source and a wavelength of 1.54 Å. The XRPD patterns were used to evaluate the crystal structure of the materials and the presence of boric acid by the RIR method.

Prior to the measurements for the FTIR spectra and XRD patterns, the samples were dehydrated overnight at 110 °C in an oven. For both techniques all the samples were crushed with a pestle and mortar before each measurement.

Scanning Electron Microscopy was performed with a SEM-FID ZEISS Crossbeam 340 equipped with energy dispersive X-ray spectroscopy microprobe EDS Oxford Aztec, Silicon drift 80 mm<sup>2</sup>.

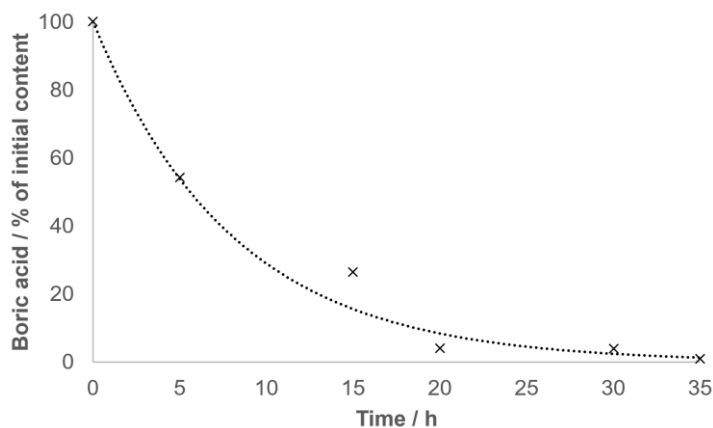


**Figure 5-2.** Percent of remaining initial boric acid content determined using the reference intensity ratio (RIR) method with the XRD patterns during post treatment with humid air at 600 °C. The initial sample was a thermally treated hBN sample.



## Catalytic activity

The catalytic activity was evaluated in a quartz tubular reactor (internal diameter = 12 mm) with a continuous flow operating at atmospheric pressure. The catalyst was packed into the reactor between quartz wool. The reactor tube was encased in an electrically heated tube furnace with a PID temperature controller connected to a coaxial thermocouple. The reactor effluent gases were analyzed by an on-line gas chromatograph (SRI 8610C GC) equipped with a silica gel column connected in series with a Molsieve MS13x 6 column and two detectors, TCD and FID with methanizer. For all reactions, except for those with hBN\*, the reactor was heated from room temperature with a stream of N<sub>2</sub>/O<sub>2</sub>/C<sub>2</sub>H<sub>6</sub> (60:20:20). For hBN\* the reactor was heated with a stream of 100% N<sub>2</sub>, and once the reaction temperature was reached, O<sub>2</sub> and C<sub>2</sub>H<sub>6</sub>, were added to the stream.

## Result and discussion

### Characterization

The morphology of the materials was evaluated using SEM images (**Figure 5-3** a-c). **Figure 5-3a** shows untreated hBN, which is the starting material. Due to the layered structure of hBN, most of the particles are thinner along the [002] direction. **Figure 5-3b** is hBNO before the 24 h purification. There is a material deposited on the surface of this sample. We attribute this to boron oxide species formed during the thermal treatment. After the purification step (with humid air at 600 °C for 24 h) the boron oxide compounds were removed from the surface of hBNO and the morphology was revealed to be similar to hBN (**Figure 5-3c**)

According with the XRD patterns the crystalline structure of hBN (PDF No: 01-085-1068) was preserved after the thermal treatments (**Figure 5-3d**). A left shift in the hBN 002 plane for hBNO suggests that the hBNO surface is oxidized, causing an increase in the crystal plane spacing.

FTIR spectroscopy for all samples is shown in **Figure 5-4**. The peak at  $\approx 3200\text{ cm}^{-1}$  is assigned to boric acid formation or concerted hydroxyl groups<sup>80</sup>. The peak at  $1190\text{ cm}^{-1}$  is assigned to B-N-O vibration<sup>75-78</sup>. **Figure 5-4a** shows hBNO before (hBNO) and after (hBNO-P) purification with humid air. These samples are also shown in **Figure 5-3b** and **Figure 5-3c**. Contrary to the SEM images, the FTIR spectroscopy is not showing a significant difference between these two samples. We interpret that the boron compounds present in **Figure 5-3b**, and removed by the thermal purification (**Figure 5-3c**) are not contributing significantly to the FTIR spectra. Thus, the peaks shown in figure **Figure 5-4** are a representation of the structure of hBNO.

Spent hBNO, however, has weaker peaks at  $1190\text{ cm}^{-1}$ . The longer the reaction period the weaker the peak. This is coherent with the results shown in **Figure 5-11**, the deactivation of hBNO over time is explained by a change in its structure, characterized especially by the  $1190\text{ cm}^{-1}$  peak, with a more pronounced reduction than the  $3200\text{ cm}^{-1}$  peak compared with the hBN characteristic peak at  $3160\text{ cm}^{-1}$ .

On the other hand, the  $3190\text{ cm}^{-1}$  peak is not present in hBN after 6 h of reaction (**Figure 5-4b**) but it appeared after the 50 h stability test. In this case hBN is also being deactivated over time (**Figure 5-11**), but both peaks ( $\approx 3200\text{ cm}^{-1}$  and  $1190\text{ cm}^{-1}$ ) are more intense in spent hBN, a result completely opposite to the one obtained with hBNO. The activity evidence shown in selectivity profile (**Figure 5-12**) confirms that the deactivation of both materials is different, as well as its initial activity (hBNO is more active). The differences between spent hBN and hBNO after 50 h or reaction are more evident in **Figure 5-4d**, the FTIR spectrum for spent hBN is similar

to hBNO before the reaction, but its activity is much lower (**Figure 5-11**). Finally, hBN850 (**Figure 5-4c**) thermally treated for 3h (hBN860(3h)) or 6h (hBN850(6h)) does not show the 1190  $\text{cm}^{-1}$  peak, neither before or after 6 h of reaction. The only difference between hBN850 and spent hBN850 is a more intense 3200  $\text{cm}^{-1}$  peak of the latter.

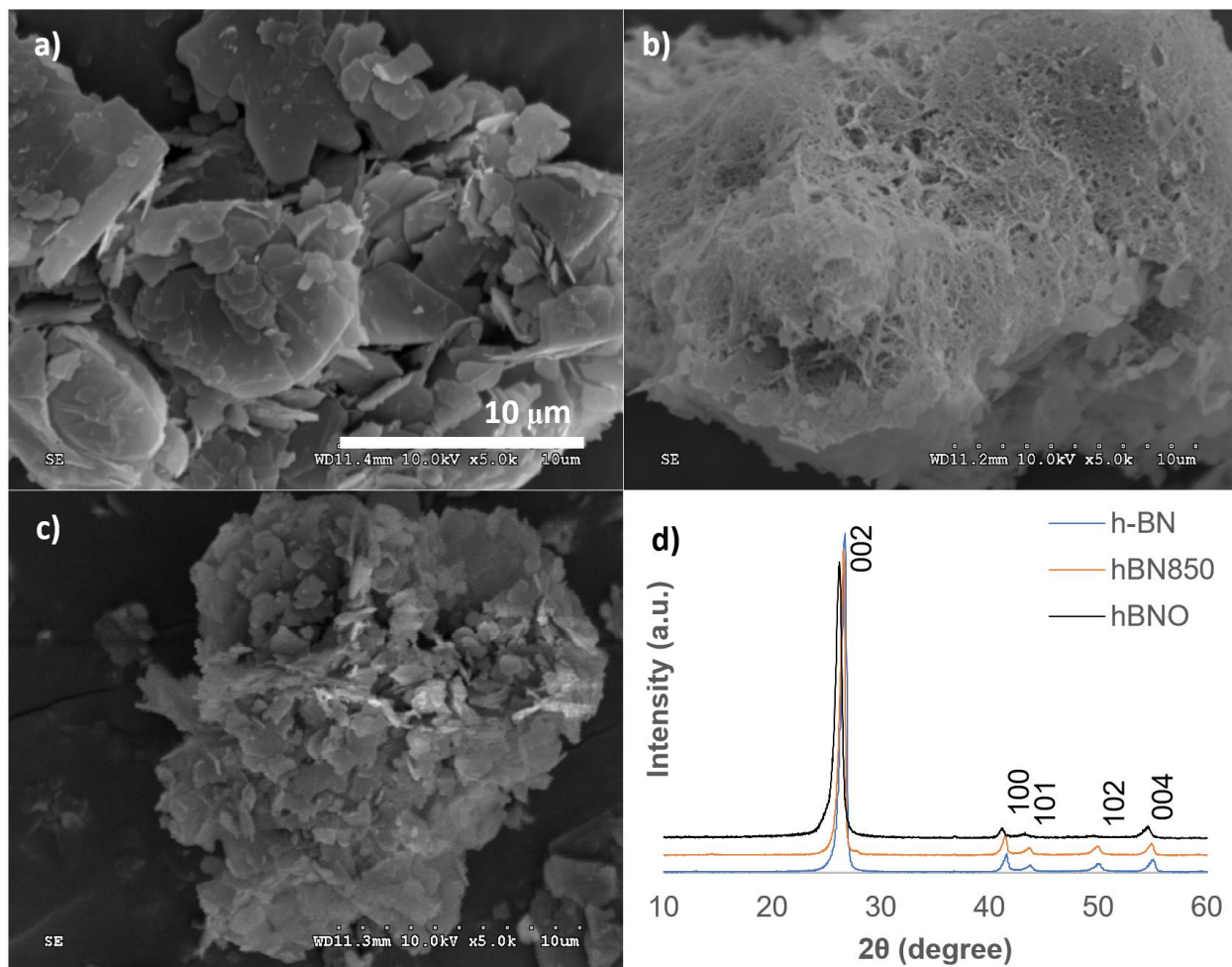


**Figure 5-3.** SEM images for untreated hBN (a), thermally treated hBN sonicated and centrifuged: hBNO (b) and thermally purified hBNO (hBNO-P) (c). (d) shows the XRD patterns for the hBN materials.

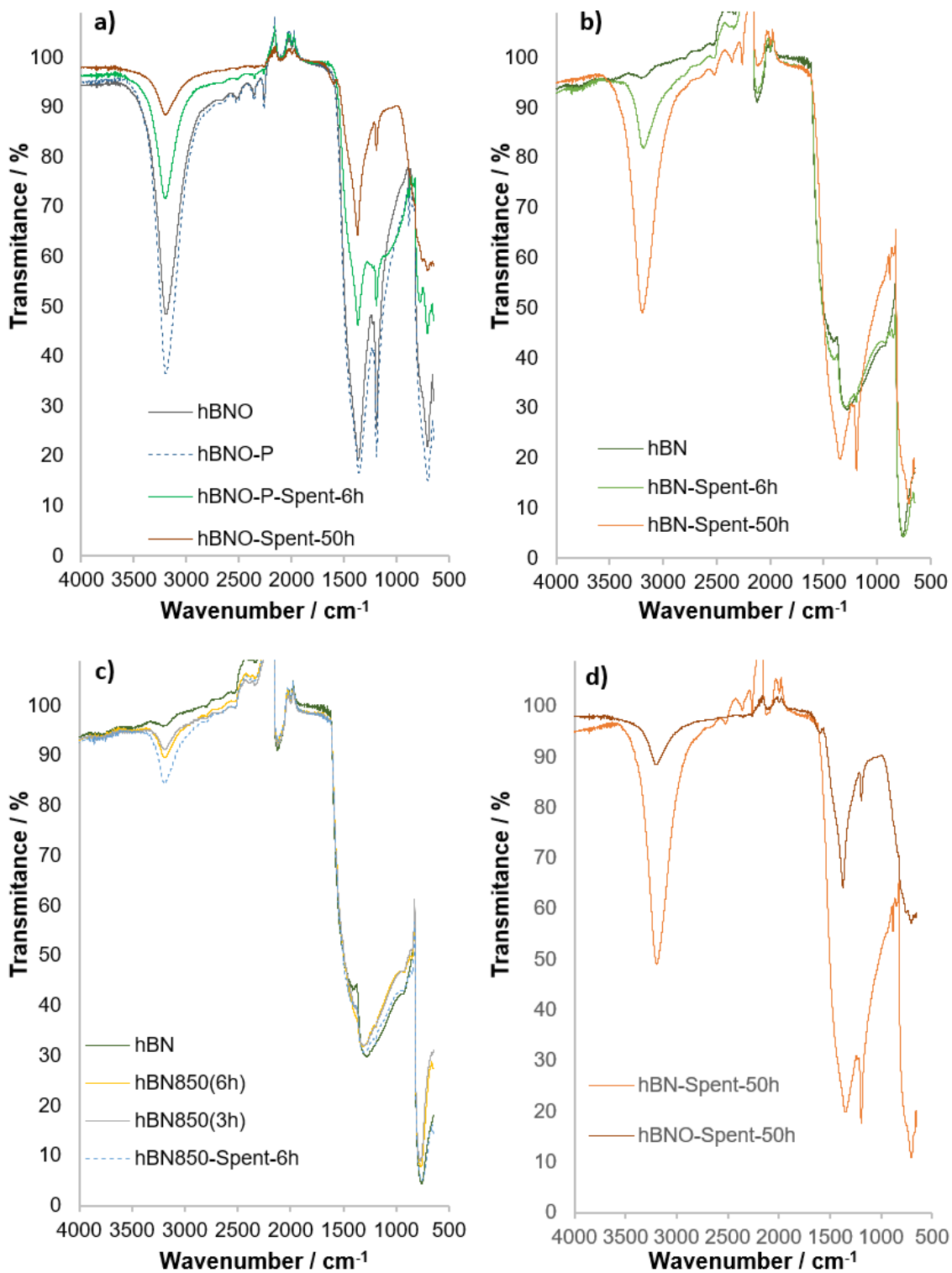


**Figure 5-4.** FTIR for; a) hBNO, b) hBN, c) hBN850 and d) spent hBN and hBNO after a 50 h stability test.

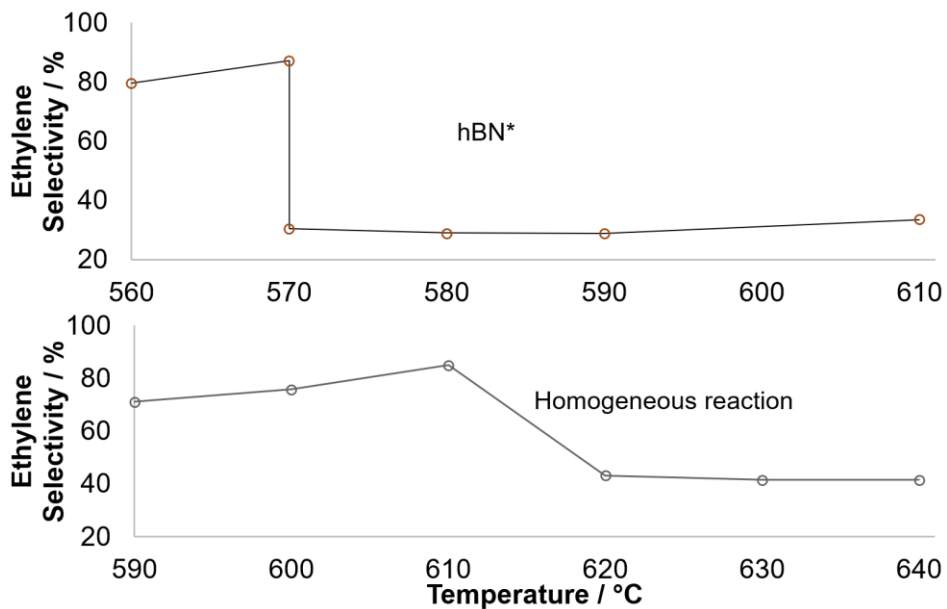


**Figure 5-5.** Ethylene selectivity for the ODH of ethane on hBN\* and the homogeneous reaction. The two different selectivity values at 570 °C for hBN\* are the result of hBN\* activation once a temperature lower than 570 °C is set.

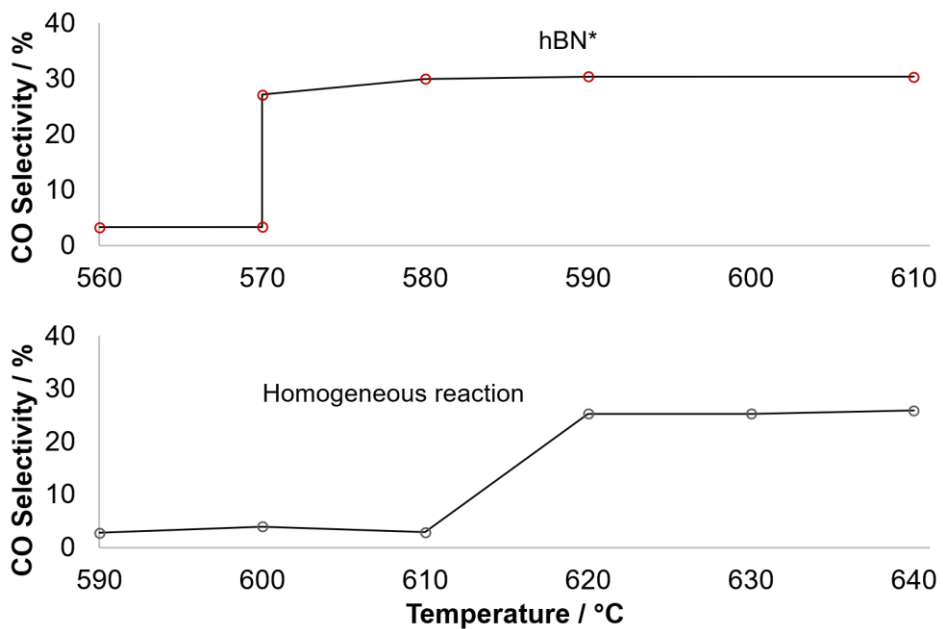


**Figure 5-6.** CO selectivity for the ODH of ethane on hBN\* and the homogeneous reaction

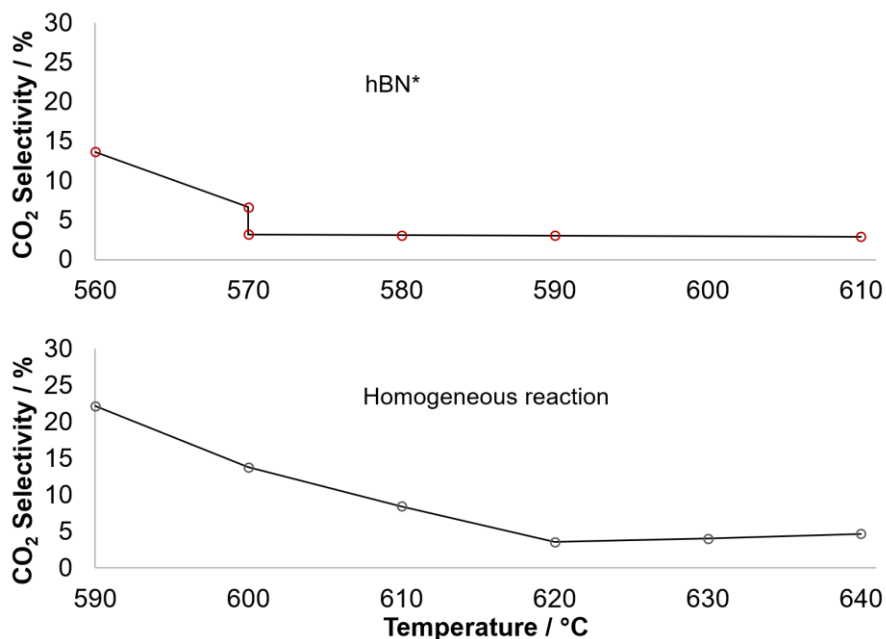


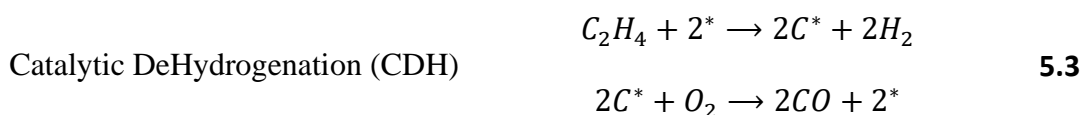
**Figure 5-7.** CO<sub>2</sub> selectivity for the ODH of ethane on hBN\* and the homogeneous reaction.

### Catalytic activity for ODH

The catalytic activity for pristine hBN, thermally treated hBN (hBN850) and thermally treated, sonicated and centrifuged hBN (hBNO) was evaluated for the oxidative dehydrogenation (ODH) of ethane with a N<sub>2</sub>:O<sub>2</sub>:C<sub>2</sub>H<sub>6</sub> ratio of 60:20:20.

We first heated up pristine hBN under N<sub>2</sub> to prevent its activation by O<sub>2</sub>/C<sub>2</sub>H<sub>6</sub>. Activation of hBN is crucial for its catalytic activity and non-activated hBN (hBN\*) is catalytically inert<sup>2,29</sup>. After reaching the reaction temperature we change the N<sub>2</sub> stream to N<sub>2</sub>/O<sub>2</sub>/C<sub>2</sub>H<sub>6</sub>. We expected hBN\* to behave similar to the homogeneous reaction (Reaction 5.2)<sup>100</sup> and then, after an induction period, to reach the same behavior shown by activated hBN. Surprisingly, hBN\* did not activate when the temperature was 570 °C or higher because the O<sub>2</sub> conversion was 100%. Only when the reactor temperature was set at 560 °C or lower did the ODH reaction (Reaction 5.1) become

predominant (hBN\* was activated). On the other hand, the homogeneous reaction (Reaction 5.2)<sup>101</sup> became important at 615 °C, 45 °C higher than the reaction on hBN\*. The selectivity profile confirms that the reaction taking place on hBN\* was the catalytic dehydrogenation of propane (Reaction 5.3) (**Figure 5-5**, **Figure 5-6** and **Figure 5-7**) not the ODH reaction (**Figure 5-8** and **Figure 5-9**). The high hydrogen selectivity shown by hBN\* (**Figure 5-9**) is another indication of catalytic dehydrogenation. If Al<sub>2</sub>O<sub>3</sub> is used instead of hBN\* the result is completely different. The reaction on Al<sub>2</sub>O<sub>3</sub> is similar to the thermal dehydrogenation (Reaction 5.2) without the catalytic effect caused by hBN\*. This means that Al<sub>2</sub>O<sub>3</sub> is certainly inert, but hBN\* promotes the dehydrogenation reaction when O<sub>2</sub>/C<sub>2</sub>H<sub>6</sub> is feed.



The next step was to evaluate the catalytic activity of hBN, hBN850 and hBNO. At temperatures higher than 590 °C the CDH reaction became significant, the ethylene selectivity dropped favoring the production of CO (**Figure 5-8**) and the H<sub>2</sub> selectivity started to grow (**Figure 5-9**). **Figure 5-10** shows the reaction rate (consumed ethane and produced ethylene) and **Figure 5-8** and **Figure 5-9** show the selectivity of the major products as a function of temperature. At temperatures lower than 580 °C there is no significant difference between the activity of hBN and hBN850 in terms of ethane consumed, but the reaction rate for ethane was significantly higher for hBNO (**Figure 5-10**). Produced ethylene is also higher for hBNO below 580 °C (**Figure 5-10**).

even though the ethylene selectivity is lower (**Figure 5-8**) because the lower selectivity is compensated with the higher reaction rate. Moreover, hBNO shows a higher selectivity for CO than hBN and hBN850 (**Figure 5-8**) but a lower selectivity for CO<sub>2</sub> below 580 °C (**Figure 5-9**).

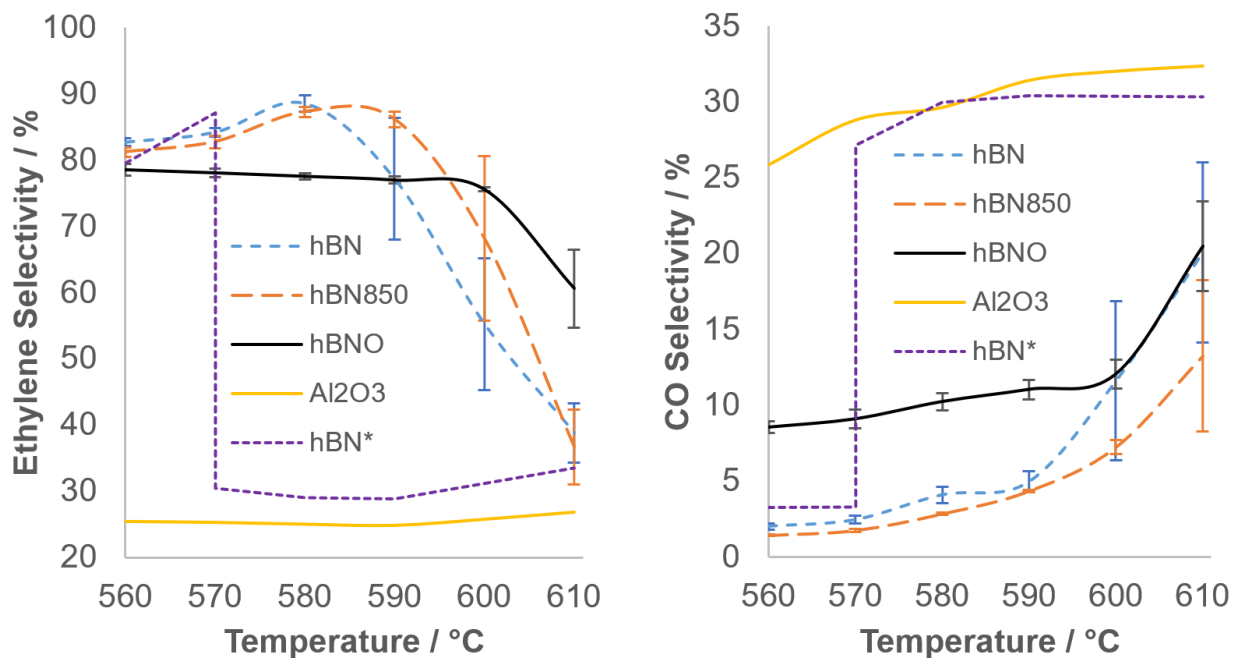


**Figure 5-8.** Ethylene and CO selectivity for the ODH of ethane on hBN materials

Neither hBNO or hBN850 needed activation, even when the samples were heated in a N<sub>2</sub> stream the catalytic activity was the same, in contrast with hBN\*.



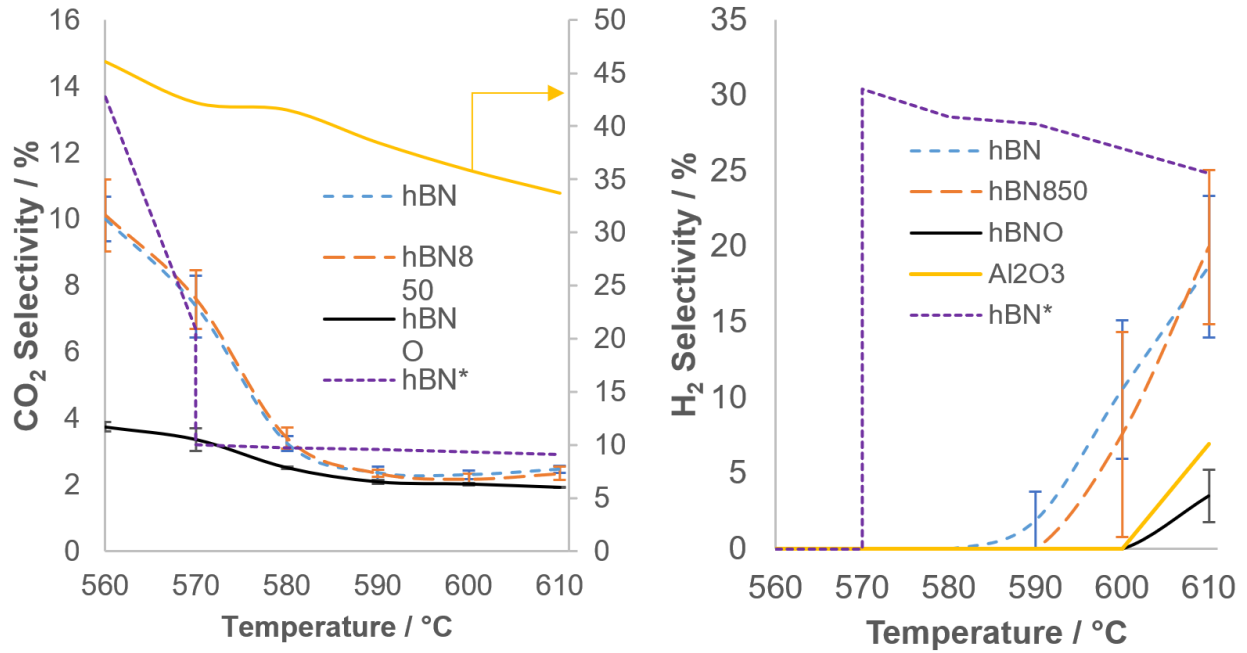


Figure 5-9. CO<sub>2</sub> and H<sub>2</sub> selectivity for the ODH of ethane on hBN materials.

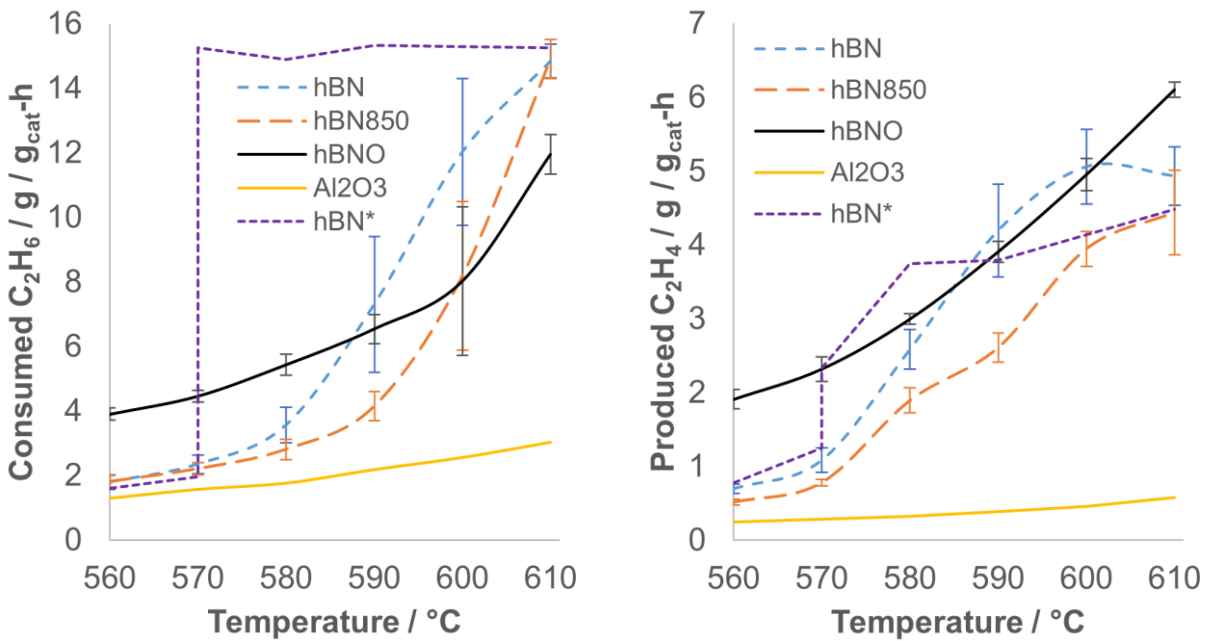


Figure 5-10. Reaction rate for the ODH of ethane on hBN materials.

## Catalyst stability

The stability of hBN and hBNO was tested at 580 °C for 50 h. The evolution of the reaction rate over time is shown in **Figure 5-11**. After 50 h the ethane reaction rate for hBN was reduced by 35%, the ethylene production by 48% and the CO production by 70%. For hBNO the ethane reaction rate dropped 51%, the ethylene production 75% and the CO production 72%.

The selectivity profile (**Figure 5-12**) reveals a clear difference between hBN and hBNO in terms of the evolution of the material over time, especially in terms of CO<sub>2</sub> selectivity. hBNO is showing a pronounced increased CO<sub>2</sub> selectivity compared to hBN. Moreover, there is no production of C<sub>2</sub>H<sub>2</sub> on hBN but there is a small amount produced on hBNO. Additionally, the ethylene selectivity is almost constant for hBN but decreased significantly for hBNO. The CO production rate was stable for hBNO during the first 12 h, meanwhile, for hBN it dropped 30% in the first 4 h (**Figure 5-13**). Other studies have shown deactivation of hBN catalysts in ODH conditions (propene yield from 28% to 8% in 24 h C<sub>3</sub>H<sub>8</sub>/O<sub>2</sub>/He = 1/50/49 at 525 °C, for example)<sup>18</sup>, in those cases the activity was easily recovered. There is also evidence of deactivation when B<sub>2</sub>O<sub>3</sub> was anchored on commercial cordierite and tested for ODH of propane, but not when it was anchored to SiO<sub>2</sub><sup>102</sup>. The authors suggested that commercial cordierite does not have enough M—OH groups for B<sub>2</sub>O<sub>3</sub> to be attached. In our case, the XRD patterns and FTIR evidence suggests that hBNO is a borated hBN. A possible structure for it is presented in **Figure 5-14b**, in contrast with the previously suggested modified N-edge<sup>29</sup> presented in **Figure 5-14a**. A significant fraction of this borated hBN (hBNO) could be attached to non-hydroxylated hBN, causing its loss at reaction conditions.

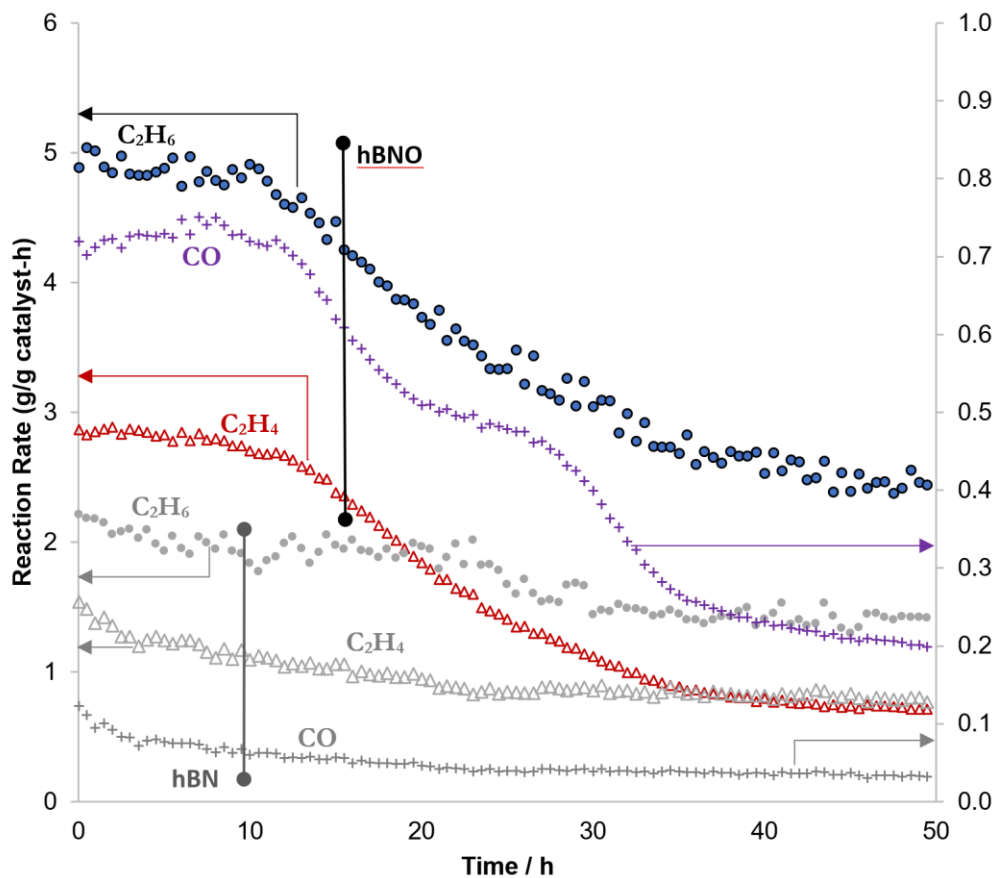


Figure 5-11. Stability test at 580 °C for hBN and hBNO during ethane ODH.

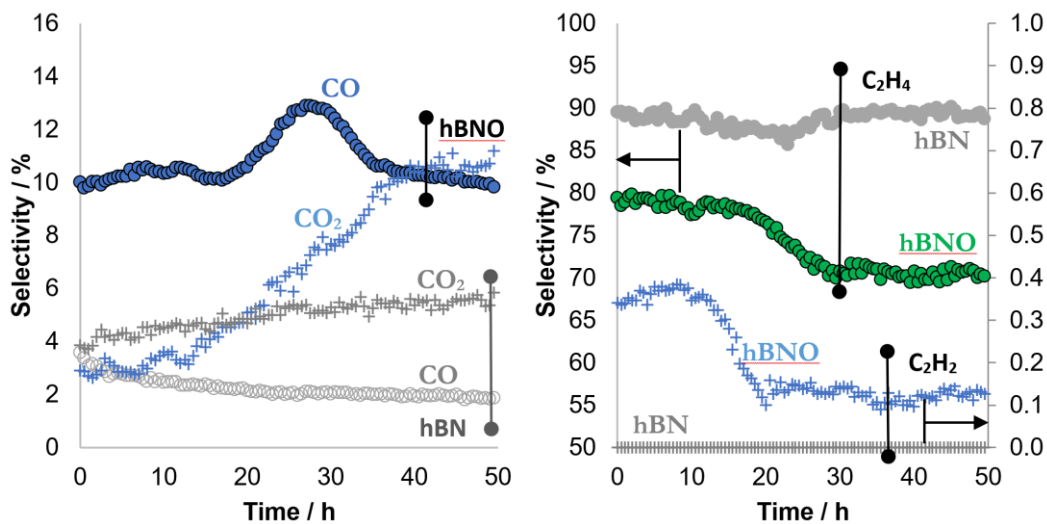
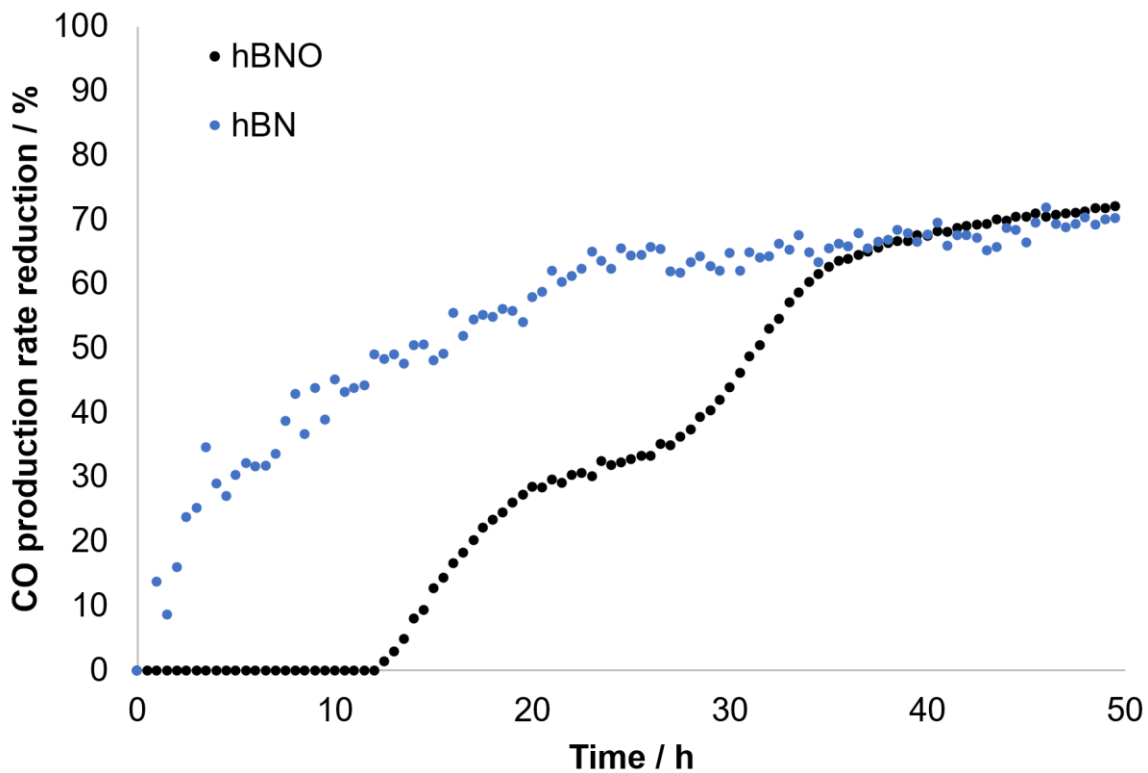
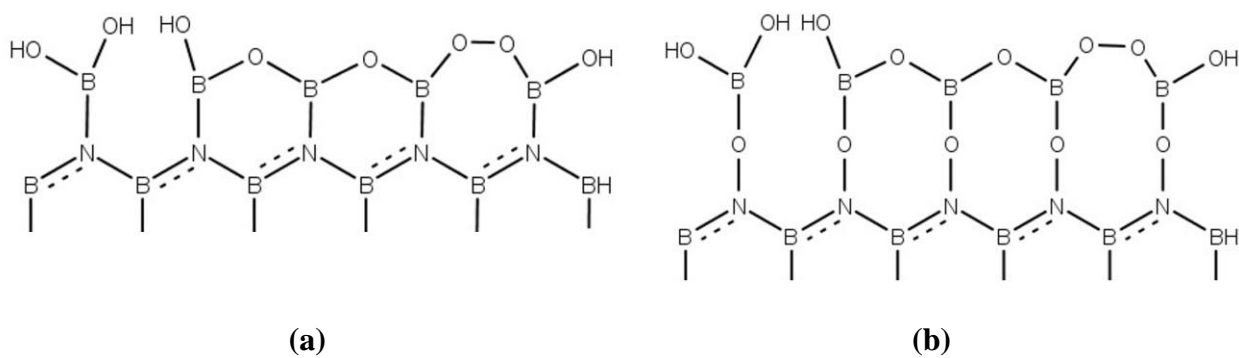


Figure 5-12. Selectivity during the stability test at 580 °C for hBN and hBNO.



**Figure 5-13.** CO selectivity for the ODH of ethane on hBN\* and the homogeneous reaction



**Figure 5-14.** Candidate active sites on hBN. a) Modified N edge<sup>29</sup>. b) Borated hBN.

## Conclusion

Thermally treated hBN has a significantly different catalytic activity compared with untreated hBN. The thermal treatment, followed by sonication and centrifugation, produced a highly active material for the oxidative dehydrogenation of ethane (hBNO). The spectroscopic evidence suggests that this hBNO is borated on its surface. This conclusion is supported by a peak at  $1190\text{ cm}^{-1}$ , assigned to B-N-O vibration, and a shift in the 002 plane peak shown by the XRD pattern, due to a change in the plane separation caused by the borated surface. The  $1190\text{ cm}^{-1}$  peak is also present in spent hBN after 50 h of reaction at  $580\text{ }^{\circ}\text{C}$ , but in this case the selectivity profile shows that the reactions taking place on hBNO and hBN are different. Even though the hBNO catalyst was significantly deactivated over time, similar to pristine hBN, our findings suggest that active sites on hBN are diverse, and its understanding will contribute to develop better and more stable catalysts.

## Chapter 6 - Conclusions and future work

This work shows how different thermal treatments can be used to hydroxylate hBN and how the final material can be tuned by changing the treatment temperature, time, atmosphere and post treatment. Boric acid is extensively formed when hBN is treated in humid air at high temperatures, but it can be removed by a thermal post treatment at low temperature using air saturated with water. This results in the formation of hBN particles without reaggregation or loss of material, which can plague alternative methods such as filtration. It was also shown that boric acid can dehydrate to  $B_2O_3$  at high temperatures, ultimately forming hBNO. These materials form more stable suspensions in water than pristine hBN. XRD and FTIR analysis can be complicated by the formation of boric acid if thermal treated hBN samples are stored in a humid environment. Analysis of samples stored in a dry environment demonstrate the absence of boric acid and the presence of  $B_2O_3$ . This is an important consideration to take into account when characterizing thermal treated samples.

Highly active catalysts for partial oxidation of methane (POM) can be produced using hBN to support Pt. The higher activity of this catalyst, compared to Pt/ $Al_2O_3$ , relies on the weaker Pt-support interaction, which increase the Pt reducibility. This higher reducibility also affects the variation of the  $H_2/CO$  ratio with temperature. The hBN supported Pt produces a stream with a  $H_2/CO$  ratio relatively constant ( $\approx 2$ ), probably due to the alterations in the POM pathway: complete combustion followed by steam and dry reforming.

Thermal treating hBN at 850 °C with humid air before the Pt impregnation generates catalysts even more active. When hBN is thermal treated, boric acid is formed. During the catalysts synthesis this boric acid forms a borated surface and Pt is deposited on it, creating an even weaker interaction with the support (Pt/Borated hBN). This result cannot be completely reproduced by

adding boric acid to hBN and then using it to synthesize the catalyst, even though the catalysts created this way are more active than those produced only with hBN because the Pt dispersion is much lower (around a third) compared with the thermal treated hBN.

Boric acid itself is detrimental for Pt activity. Borated hBN increases the activity of Pt, but if there is “free” boric acid after the catalyst synthesis, it lowers the activity. This was determined by removing the “free” boric acid after the catalyst synthesis using a purification step with humid air at 600 °C.

Oxidative dehydrogenation of ethane on hBN was evaluated. Thermally treated hBN has a significantly different catalytic activity compared with untreated hBN. The thermal treatment, followed by sonication and centrifugation, produced a highly active material for the oxidative dehydrogenation of ethane (hBNO). The spectroscopic evidence suggests that this hBNO is borated on its surface. This conclusion is supported by a peak at 1190  $\text{cm}^{-1}$ , assigned to B-N-O vibration, and a shift in the [002] plane peak shown by the XRD pattern, due to a change in the plane separation caused by the borated surface. The 1190  $\text{cm}^{-1}$  peak is also present in spent hBN after 50 h of reaction at 580 °C, but in this case the selectivity profile shows that the reactions taking place on hBNO and hBN are different. Even though the hBNO catalyst was significantly deactivated over time, as well as pristine hBN, our findings suggest that active sites on hBN are diverse, and its understanding will contribute to develop better and more stable catalysts.

The active sites on hBN remained undetermined, but there are a lot of aspects already revealed. The potential applications of hBN in the catalyst field are huge. The versatility showed by hBN when thermally modified and its dual catalyst/support role, are promising aspects that could be used to produce novel catalysts. More work is needed to explore different hBN

functionalization techniques, how those techniques affect its catalytic activity and how that activity could be maintained over time, due to the tendency of hBN catalysts to deactivate over time.

Future experiments could use our findings to obtain a deeper understanding of the active sites by, for example, using hBN, hBN850 and hBNO with different oxygen/ethane rates. By changing the oxygen rates to generate a dataset with the catalyst activity as a function of the oxygen partial pressure, additional details could be revealed if the different active sites regenerate differently. This will be possible if the oxygen interaction with hBNO, hBN850 and hBN is different. If that is the case, the XOH HOX sites ( $X = B$  or  $N$ ) will be regenerated by oxygen to produce XOOX sites (the active sites). We argue that these interactions will be different because the sites are structurally different, especially the sites on hBNO, which are probably formed on a borated hBN surface (hBNO).

Deactivation of hBNO is also a concern. Future experiments could use a higher  $N_2$  dilution and compare the deactivation with lower  $N_2$  dilutions. If the deactivation does not change with the  $N_2$  dilution, it means that it is purely thermally driven; if it changes, it is due to the reaction. In other words, a higher  $N_2$  dilution will slow down the reaction rate because the partial pressure of the reagents will be lower. If this lower reaction rate reduces the deactivation, then it is the result of the reaction, otherwise, the deactivation is a function of additional variables, such as temperature. This experiment could be repeated to generate a plot of deactivation as a function of reaction rate. The form of the plot will give information about the deactivation process, a linear relationship will indicate a deactivation due to the reaction.

In additional experiments  $N_2/O_2/C_2H_6/H_2O$  could be used to determine if the deactivation is caused by the water formed during ODH. If adding a small amount of water, just enough to saturate the inlet stream at room temperature, accelerates the deactivation, this will be a clear sign that



water causes deactivation. If this is the case the deactivation will a function of the reaction rate because one of the products of the ODH of ethane is water.

## References

- (1) Shi, L.; Yan, B.; Shao, D.; Jiang, F.; Wang, D.; Lu, A.-H. Selective Oxidative Dehydrogenation of Ethane to Ethylene over a Hydroxylated Boron Nitride Catalyst. *Chin. J. Catal.* **2017**, *38* (2), 389–396. [https://doi.org/10.1016/S1872-2067\(17\)62786-4](https://doi.org/10.1016/S1872-2067(17)62786-4).
- (2) Zhou, Y.; Lin, J.; Li, L.; Pan, X.; Sun, X.; Wang, X. Enhanced Performance of Boron Nitride Catalysts with Induction Period for the Oxidative Dehydrogenation of Ethane to Ethylene. *J. Catal.* **2018**, *365*, 14–24. <https://doi.org/10.1016/j.jcat.2018.05.023>.
- (3) Loiland, J. A.; Zhao, Z.; Patel, A.; Hazin, P. Boron-Containing Catalysts for the Oxidative Dehydrogenation of Ethane/Propane Mixtures. *Ind. Eng. Chem. Res.* **2019**, *58* (6), 2170–2181. <https://doi.org/10.1021/acs.iecr.8b04906>.
- (4) Huang, R.; Zhang, B.; Wang, J.; Wu, K.-H.; Shi, W.; Zhang, Y.; Liu, Y.; Zheng, A.; Schlögl, R.; Su, D. S. Direct Insight into Ethane Oxidative Dehydrogenation over Boron Nitrides. *ChemCatChem* **2017**, *9* (17), 3293–3298. <https://doi.org/10.1002/cctc.201700725>.
- (5) Ascoop, I.; Galvita, V. V.; Alexopoulos, K.; Reyniers, M.-F.; Van, D. V.; Bliznuk, V.; Marin, G. B. The Role of CO<sub>2</sub> in the Dehydrogenation of Propane over WO<sub>x</sub>-VO<sub>x</sub>/SiO<sub>2</sub>. *J. Catal.* **2016**, *335*, 1–11. <https://doi.org/10.1016/j.jcat.2015.12.015>.
- (6) Saravanan Vaithi. Trends and Outlook for the Global Olefins Market. *Chem. Ind. Dig. Mumbai* **2016**.
- (7) Ethylene Market Size, Share, Trends, Value | Industry Report 2020-2026 <https://www.polarismarketresearch.com/industry-analysis/ethylene-market> (accessed Nov 16, 2020).
- (8) Zhu, J.; Yang, M.-L.; Yu, Y.; Zhu, Y.-A.; Sui, Z.-J.; Zhou, X.-G.; Holmen, A.; Chen, D. Size-Dependent Reaction Mechanism and Kinetics for Propane Dehydrogenation over Pt Catalysts. *ACS Catal.* **2015**, *5* (11), 6310–6319. <https://doi.org/10.1021/acscatal.5b01423>.
- (9) Qiao, A.; Kalevaru, V. N.; Radnik, J.; Srihari Kumar, A.; Lingaiah, N.; Sai Prasad, P. S.; Martin, A. Oxidative Dehydrogenation of Ethane to Ethylene over V<sub>2</sub>O<sub>5</sub>/Nb<sub>2</sub>O<sub>5</sub> Catalysts. *Catal. Commun.* **2013**, *30*, 45–50. <https://doi.org/10.1016/j.catcom.2012.10.018>.
- (10) Khan, M. I.; Aydemir, K.; Siddiqui, M. R. H.; Alwarthan, A. A.; Marshall, C. L. Oxidative Dehydrogenation Properties of Novel Nanostructured Polyoxovanadate Based Materials. *Catal. Lett.* **2011**, *141* (4), 538–543. <https://doi.org/10.1007/s10562-011-0547-9>.
- (11) Galvita, V.; Siddiqi, G.; Sun, P.; Bell, A. T. Ethane Dehydrogenation on Pt/Mg(Al)O and PtSn/Mg(Al)O Catalysts. *J. Catal.* **2010**, *271* (2), 209–219. <https://doi.org/10.1016/j.jcat.2010.01.016>.
- (12) Eric McFarland. Unconventional Chemistry for Unconventional Natural Gas. *Sci. Am. Assoc. Adv. Sci.* **2012**, *338* (6105), 340–342. <https://doi.org/10.1126/science.1226840>.
- (13) Testova, N. V.; Shalygin, A. S.; Kaichev, V. V.; Glazneva, T. S.; Paukshtis, E. A.; Parmon, V. N. Oxidative Dehydrogenation of Propane by Molecular Chlorine. *Appl. Catal. Gen.* **2015**, *505*, 441–446. <https://doi.org/10.1016/j.apcata.2015.05.018>.
- (14) Kung, H. H. Oxidative Dehydrogenation of Light (C<sub>2</sub> to C<sub>4</sub>) Alkanes. *Adv. Catal.* **1994**, *40*, 1–38. [https://doi.org/10.1016/S0360-0564\(08\)60655-0](https://doi.org/10.1016/S0360-0564(08)60655-0).
- (15) Cavani, F.; Ballarini, N.; Cericola, A. Oxidative Dehydrogenation of Ethane and Propane: How Far from Commercial Implementation? *Catal. Today* **2007**, *127* (1), 113–132. <https://doi.org/10.1016/j.cattod.2007.05.009>.

- (16) Khan, M. I.; Deb, S.; Aydemir, K.; Alwarthan, A. A.; Chattopadhyay, S.; Miller, J. T.; Marshall, C. L. Vanadium Oxide Based Nanostructured Materials for Catalytic Oxidative Dehydrogenation of Propane : Effect of Heterometallic Centers on the Catalyst Performance. *Catal. Lett.* **2010**, *135* (2010). <https://doi.org/10.1007/s10562-010-0275-6>.
- (17) Carrero, C.; Kauer, M.; Dinse, A.; Wolfram, T.; Hamilton, N.; Trunschke, A.; Schlögl, R.; Schomäcker, R. High Performance (VO<sub>x</sub>)<sub>n</sub>–(TiO<sub>x</sub>)<sub>m</sub>/SBA-15 Catalysts for the Oxidative Dehydrogenation of Propane. *Catal. Sci. Technol.* **2014**, *4* (3), 786–795. <https://doi.org/10.1039/C3CY00625E>.
- (18) Chaturbedy, P.; Ahamed, M.; Eswaramoorthy, M. Oxidative Dehydrogenation of Propane over a High Surface Area Boron Nitride Catalyst: Exceptional Selectivity for Olefins at High Conversion. *ACS Omega* **2018**, *3* (1), 369–374. <https://doi.org/10.1021/acsomega.7b01489>.
- (19) Wachs, I. E.; Weckhuysen, B. M. Structure and reactivity of surface vanadium oxide species on oxide supports (accessed Jan 1, 157AD).
- (20) Wachs, I. E. Catalysis Science of Supported Vanadium Oxide Catalysts. *Dalton Trans.* **2013**, *42* (33), 11762–11770. <https://doi.org/10.1039/C3DT50692D>.
- (21) Martínez-Huerta, M. V.; Gao, X.; Tian, H.; Wachs, I. E.; Fierro, J. L. G.; Bañares, M. A. Oxidative Dehydrogenation of Ethane to Ethylene over Alumina-Supported Vanadium Oxide Catalysts: Relationship between Molecular Structures and Chemical Reactivity. *Catal. Today* **2006**, *118* (3–4), 279–288. <https://doi.org/10.1016/j.cattod.2006.07.034>.
- (22) Grabowski, R. Kinetics of Oxidative Dehydrogenation of C<sub>2</sub>–C<sub>3</sub> Alkanes on Oxide Catalysts. *Catal. Rev.* **2006**, *48* (2), 199–269. <https://doi.org/10.1080/01614940600631413>.
- (23) Rozanska, X.; Fortrie, R.; Sauer, J. Oxidative Dehydrogenation of Propane by Monomeric Vanadium Oxide Sites on Silica Support. *J. Phys. Chem. C* **2007**, *111* (16), 6041–6051. <https://doi.org/10.1021/jp071409e>.
- (24) Grant, J. T.; McDermott, W. P.; Venegas, J. M.; Burt, S. P.; Micka, J.; Phivilay, S. P.; Carrero, C. A.; Hermans, I. Boron and Boron-Containing Catalysts for the Oxidative Dehydrogenation of Propane. *ChemCatChem* **2017**, *9* (19), 3622–3622. <https://doi.org/10.1002/cctc.201701473>.
- (25) Shi, L.; Yan, B.; Shao, D.; Jiang, F.; Wang, D.; Lu, A.-H. Selective Oxidative Dehydrogenation of Ethane to Ethylene over a Hydroxylated Boron Nitride Catalyst. *Chin. J. Catal.* **2017**, *38* (2), 389–395. [https://doi.org/10.1016/S1872-2067\(17\)62786-4](https://doi.org/10.1016/S1872-2067(17)62786-4).
- (26) Grant, J. T.; Carrero, C. A.; Goeltl, F.; Venegas, J.; Mueller, P.; Burt, S. P.; Specht, S. E.; McDermott, W. P.; Chiericato, A.; Hermans, I. Selective Oxidative Dehydrogenation of Propane to Propene Using Boron Nitride Catalysts. *Sci. Am. Assoc. Adv. Sci.* **2016**, *354* (6319), 1570–1573. <https://doi.org/10.1126/science.aaf7885>.
- (27) Tian, J.; Lin, J.; Xu, M.; Wan, S.; Lin, J.; Wang, Y. Hexagonal Boron Nitride Catalyst in a Fixed-Bed Reactor for Exothermic Propane Oxidation Dehydrogenation. *Chem. Eng. Sci.* **2018**, *186* (C), 142–151. <https://doi.org/10.1016/j.ces.2018.04.029>.
- (28) Venegas, J. M.; Grant, J. T.; McDermott, W. P.; Burt, S. P.; Micka, J.; Carrero, C. A.; Hermans, I. Selective Oxidation of N-Butane and Isobutane Catalyzed by Boron Nitride. *ChemCatChem* **2017**, *9* (12), 2118–2128. <https://doi.org/10.1002/cctc.201601686>.
- (29) Shi, L.; Wang, D.; Lu, A.-H. A Viewpoint on Catalytic Origin of Boron Nitride in Oxidative Dehydrogenation of Light Alkanes. *Chin. J. Catal.* **2018**, *39* (5), 908–913. [https://doi.org/10.1016/S1872-2067\(18\)63060-8](https://doi.org/10.1016/S1872-2067(18)63060-8).

- (30) Lee, K. H.; Shin, H.-J.; Kumar, B.; Kim, H. S.; Lee, J.; Bhatia, R.; Kim, S.-H.; Lee, I.-Y.; Lee, H. S.; Kim, G.-H.; Yoo, J.-B.; Choi, J.-Y.; Kim, S.-W. Nanocrystalline-Graphene-Tailored Hexagonal Boron Nitride Thin Films. *Angew. Chem.* **2014**, *126* (43), 11677–11681. <https://doi.org/10.1002/ange.201405762>.
- (31) Huang, R.; Zhang, B.; Wang, J.; Wu, K.-H.; Shi, W.; Zhang, Y.; Liu, Y.; Zheng, A.; Schlögl, R.; Su, D. S. Direct Insight into Ethane Oxidative Dehydrogenation over Boron Nitrides. *ChemCatChem* **2017**, *9* (17), 3293–3297. <https://doi.org/10.1002/cctc.201700725>.
- (32) Cui, Z.; Oyer, A. J.; Glover, A. J.; Schniepp, H. C.; Adamson, D. H. Large Scale Thermal Exfoliation and Functionalization of Boron Nitride. *Small* **2014**, *10* (12), 2352–2356. <https://doi.org/10.1002/sml.201303236>.
- (33) Li, L. H.; Cervenka, J.; Watanabe, K.; Taniguchi, T.; Chen, Y. Strong Oxidation Resistance of Atomically Thin Boron Nitride Nanosheets. *ACS Nano* **2014**, *8* (2), 1457–1462. <https://doi.org/10.1021/nn500059s>.
- (34) Yu, Z.; Hou, X.; Chen, Z.; Chou, K.-C. Effect of Water-Vapor Content on Reaction Rate of Hexagonal BN Powder at 1273 K. *High Temp. Mater. Process.* **2013**, *32* (3), 275–281. <https://doi.org/10.1515/htmp-2012-0138>.
- (35) Buyevskaya, O. V.; Kubik, M.; Baerns, M. Factors Determining the Selectivity in the Oxidative Dehydrogenation of Propane over Boria—Alumina Catalysts. In *Heterogeneous Hydrocarbon Oxidation*; ACS Symposium Series; American Chemical Society, 1996; Vol. 638, pp 155–169. <https://doi.org/10.1021/bk-1996-0638.ch011>.
- (36) Sibeijn, M.; Vanveen, J.; Blik, A.; Moulijn, J. On The Nature And Formation Of The Active-Sites In Re<sub>2</sub>O<sub>7</sub> Metathesis Catalysts Supported On Borated Alumina. *J. Catal.* **1994**, *145* (2), 416–429. <https://doi.org/10.1006/jcat.1994.1052>.
- (37) Colorio, G.; Védrine, J. C.; Auroux, A.; Bonnetot, B. Partial Oxidation of Ethane over Alumina-Boria Catalysts. *Appl. Catal. Gen.* **1996**, *137* (1), 55–68. [https://doi.org/10.1016/0926-860X\(95\)00273-1](https://doi.org/10.1016/0926-860X(95)00273-1).
- (38) Buyevskaya, O. V.; Müller, D.; Pitsch, I.; Baerns, M. Selective Oxidative Conversion of Propane to Olefins and Oxygenates on Boria-Containing Catalysts. In *Studies in Surface Science and Catalysis*; Parmaliana, A., Sanfilippo, D., Frusteri, F., Vaccari, A., Arena, F., Eds.; Natural Gas Conversion V; Elsevier, 1998; Vol. 119, pp 671–676. [https://doi.org/10.1016/S0167-2991\(98\)80509-0](https://doi.org/10.1016/S0167-2991(98)80509-0).
- (39) U. S. Energy Information Administration. *Natural Gas Annual*; Energy Information Administration: Washington, DC, 2019.
- (40) da Silva, M. J. Synthesis of Methanol from Methane: Challenges and Advances on the Multi-Step (Syngas) and One-Step Routes (DMTM). *Fuel Process. Technol.* **2016**, *145*, 42–61. <https://doi.org/10.1016/j.fuproc.2016.01.023>.
- (41) Abdullah, B.; Abd Ghani, N. A.; Vo, D.-V. N. Recent Advances in Dry Reforming of Methane over Ni-Based Catalysts. *J. Clean. Prod.* **2017**, *162* (C), 170–185. <https://doi.org/10.1016/j.jclepro.2017.05.176>.
- (42) Korup, O.; Schlögl, R.; Horn, R. Carbon Formation in Catalytic Partial Oxidation of Methane on Platinum: Model Studies on a Polycrystalline Pt Foil. *Catal. Today* **2012**, *181* (1), 177–183. <https://doi.org/10.1016/j.cattod.2011.04.051>.
- (43) Figen, H. E.; Baykara, S. Z. Effect of Ruthenium Addition on Molybdenum Catalysts for Syngas Production via Catalytic Partial Oxidation of Methane in a Monolithic Reactor.

- Int. J. Hydrog. Energy* **2018**, *43* (2), 1129–1138.  
<https://doi.org/10.1016/j.ijhydene.2017.10.173>.
- (44) Koh, A. C. W.; Chen, L.; Kee Leong, W.; Johnson, B. F. G.; Khimyak, T.; Lin, J. Hydrogen or Synthesis Gas Production via the Partial Oxidation of Methane over Supported Nickel–Cobalt Catalysts. *Int. J. Hydrog. Energy* **2007**, *32* (6), 725–730.  
<https://doi.org/10.1016/j.ijhydene.2006.08.002>.
- (45) Sengodan, S.; Lan, R.; Humphreys, J.; Du, D.; Xu, W.; Wang, H.; Tao, S. Advances in Reforming and Partial Oxidation of Hydrocarbons for Hydrogen Production and Fuel Cell Applications. *Renew. Sustain. Energy Rev.* **2018**, *82*, 761–780.  
<https://doi.org/10.1016/j.rser.2017.09.071>.
- (46) Christian Enger, B.; Lødeng, R.; Holmen, A. A Review of Catalytic Partial Oxidation of Methane to Synthesis Gas with Emphasis on Reaction Mechanisms over Transition Metal Catalysts. *Appl. Catal. Gen.* **2008**, *346* (1), 1–27.  
<https://doi.org/10.1016/j.apcata.2008.05.018>.
- (47) Kondratenko, E. V.; Peppel, T.; Seeburg, D.; Kondratenko, V. A.; Kalevaru, N.; Martin, A.; Wohlrab, S. Methane Conversion into Different Hydrocarbons or Oxygenates: Current Status and Future Perspectives in Catalyst Development and Reactor Operation. *Catal. Sci. Technol.* **2017**, *7* (2), 366–381. <https://doi.org/10.1039/c6cy01879c>.
- (48) van Looij, F.; van Giezen, J. C.; Stobbe, E. R.; Geus, J. W. Mechanism of the Partial Oxidation of Methane to Synthesis Gas on a Silica-Supported Nickel Catalyst. *Catal. Today* **1994**, *21* (2), 495–503. [https://doi.org/10.1016/0920-5861\(94\)80172-X](https://doi.org/10.1016/0920-5861(94)80172-X).
- (49) Albertazzi, S.; Arpentinier, P.; Basile, F.; Del Gallo, P.; Fornasari, G.; Gary, D.; Vaccari, A. Deactivation of a Pt/ $\gamma$ -Al<sub>2</sub>O<sub>3</sub> Catalyst in the Partial Oxidation of Methane to Synthesis Gas. *Appl. Catal. Gen.* **2003**, *247* (1), 1–7. [https://doi.org/10.1016/S0926-860X\(03\)00083-8](https://doi.org/10.1016/S0926-860X(03)00083-8).
- (50) Geske, M.; Pelzer, K.; Horn, R.; Jentoft, F. C.; Schlögl, R. In-Situ Investigation of Gas Phase Radical Chemistry in the Catalytic Partial Oxidation of Methane on Pt. *Catal. Today* **2009**, *142* (1), 61–69. <https://doi.org/10.1016/j.cattod.2009.01.005>.
- (51) Lanza, R.; Canu, P.; Järås, S. G. Methane Partial Oxidation over Pt–Ru Catalyst: An Investigation on the Mechanism. *Appl. Catal. Gen.* **2010**, *375* (1), 92–100.  
<https://doi.org/10.1016/j.apcata.2009.12.021>.
- (52) Mattos, L. V.; Rodino, E.; Resasco, D. E.; Passos, F. B.; Noronha, F. B. Partial Oxidation and CO<sub>2</sub> Reforming of Methane on Pt/Al<sub>2</sub>O<sub>3</sub>, Pt/ZrO<sub>2</sub>, and Pt/Ce–ZrO<sub>2</sub> Catalysts. *Fuel Process. Technol.* **2003**, *83* (1–3), 147–161. [https://doi.org/10.1016/S0378-3820\(03\)00063-8](https://doi.org/10.1016/S0378-3820(03)00063-8).
- (53) Wu, J. C.; Cheng, T.-S.; Lai, C.-L. Boron Nitride Supported PtFe Catalysts for Selective Hydrogenation of Crotonaldehyde. *Appl. Catal. Gen.* **2006**, *314* (2), 233–239.  
<https://doi.org/10.1016/j.apcata.2006.08.022>.
- (54) Lin, C.-A.; Wu, J. C. S.; Pan, J.-W.; Yeh, C.-T. Characterization of Boron-Nitride-Supported Pt Catalysts for the Deep Oxidation of Benzene. *J. Catal.* **2002**, *210* (1), 39–45.  
<https://doi.org/10.1006/jcat.2002.3638>.
- (55) Wu, J. C. S.; Fan, Y.-C.; Lin, C.-A. Deep Oxidation of Methanol Using a Novel Pt/Boron Nitride Catalyst. *Ind. Eng. Chem. Res.* **2003**, *42* (14), 3225–3229.  
<https://doi.org/10.1021/ie020880l>.
- (56) Au, C. T.; Hu, Y. H.; Wan, H. L. Pulse Studies of CH<sub>4</sub> Interaction with NiO/Al<sub>2</sub>O<sub>3</sub> Catalysts. *Catal. Lett.* **1994**, *27* (1–2), 199–206. <https://doi.org/10.1007/BF00806993>.

- (57) Goula, M. A.; Lemonidou, A. A.; Grünert, W.; Baerns, M. Methane Partial Oxidation to Synthesis Gas Using Nickel on Calcium Aluminate Catalysts. *Catal. Today* **1996**, *32* (1), 149–156. [https://doi.org/10.1016/S0920-5861\(96\)00168-X](https://doi.org/10.1016/S0920-5861(96)00168-X).
- (58) Aryafar, M.; Zaera, F. Kinetic Study of the Catalytic Oxidation of Alkanes over Nickel, Palladium, and Platinum Foils. *Catal. Lett.* **1997**, *48* (3), 173–183. <https://doi.org/10.1023/A:1019055810760>.
- (59) Völter, J.; Lietz, G.; Spindler, H.; Lieske, H. Role of Metallic and Oxidic Platinum in the Catalytic Combustion of N-Heptane. *J. Catal.* **1987**, *104* (2), 375–380. [https://doi.org/10.1016/0021-9517\(87\)90370-8](https://doi.org/10.1016/0021-9517(87)90370-8).
- (60) Wu, J.; Chen, C.-Y.; Lin, S. Boron Nitride Supported Pt Catalyst for Selective Hydrogenation. *Catal. Lett.* **2005**, *102* (3–4), 223–227. <https://doi.org/10.1007/s10562-005-5860-8>.
- (61) Feng Xiao, S. N., Gilberto Casillas, Majharul H. Khan, Tomas Katkus, Lei Jiang, Huakun Liu, Huijun Li, Zhenguo Huang. Edge-Hydroxylated Boron Nitride Nanosheets as an Effective Additive to Improve the Thermal Response of Hydrogels. *Adv. Mater.* **2015**, *27*, 7196–7204.
- (62) Jin, H.; Li, Y.; Li, X.; Shi, Z.; Xia, H.; Xu, Z.; Qiao, G. Functionalization of Hexagonal Boron Nitride in Large Scale by a Low-Temperature Oxidation Route. *Mater. Lett.* **2016**, *175*, 244–248. <https://doi.org/10.1016/j.matlet.2016.04.008>.
- (63) Yi Lin; Tiany V. Williams; Tian-Bing Xu; Wei Cao; Hani E. Elsayed-Ali; John W. Connell. Aqueous Dispersions of Few-Layered and Monolayered Hexagonal Boron Nitride Nanosheets from Sonication-Assisted Hydrolysis: Critical Role of Water. *J. Phys. Chem. C* **2011**, *115* (6), 2679–2686. <https://doi.org/10.1021/jp110985w>.
- (64) Wu, K.; Lei, C.; Yang, W.; Chai, S.; Chen, F.; Fu, Q. Surface Modification of Boron Nitride by Reduced Graphene Oxide for Preparation of Dielectric Material with Enhanced Dielectric Constant and Well-Suppressed Dielectric Loss. *Compos. Sci. Technol. Compos. Sci. Technol.* **2016**, *134*, 191–201. <https://doi.org/10.1016/j.compscitech.2016.08.015>.
- (65) Lee, D.; Lee, B.; Park, K. H.; Ryu, H. J.; Jeon, S.; Hong, S. H. Scalable Exfoliation Process for Highly Soluble Boron Nitride Nanoplatelets by Hydroxide-Assisted Ball Milling. *Nano Lett.* **2015**, *15* (2), 1238. <https://doi.org/10.1021/nl504397h>.
- (66) Zhu, W.; Gao, X.; Li, Q.; Li, H.; Chao, Y.; Li, M.; Mahurin, S. M.; Li, H.; Zhu, H.; Dai, S. Controlled Gas Exfoliation of Boron Nitride into Few-Layered Nanosheets. *Angew. Chem. Int. Ed.* **2016**, *55* (36), 10766–10771. <https://doi.org/10.1002/anie.201605515>.
- (67) Pakdel, A.; Bando, Y.; Golberg, D. Nano Boron Nitride Flatland. *Chem. Soc. Rev.* *ChemSocRev* **2014**, *43* (3), 934–960. <https://doi.org/10.1039/c3cs60260e>.
- (68) Shi, Z.; Wang, J.; Qiao, G.; Jin, Z. Effects of Weak Boundary Phases (WBP) on the Microstructure and Mechanical Properties of Pressureless Sintered Al<sub>2</sub>O<sub>3</sub>/h-BN Machinable Composites. *Mater. Sci. Eng. A* **2008**, *492* (1), 29–35. <https://doi.org/10.1016/j.msea.2008.03.004>.
- (69) Golberg, D.; Bando, Y.; Huang, Y.; Terao, T.; Mitome, M.; Tang, C.; Zhi, C. Boron Nitride Nanotubes and Nanosheets. *Acs Nano ACS Nano* **2010**, *4* (6), 2979–2994. <https://doi.org/10.1021/nn1006495>.
- (70) Nazarov, A. S.; Demin, V. N.; Grayfer, E. D.; Bulavchenko, A. I.; Arymbaeva, A. T.; Shin, H.; Choi, J.; Fedorov, V. E. Functionalization and Dispersion of Hexagonal Boron Nitride (h-BN) Nanosheets Treated with Inorganic Reagents. *Chem. – Asian J.* **2012**, *7* (3), 554–561. <https://doi.org/10.1002/asia.201100710>.

- (71) Bhimanapati, G. R.; Kozuch, D.; Robinson, J. A. Large-Scale Synthesis and Functionalization of Hexagonal Boron Nitride Nanosheets. *Nanoscale Nanoscale* **2014**, *6* (20), 11671–11676. <https://doi.org/10.1039/c4nr01816h>.
- (72) Weng, Q.; Wang, B.; Wang, X.; Hanagata, N.; Li, X.; Liu, D.; Wang, X.; Jiang, X.; Bando, Y.; Golberg, D. Highly Water-Soluble, Porous, and Biocompatible Boron Nitrides for Anticancer Drug Delivery. *ACS Nano* **2014**, *8* (6), 6123–6131. <https://doi.org/10.1021/nn5014808>.
- (73) Venegas, J. M.; Mcdermott, W. P.; Hermans, I. Serendipity in Catalysis Research: Boron-Based Materials for Alkane Oxidative Dehydrogenation. *Acc. Chem. Res.* **2018**, *51* (10), 2556. <https://doi.org/10.1021/acs.accounts.8b00330>.
- (74) Fu, L.; Wang, T.; Yu, J.; Dai, W.; Sun, H.; Liu, Z.; Sun, R.; Jiang, N.; Yu, A.; Lin, C.-T. An Ultrathin High-Performance Heat Spreader Fabricated with Hydroxylated Boron Nitride Nanosheets. *2D Mater.* **2017**, *4* (2), 7. <https://doi.org/10.1088/2053-1583/aa636e>.
- (75) Liao, Y.; Tu, K.; Han, X.; Hu, L.; Connell, J. W.; Chen, Z.; Lin, Y. Oxidative Etching of Hexagonal Boron Nitride Toward Nanosheets with Defined Edges and Holes. *Sci. Rep.* **2015**, *5*, 14510. <https://doi.org/10.1038/srep14510>.
- (76) Zhan, Y.; Yan, J.; Wu, M.; Guo, L.; Lin, Z.; Qui, B.; Chen, G.; Wong, K. Boron Nitride Nanosheets as a Platform for Fluorescence Sensing. *Talanta* **2017**, *174*, 365–372. <https://doi.org/10.1016/j.talanta.2017.06.032>.
- (77) M. Sudeep, P.; Vinod, S.; Ozden, S.; Sruthi, R.; Kukovecz, A.; Konya, Z.; Vajtai, R.; R. Anantharaman, M.; M. Ajayan, P.; N. Narayanan, T. Functionalized Boron Nitride Porous Solids. *RSC Adv.* **2015**, *5* (114), 93964–93969. <https://doi.org/10.1039/C5RA19091F>.
- (78) Lei, Z.; Xu, S.; Wan, J.; Wu, P. Facile Preparation and Multifunctional Applications of Boron Nitride Quantum Dots. *Nanoscale* **2015**, *7* (45), 18902–18908. <https://doi.org/10.1039/C5NR05960G>.
- (79) Aghili, S.; Panjepour, M.; Meratian, M. Kinetic Analysis of Formation of Boron Trioxide from Thermal Decomposition of Boric Acid under Non-Isothermal Conditions. *J. Therm. Anal. Calorim.* **2018**, *131* (3), 2443–2456. <https://doi.org/10.1007/s10973-017-6740-3>.
- (80) Gautam, C.; Yadav, A. K.; Singh, A. K. A Review on Infrared Spectroscopy of Borate Glasses with Effects of Different Additives. *ISRN Ceram.* **2012**, *2012*. <https://doi.org/10.5402/2012/428497>.
- (81) Shi, L.; Wang, Y.; Yan, B.; Song, W.; Shao, D.; Lu, A.-H. Progress in Selective Oxidative Dehydrogenation of Light Alkanes to Olefins Promoted by Boron Nitride Catalysts. *Chem. Commun.* **2018**, *54* (78), 10936–10947. <https://doi.org/10.1039/c8cc04604b>.
- (82) Méthivier, Ch.; Béguin, B.; Brun, M.; Massardier, J.; Bertolini, J. C. Pd/SiC Catalysts: Characterization and Catalytic Activity for the Methane Total Oxidation. *J. Catal.* **1998**, *173* (2), 374–382. <https://doi.org/10.1006/jcat.1997.1924>.
- (83) Postole, G.; Caldararu, M.; Ionescu, N. I.; Bonnetot, B.; Auroux, A.; Guimon, C. Boron Nitride: A High Potential Support for Combustion Catalysts. *Thermochim. Acta* **2005**, *434* (1), 150–157. <https://doi.org/10.1016/j.tca.2005.01.007>.
- (84) Hohn, K. L.; Schmidt, L. D. Partial Oxidation of Methane to Syngas at High Space Velocities over Rh-Coated Spheres. *Appl. Catal. Gen.* **2001**, *211* (1), 53–68. [https://doi.org/10.1016/S0926-860X\(00\)00835-8](https://doi.org/10.1016/S0926-860X(00)00835-8).

- (85) Carstens, J. N.; Su, S. C.; Bell, A. T. Factors Affecting the Catalytic Activity of Pd/ZrO<sub>2</sub> for the Combustion of Methane. *J. Catal.* **1998**, *176* (1), 136–142. <https://doi.org/10.1006/jcat.1998.2029>.
- (86) Murata, K.; Mahara, Y.; Ohyama, J.; Yamamoto, Y.; Arai, S.; Satsuma, A. The Metal–Support Interaction Concerning the Particle Size Effect of Pd/Al<sub>2</sub>O<sub>3</sub> on Methane Combustion. *Angew. Chem. Int. Ed.* **2017**, *56* (50), 15993–15997. <https://doi.org/10.1002/anie.201709124>.
- (87) Balcı, S.; Sezgi, N. A.; Eren, E. Boron Oxide Production Kinetics Using Boric Acid as Raw Material. *Ind. Eng. Chem. Res.* **2012**, *51* (34), 11091–11096. <https://doi.org/10.1021/ie300685x>.
- (88) Zhu, T.; van Grootel, P. W.; Filot, I. A.; Sun, S.-G.; van Santen, R. A.; Hensen, E. J. Microkinetics of Steam Methane Reforming on Platinum and Rhodium Metal Surfaces. *J. Catal.* **2013**, *297*, 227–235. <https://doi.org/10.1016/j.jcat.2012.10.010>.
- (89) Niu, J.; Wang, Y.; Qi, Y.; Dam, A. H.; Wang, H.; Zhu, Y.-A.; Holmen, A.; Ran, J.; Chen, D. New Mechanism Insights into Methane Steam Reforming on Pt/Ni from DFT and Experimental Kinetic Study. *Fuel Guildf.* **2020**, *266*, 117143-. <https://doi.org/10.1016/j.fuel.2020.117143>.
- (90) Maier, L.; Schädel, B.; Herrera Delgado, K.; Tischer, S.; Deutschmann, O. Steam Reforming of Methane Over Nickel: Development of a Multi-Step Surface Reaction Mechanism. *Top. Catal.* **2011**, *54* (13–15), 845–858. <https://doi.org/10.1007/s11244-011-9702-1>.
- (91) Choi, I.; Lee, K. G.; Ahn, S. H.; Kim, D. H.; Kwon, O. J.; Kim, J. J. Sonochemical Synthesis of Pt-Deposited SiO<sub>2</sub> Nanocomposite and Its Catalytic Application for Polymer Electrolyte Membrane Fuel Cell under Low-Humidity Conditions. *Catal. Commun.* **2012**, *21*, 86–90. <https://doi.org/10.1016/j.catcom.2012.02.005>.
- (92) Gümeçi, C.; Li, Z.; Casadonte, D. J.; Korzeniewski, C. Pt-Ni Nanoparticles for Oxygen Reduction Prepared by a Sonochemical Method. *J. Electrochem. Soc.* **2012**, *159* (3), F35–F41. <https://doi.org/10.1149/2.029203jes>.
- (93) Perkasi, N.; Zhong, Z.; Chen, L.; Besson, M.; Gedanken, A. Sonochemically Prepared High Dispersed Ru/TiO<sub>2</sub> Mesoporous Catalyst for Partial Oxidation of Methane to Syngas. *Catal. Lett.* **2005**, *103* (1), 9–14. <https://doi.org/10.1007/s10562-005-6496-4>.
- (94) Xu, D.; Liu, Y.-J.; Zhao, J.-X.; Cai, Q.-H.; Wang, X.-Z. Theoretical Study of the Deposition of Pt Clusters on Defective Hexagonal Boron Nitride (h-BN) Sheets: Morphologies, Electronic Structures, and Interactions with O. *J. Phys. Chem. C* **2014**, *118* (17), 8868–8876. <https://doi.org/10.1021/jp4087943>.
- (95) Aly, M.; Fornero, E. L.; Leon-Garzon, A. R.; Galvita, V. V.; Saeys, M. Effect of Boron Promotion on Coke Formation during Propane Dehydrogenation over Pt/γ-Al<sub>2</sub>O<sub>3</sub> Catalysts. *ACS Catal.* **2020**, *10* (9), 5208–5216. <https://doi.org/10.1021/acscatal.9b05548>.
- (96) Munnik, P.; de Jongh, P. E.; de Jong, K. P. Recent Developments in the Synthesis of Supported Catalysts. *Chem. Rev.* **2015**, *115* (14), 6687–6718. <https://doi.org/10.1021/cr500486u>.
- (97) Si, C.; Lian, Z.; Olanrele, S. O.; Sun, X.; Li, B. Revealing the Origin of the Reactivity of Metal-Free Boron Nitride Catalysts in Oxidative Dehydrogenation of Propane. *Appl. Surf. Sci.* **2020**, *519*, 146241-. <https://doi.org/10.1016/j.apsusc.2020.146241>.



- (98) Lu, W.-D.; Wang, D.; Zhao, Z.; Song, W.; Li, W.-C.; Lu, A.-H. Supported Boron Oxide Catalysts for Selective and Low-Temperature Oxidative Dehydrogenation of Propane. *ACS Catal.* **2019**, *9* (9), 8263–8270. <https://doi.org/10.1021/acscatal.9b02284>.
- (99) Shi, L.; Wang, D.; Song, W.; Shao, D.; Zhang, W.-P.; Lu, A.-H. Edge-hydroxylated Boron Nitride for Oxidative Dehydrogenation of Propane to Propylene. *ChemCatChem* **2017**, *9* (10), 1788–1793. <https://doi.org/10.1002/cctc.201700004>.
- (100) Heracleous, E.; Lemonidou, A. A. Homogeneous and Heterogeneous Pathways of Ethane Oxidative and Non-Oxidative Dehydrogenation Studied by Temperature-Programmed Reaction. *Appl. Catal. Gen.* **2004**, *269* (1), 123–135. <https://doi.org/10.1016/j.apcata.2004.04.007>.
- (101) Parishan, S.; Nowicka, E.; Fleischer, V.; Schulz, C.; Colmenares, M. G.; Rosowski, F.; Schomäcker, R. Investigation into Consecutive Reactions of Ethane and Ethene Under the OCM Reaction Conditions over  $\text{MnxOy-Na}_2\text{WO}_4/\text{SiO}_2$  Catalyst. *Catal. Lett.* **2018**, *148* (6), 1659–1675. <https://doi.org/10.1007/s10562-018-2384-6>.
- (102) Zhou, Y.; Wang, Y.; Lu, W.; Yan, B.; Lu, A. A High Propylene Productivity over  $\text{B}_2\text{O}_3/\text{SiO}_2$ @honeycomb Cordierite Catalyst for Oxidative Dehydrogenation of Propane. *Chin. J. Chem. Eng.* **2020**. <https://doi.org/10.1016/j.cjche.2020.07.040>.

## Appendix A - hBN functionalization

In this section you will find information related to hBN samples treated with different techniques. The information presented here is for preliminary explorations, that is why it was not included as part of the previous sections.

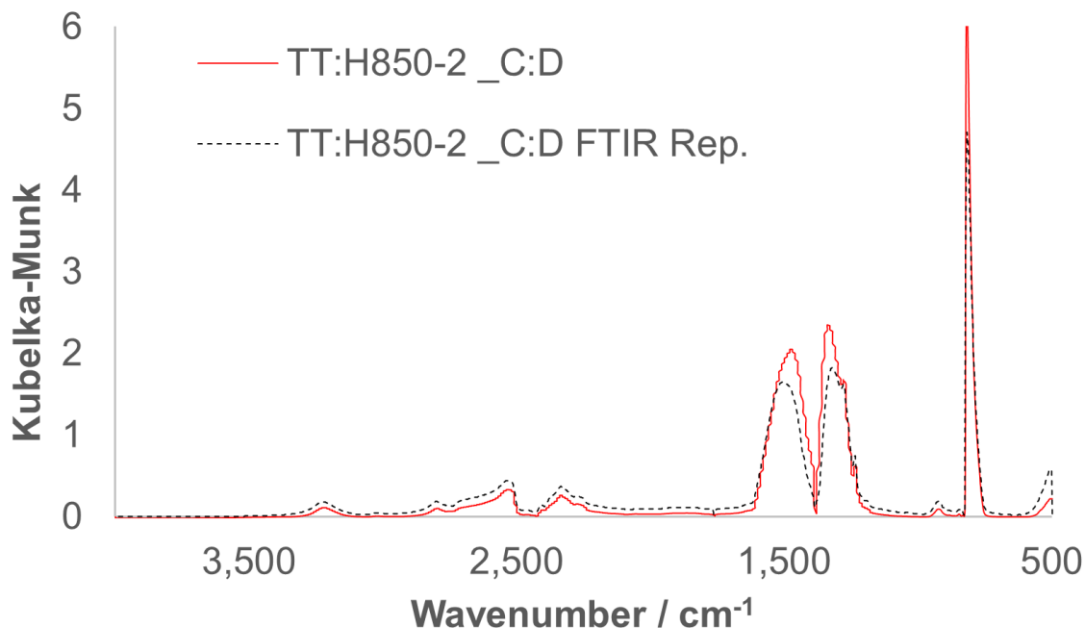


**Figure A 1** hBN thermally treated at 850 °C for 2 h. The same sample was measured twice to evaluate the repeatability of the FTIR equipment.

### Quenching

Quenching consists in the immersion of hBN at 850 °C in liquid nitrogen. For each quenching cycle hBN was heated at 850 °C at 10 °C/minute, once the temperature was

reached it was hold for 5 minutes before throwing hBN in liquid nitrogen. After the immersion, liquid nitrogen was vaporized at room temperature before the next cycle.

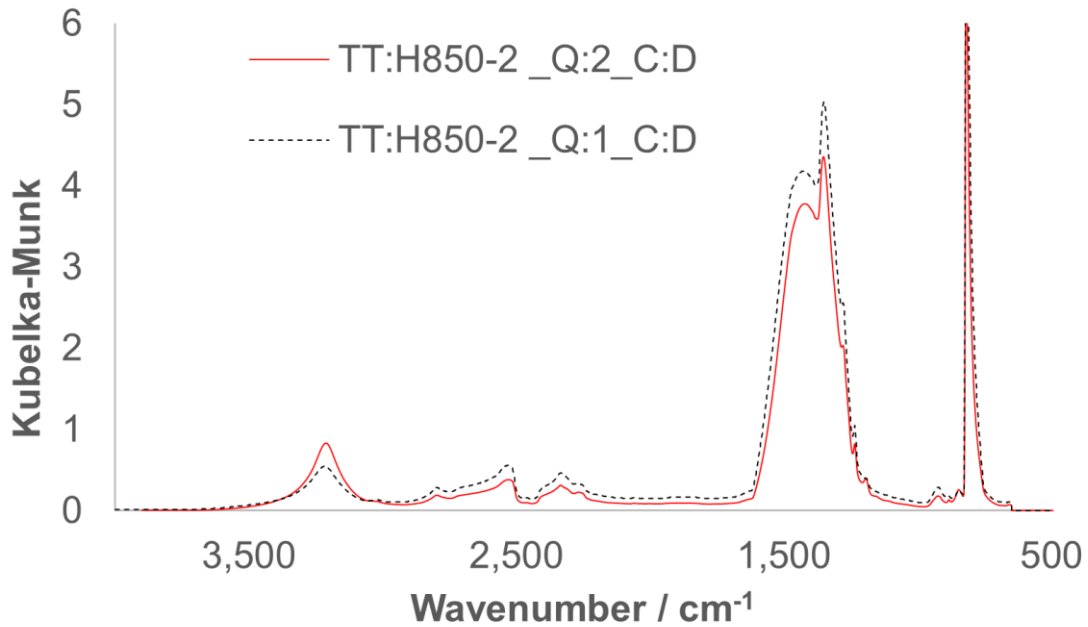
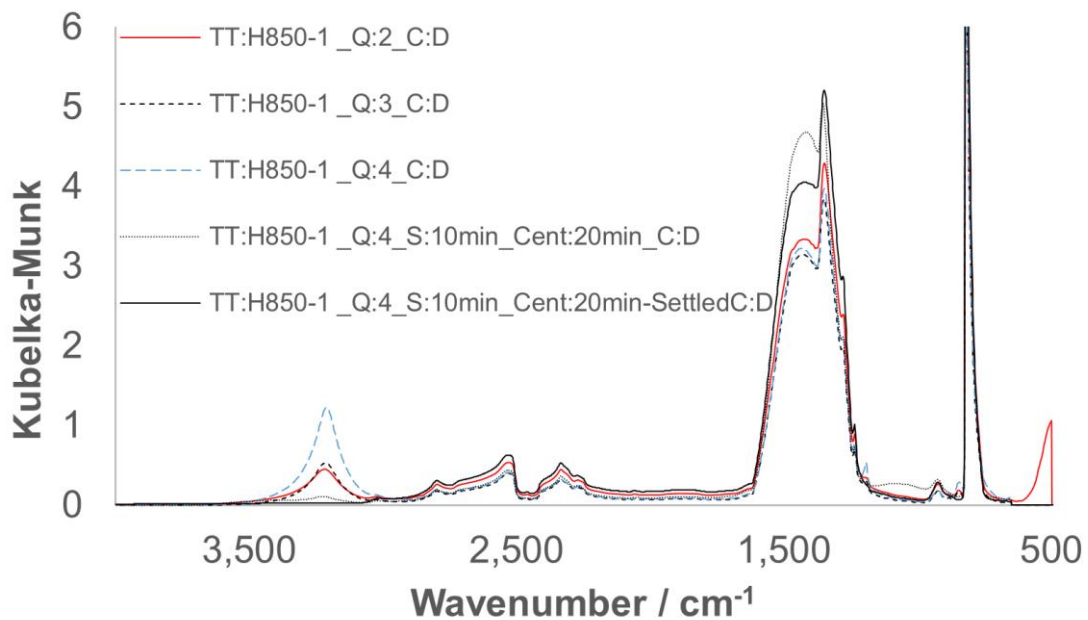


**Figure A 2** hBN thermally treated at 850 °C for 2 h and then quenched in liquid nitrogen 1 (Q:1) or 2 (Q:2) times.

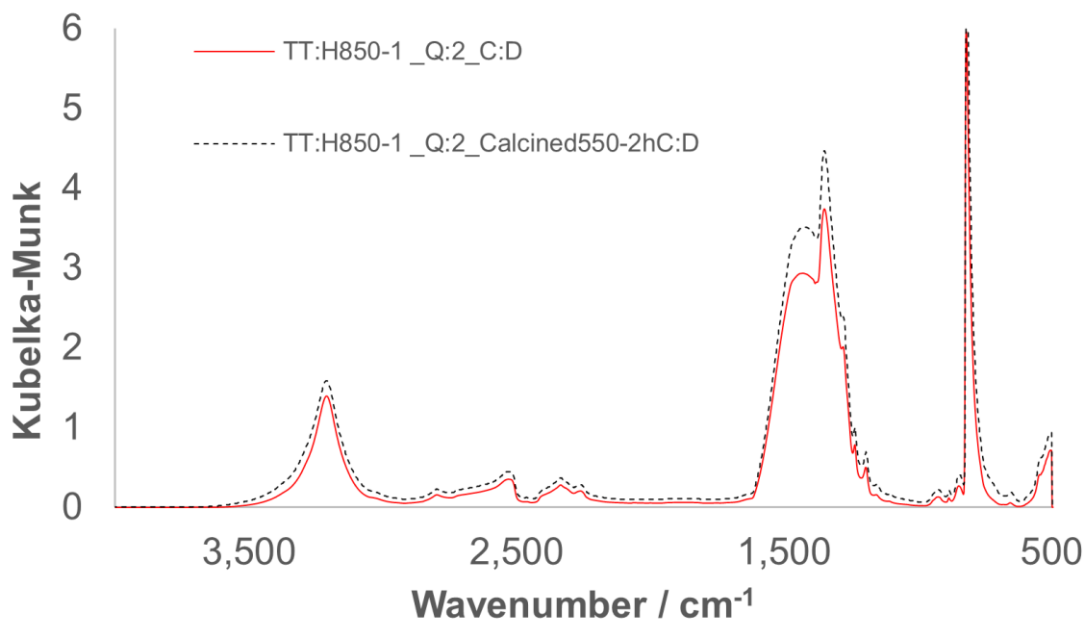
Figure A 3 shows the FTIR spectra for a thermally treated hBN sample. All the spectra shown are for different stages of the treatment process. The first 3 lines are for different number of quenching cycles. The TT:H850-1\_Q4\_S:10 min\_Cent:20min\_C:D sample was sonicated for 10 minutes and centrifuged at 1000 rpm for 20 minutes, then

the liquid was dried overnight at 110 °C. TT:H850-1\_Q4\_S:10 min\_Cent:20min-Settled\_C:D is the precipitate of the centrifuged sample.

In this sample we can see that the precipitate (black line in Figure A 3) looks just like untreated hBN. The quenched samples show the typical 3200  $\text{cm}^{-1}$  peak, and the sonicated and centrifuged (liquid part) sample shows the 1090  $\text{cm}^{-1}$  peak assigned to hBNO (borated hBN).



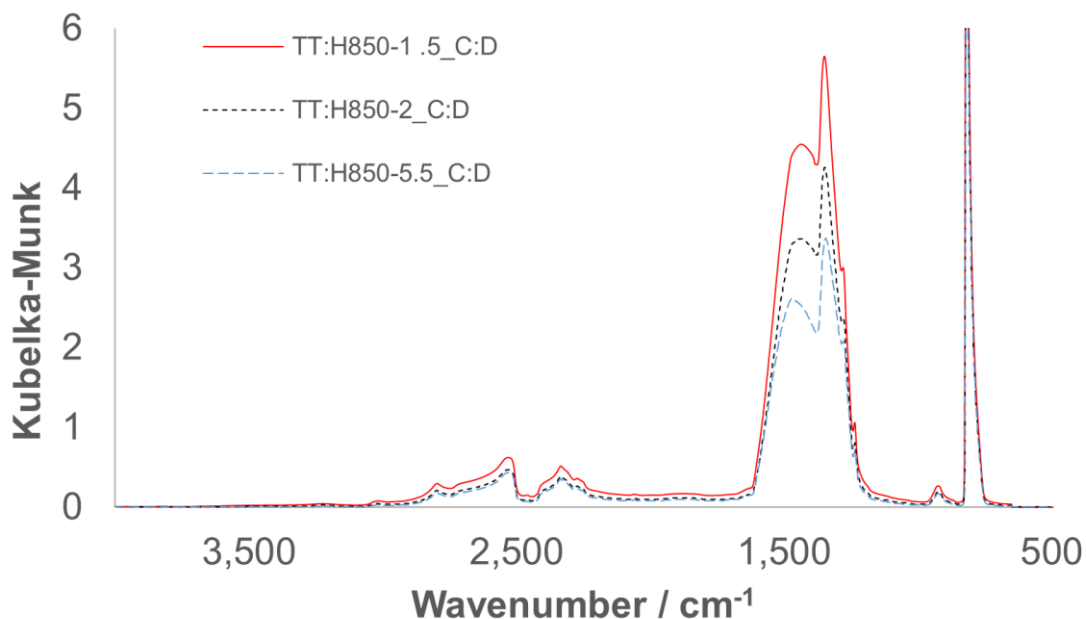
**Figure A 3** hBN thermally treated at 850 °C for 1 h and then quenched in liquid nitrogen for several cycles. Sonication and centrifugation were also applied at the end of the last quenching cycle.



**Figure A 4** hBN thermally treated at 850 °C for 1 h and then quenched in liquid nitrogen for 2 cycles. After the quenching, the sample was calcined at 550 °C for 2 h. The spectra show the samples before and after the calcination.

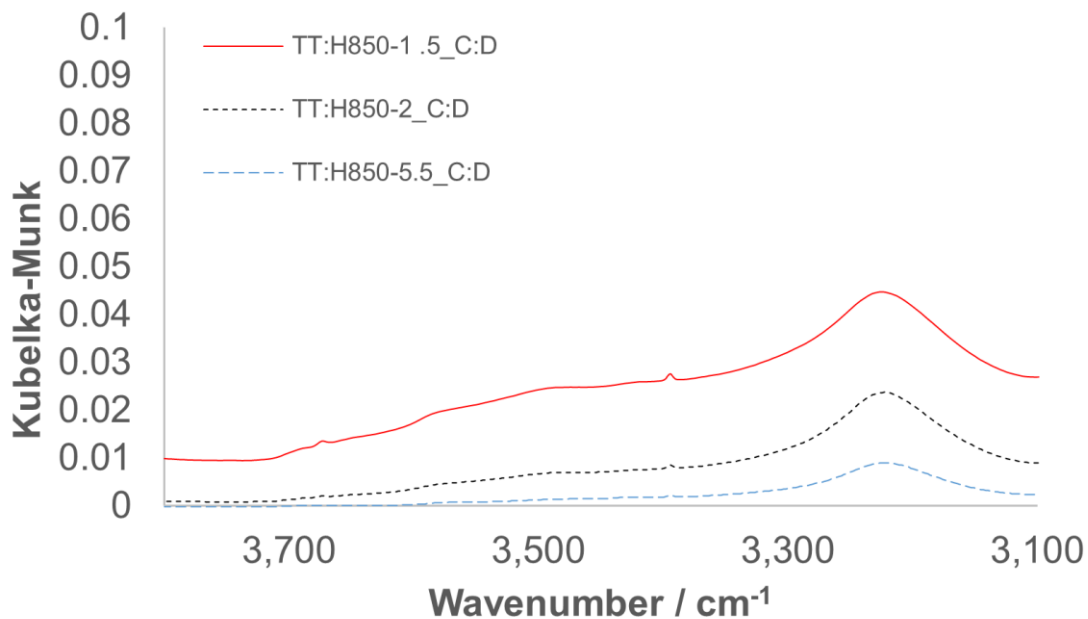
### Thermal treatment with intermediate cooling

Figure A 5 shows an hBN sample treated at 850 °C with humid air. At 90 minutes the sample was cool down to room temperature (TT:H850-1.5\_C:D). The process was repeated at 120 (TT:H850-2\_C:D) and 334 (TT:H850-5.5\_C:D) minutes.



**Figure A 5** hBN thermally treated at 850 °C. The sample was cool down to room temperature at 90, 120 and 334 minutes to take a sample.

Figure A 6 shows a zoom in of the OH zone for these samples. Interestingly, the longer the treatment the weaker the FTIR peaks. Due to this counterintuitive result, we repeated the treatment taking samples at 1, 3 and 6 hours (Figure A 7). This time the results were as expected, the FTIR peak was more intense the longer the treatment. A repetition of this experiment was made to confirm the results (Figure A 8).



**Figure A 6** Zoom in of the OH region shown in **Figure A 5**.

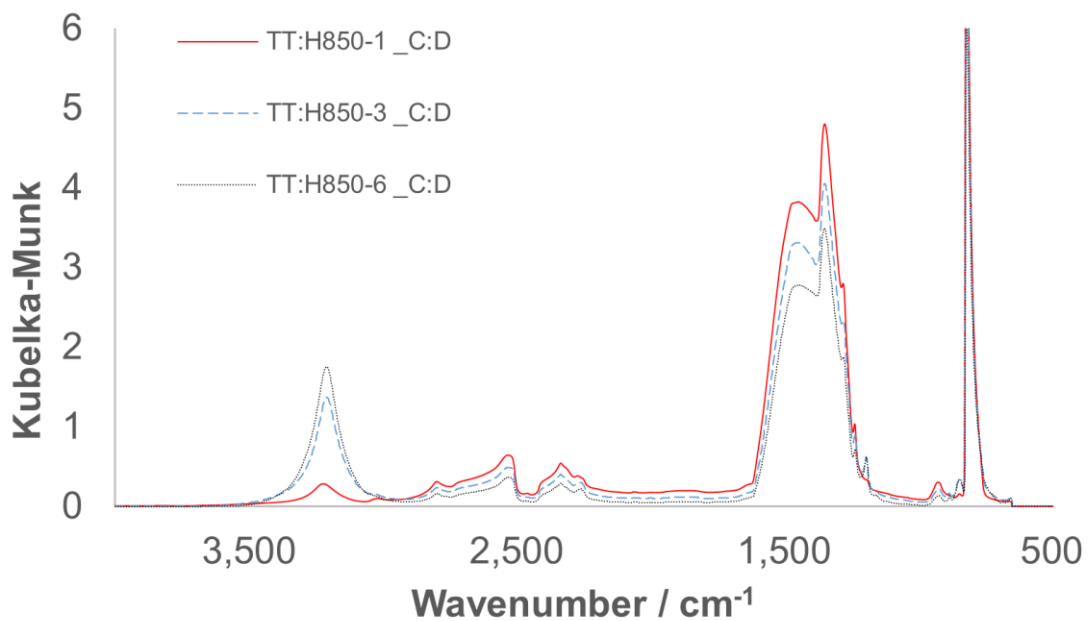


**Figure A 7** hBN thermally treated at 850 °C. The sample was cool down to room temperature at 1, 3 and 6 hours to take each sample.

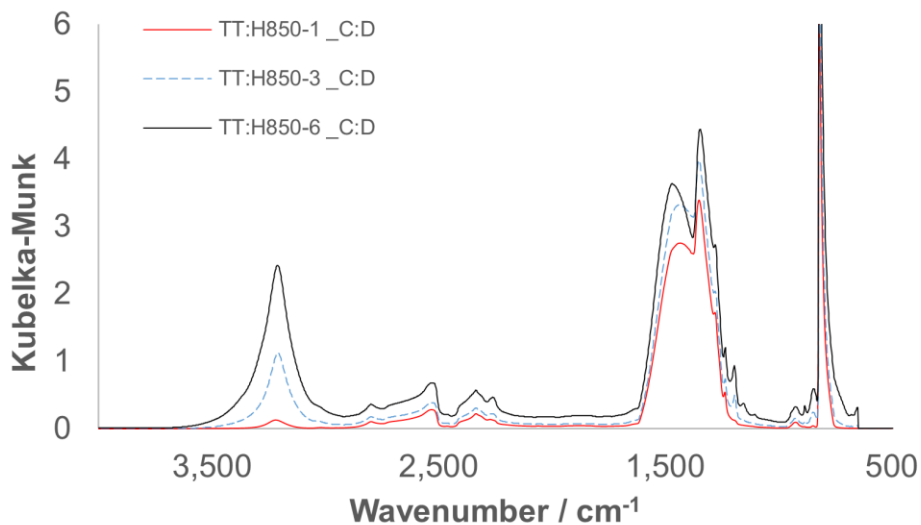


**Figure A 8** hBN thermally treated at 850 °C. The sample was cool down to room temperature at 1, 3 and 6 hours to take each sample.

### Samples storage

To evaluate if the storage of the samples has a significant impact on the FTIR spectrum, the same thermally treated sample was stored in three different environments (Figure A 9).



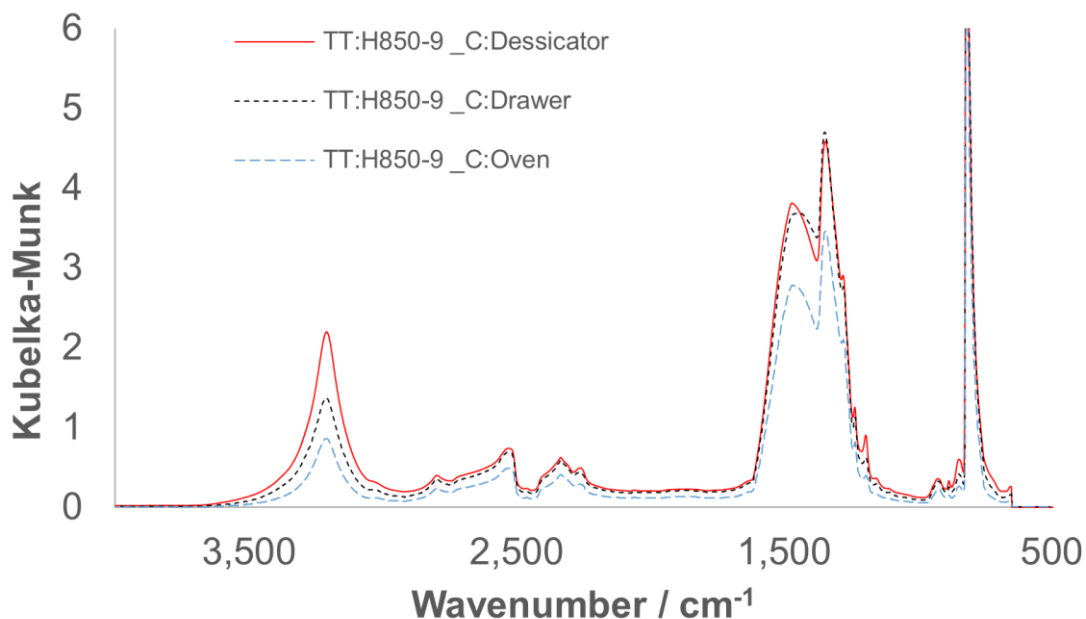
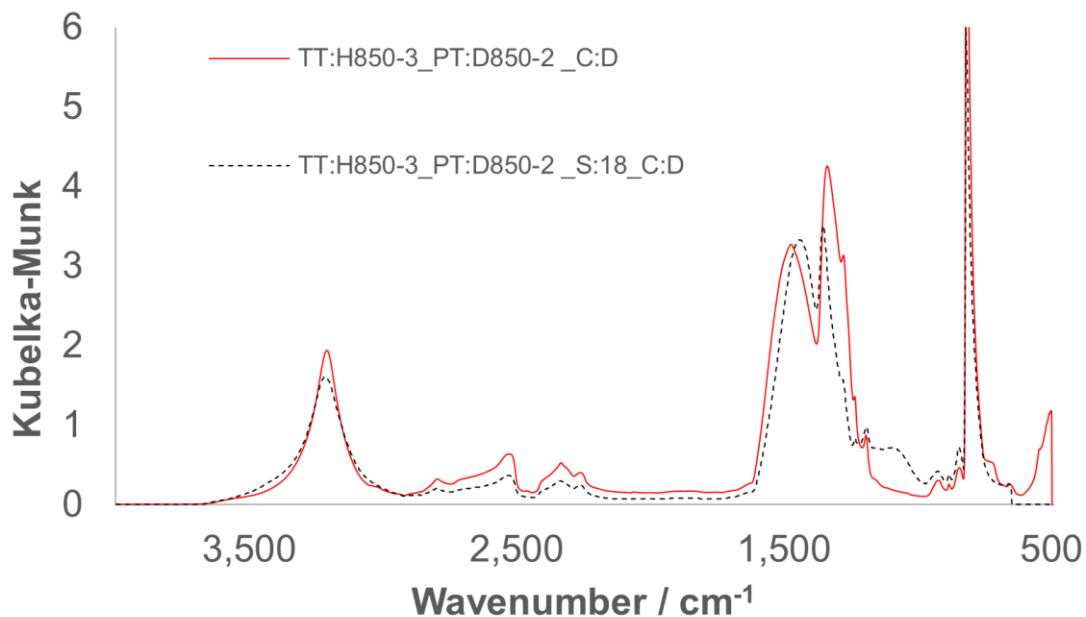


**Figure A 9** hBN thermally treated at 850 °C for 9 hours. The sample was stored in a closed vial in a desiccator (TT:850-9\_C:Dessicator), in a closed vial in a drawer (TT:850-9\_C:Drawer) and in an open vial in an oven at 110 °C overnight (TT:850-9\_C:Oven).

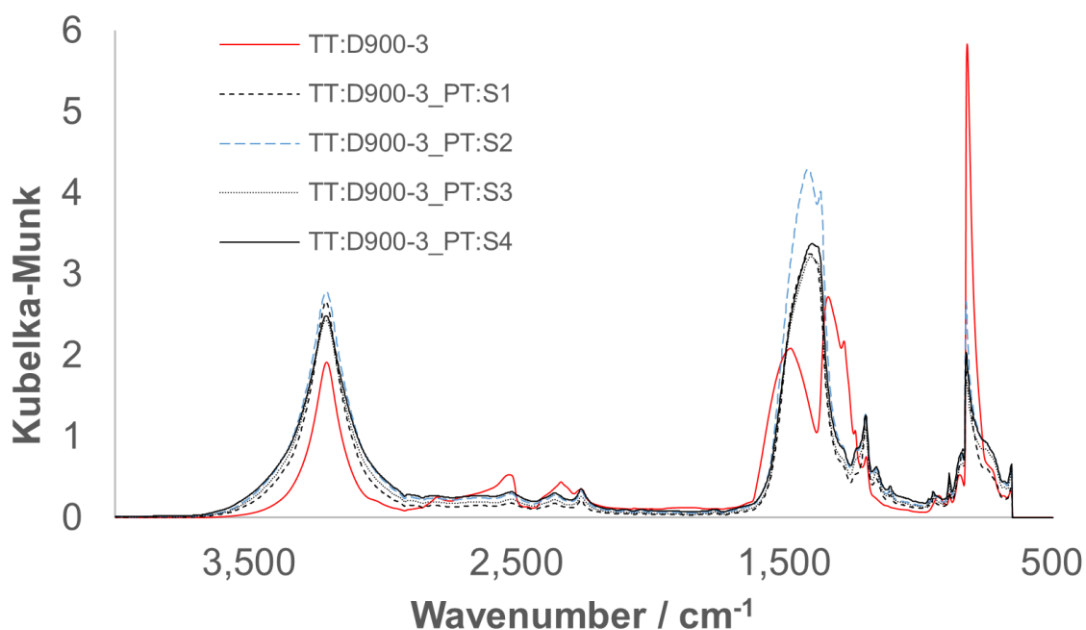
### hBN treatment stages

During the exploration of hBN modification by thermal treatments we tried combining thermal treatments since boric acid was being produced. With the thermal treatment combinations, we wanted to dehydrate boric acid, eliminate or convert it to a borated layer using different combinations, such as the one shown in Figure A 10.

We also evaluated the effect of sonication after a thermal treatment (Figure A 11). There were no significant changes with the sonication time, but the FTIR spectrum for the sonicated samples is slightly different from the non-sonicated one.



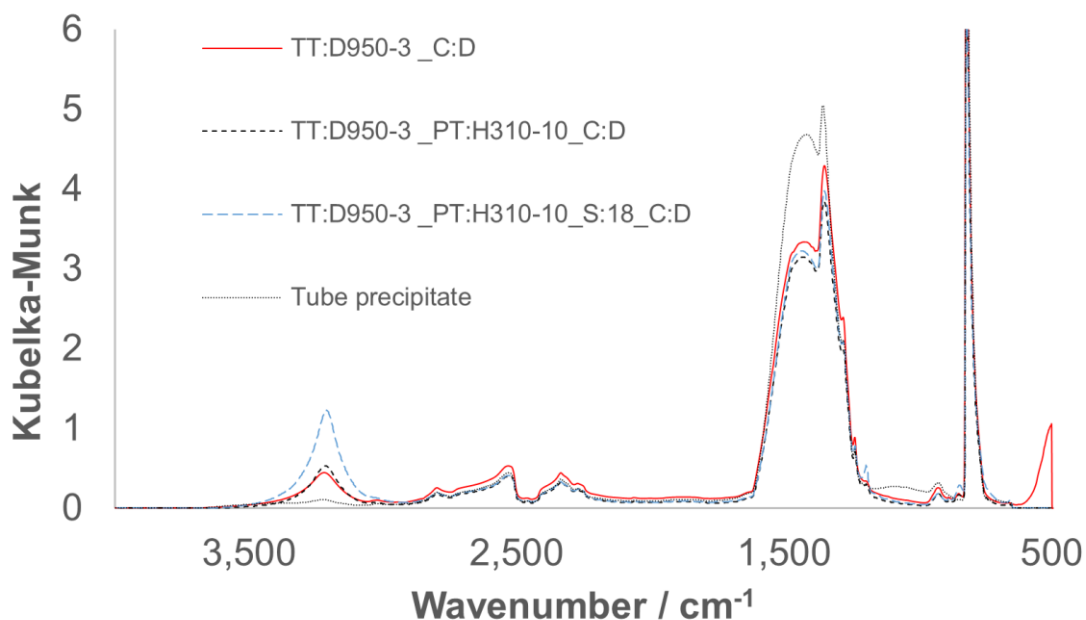
**Figure A 10** hBN thermally treated at 850 °C for 3 hours in humid air and then post treated in dry air for 2 h at the same temperature. A sonication step was performed for 18 h. Samples were taken before and after the sonication.



**Figure A 11** FTIR for hBN thermally treated at 900 °C for 3 h in dry air. A sonication step was performed for 4 h. Samples were taken each hour during the sonication.

## Boric acid identification

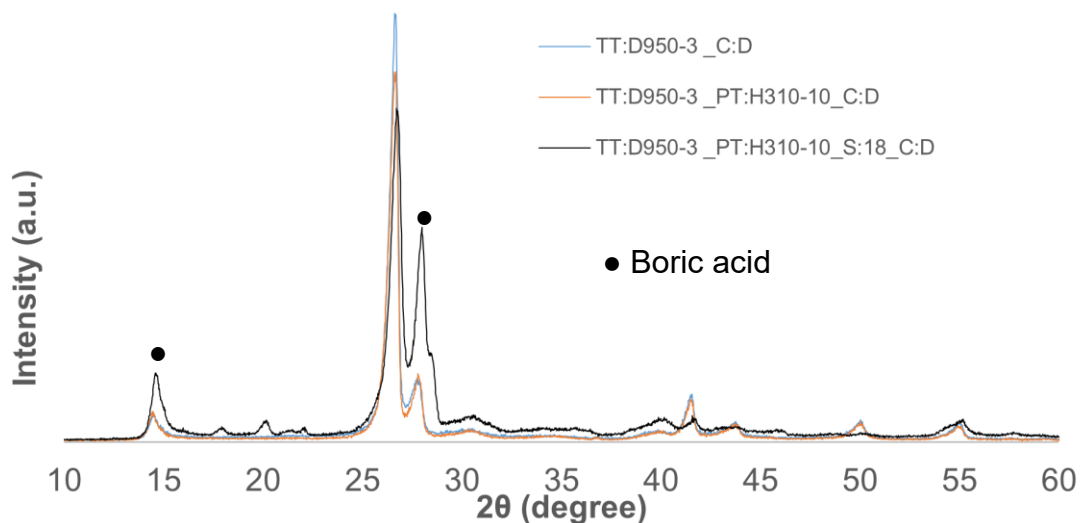
hBN was treated at 950 °C with dry air for 3 hours. The furnace outlet was connected to a quartz tube where the gas stream was cooled down, so the vapors deposited on the inner wall of the tube. The hBN samples were analyzed after the thermal treatment and also after a post treatment with humid air at 310 °C and sonication. The powder deposited on the tube wall was also analyzed using FTIR (Figure A 12).



**Figure A 12** FTIR for hBN thermally treated at 950 °C for 3 hours in dry air and then post treated in humid air for 10 h at 310 °C. A sonication step was performed for 18 h after the thermal treatment. During the thermal treatment, a quartz tube was placed in the furnace outlet, the powder precipitated there during the treatment was also analyzed (Tube precipitate).

**The presence of boric acid was determined by XRPD (**

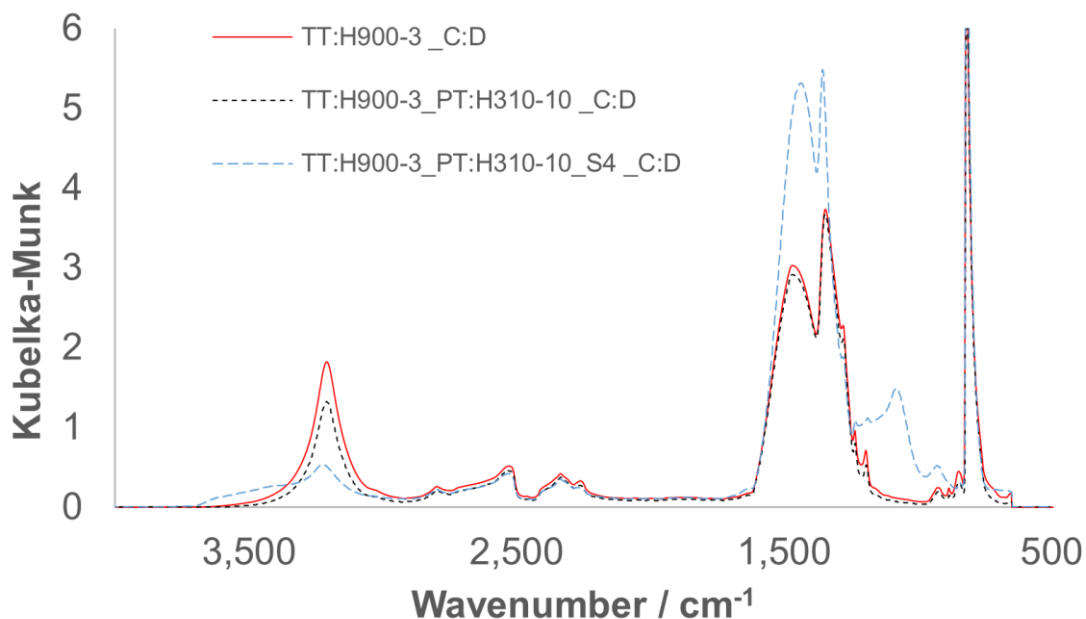
Figure A 13).



**Figure A 13** XRPD patterns for hBN thermally treated at 950 °C for 3 hours in dry air and then post treated in humid air for 10 h at 310 °C. A sonication step was performed for 18 h after the thermal treatment.

### Thermal treatment and characterization by chemisorption

hBN was thermally treated at 900 °C for 3 hours in humid air and then post treated in humid air for 10 h at 310 °C. A sonication step was performed for 4 h after the thermal treatment. The presence of several functional groups was revealed by FTIR (Figure A 14). In order to find the nature of those active sites we used chemisorption (Temperature Programmed Reduction (TPR) and Oxidation (TPO)). We expected the active sites to react and generate a signal in the thermal conductivity detector (TCD) due to the consumption of hydrogen or oxygen. The treatment protocols are shown in **Table A 1** and the potential reactions in **Table A 2**.

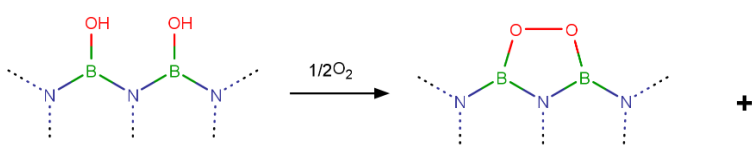
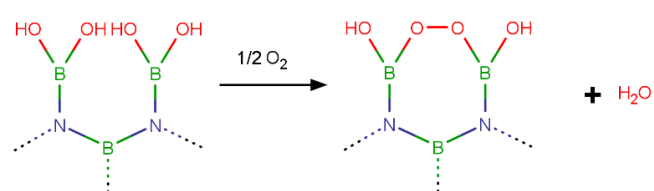
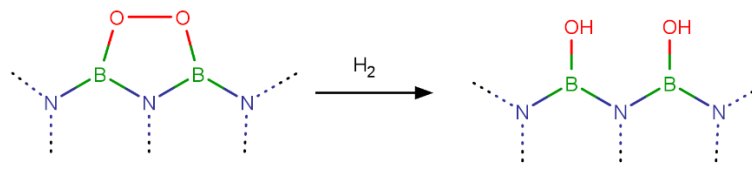
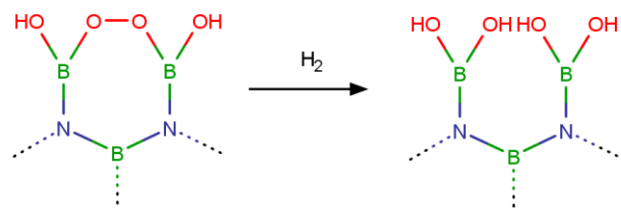


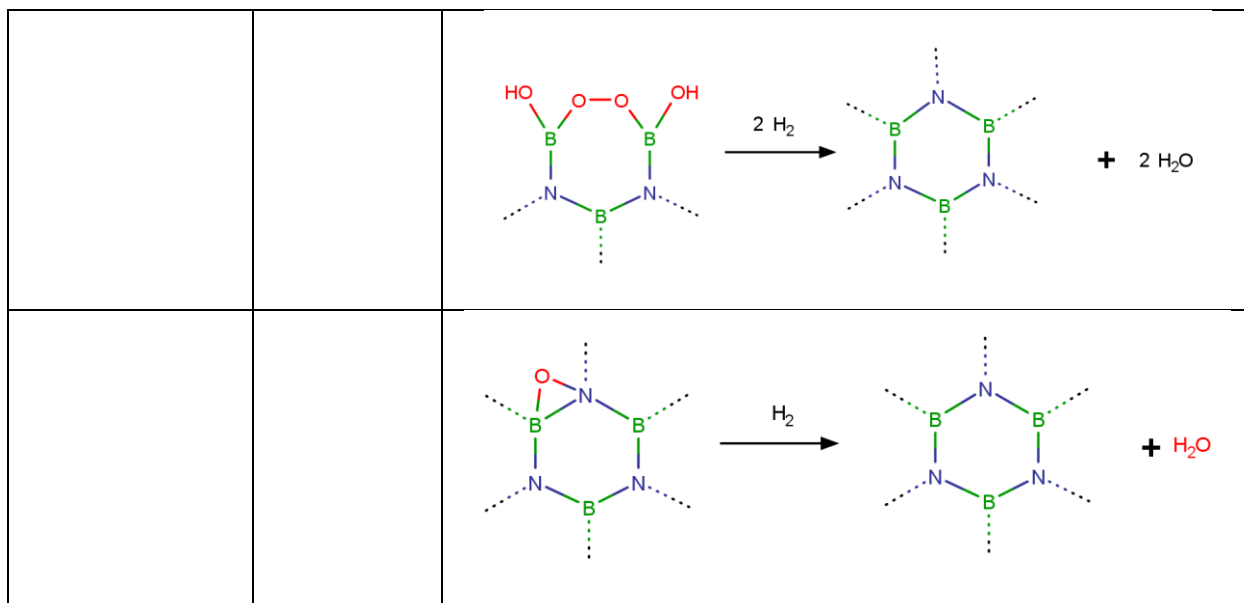
**Figure A 14** FTIR for hBN thermally treated at 900 °C for 3 hours in humid air and then post treated in humid air for 10 h at 310 °C. A sonication step was performed for 4 h after the thermal treatment.

<b>Table A 1</b> Steps for the analysis of h-BN samples using TPR and TPO.		
<b>Step</b>	<b>Conditions</b>	<b>Objective</b>
1-Treatment	Ar-550 °C / 60 min	Water removal
2-Treatment	Oxygen-450 °C / 30 min	Oxidation (to normalize sample)
3-TPR	10% H <sub>2</sub> /Ar. 40 °C – 800 °C. 30 min hold	
4-Pulse chem.	O <sub>2</sub> /He 400 °C	Quantification of the oxygen absorption
5-Treatment	10% H <sub>2</sub> /Ar 400 °C / 60 min	Reduction
6-TPO	10% O <sub>2</sub> /He 50 °C – 800 °C. 30 min hold	

7-Pulse chem.	10% H <sub>2</sub> /Ar 400 °C	Quantification of the hydrogen absorption
8-Calibration	O <sub>2</sub> /He	
9-Calibration	H <sub>2</sub> /Ar	

**Table A 2** TPR/TPO analysis for h-BN treated at 850°C with humid air + sonication centrifugation.

Step	Conditions	Objective / Chemical paths /Results
1-Treatment	Ar-550 °C / 60 min	Water removal
2-Treatment	Oxygen-450 °C / 30 min	
		
3-TPR	10% H <sub>2</sub> /Ar 40 °C – 800 °C. 30 min hold	
		



The result for the TPR is shown in Figure A 15 (with a repetition). There is not a significant difference between this result and the TPR for untreated hBN (Figure A 16). Therefore, we concluded that this technique is not conclusive. The reason could be a low sensitivity of the equipment compared with the number of active sites found in treated hBN.

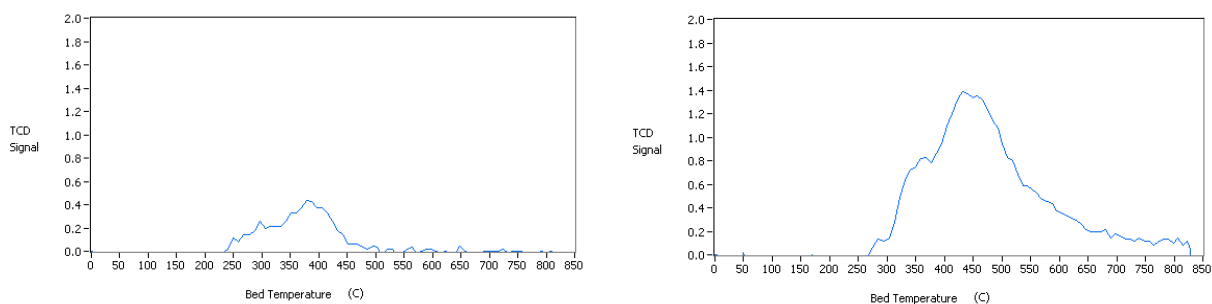


**Figure A 15** TPR plot for functionalized h-BN with repetition.

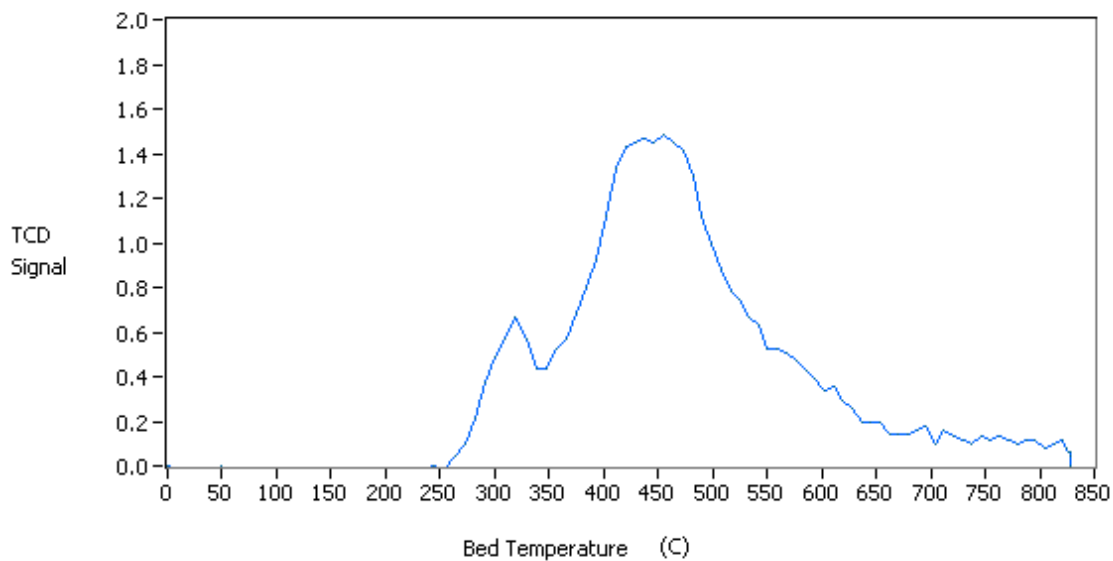


**Figure A 16** TPR plot for untreated h-BN.

Oxygen pulse chemisorption and hydrogen pulse chemisorption did not give conclusive results either (Figure A 17).

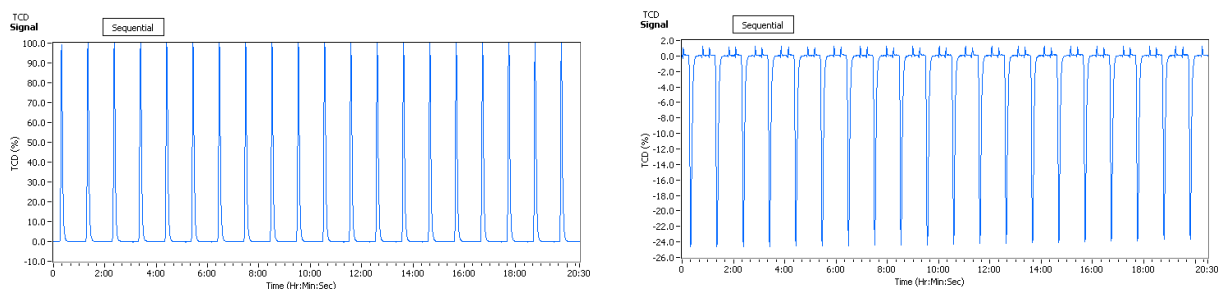


**Figure A 17** Oxygen pulse chemisorption (left) and hydrogen pulse chemisorption (right) for functionalized h-BN.

Finally, the temperature programmed oxidation (TPO) also produce an arbitrary result (Figure A 18).



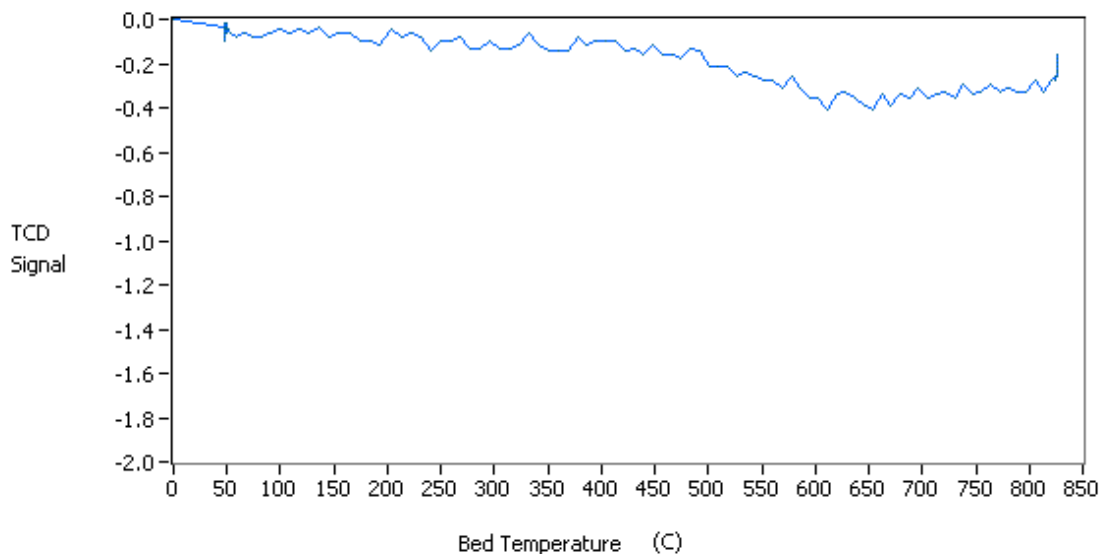


**Figure A 18** Temperature programmed oxidation (TPO) for functionalized hBN.

### Water adsorption by thermally treated hBN

hBN was thermally treated at 850 °C in humid air for 3 h and post treated at 600 °C for 5 h (Figure A 19). The sample was stored in a desiccator, once it reached the room temperature it was exposed to the ambient atmosphere and weighted over time. Untreated hBN was heated to 550 °C in dry air for 2 h, stored in a desiccator and then weighted. We expected a difference between the weight variation for thermally treated hBN (TT:H850-3\_PT:H600-5\_C:D) and untreated hBN (TT:D550-2) because the thermally treated hBN should have more sites (functional groups) where water could be adsorbed. The results confirmed the higher water adsorption by TT:H850-3\_PT:H600-5\_C:D (Figure A 20).

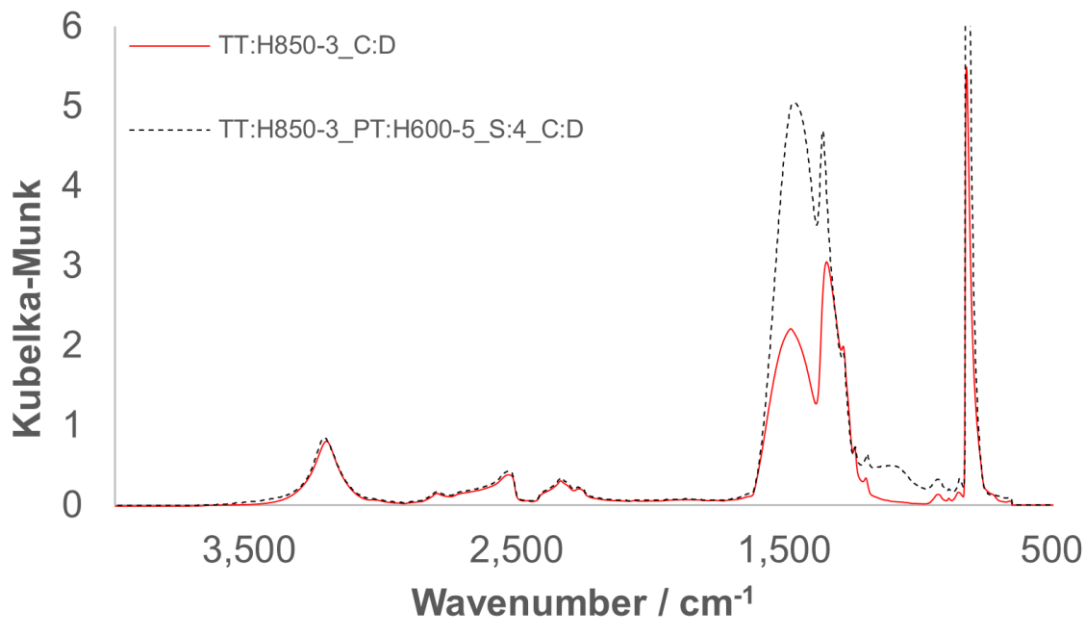


**Figure A 19** FTIR for hBN thermally treated at 850 °C for 3 hours in humid air.

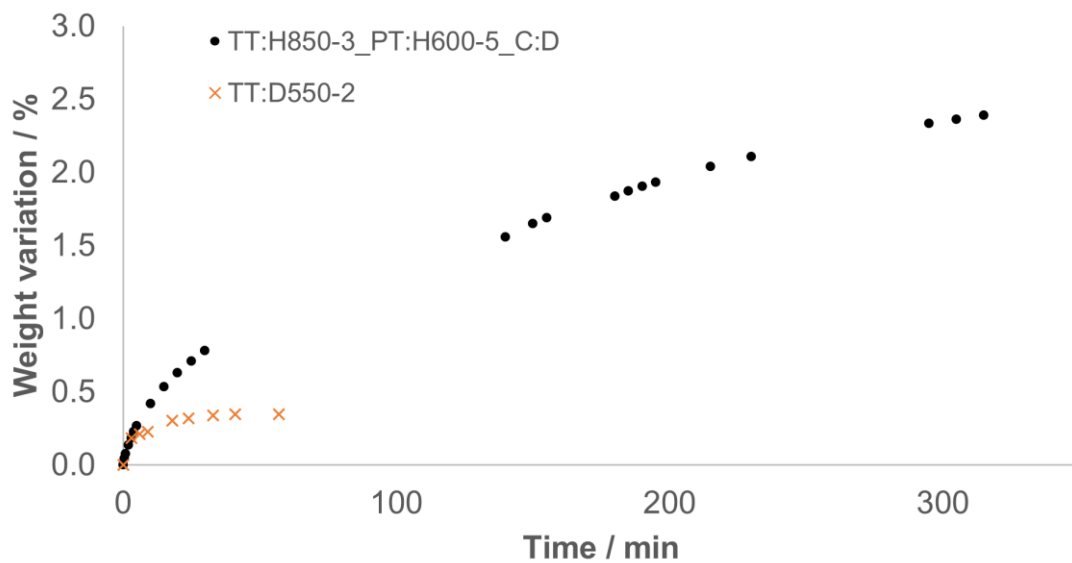


**Figure A 20** Weight variation in thermally treated hBN at 850 °C for 3 h (TT:H850-3\_PT:H600-5\_C:D) and dried pristine hBN (TT:D550-2).

## Appendix B - Pt/hBN catalyst

In this section we present the preliminary work we did as part of our explorations in the search of a Pt/hBN catalyst. Figure B 1 presents a general overview of the different catalysts we synthesized. The information presented here is in terms of conversion and selectivity, not in terms of TOF as in the previous chapters, this is because the dispersion information was not determined for all the samples.

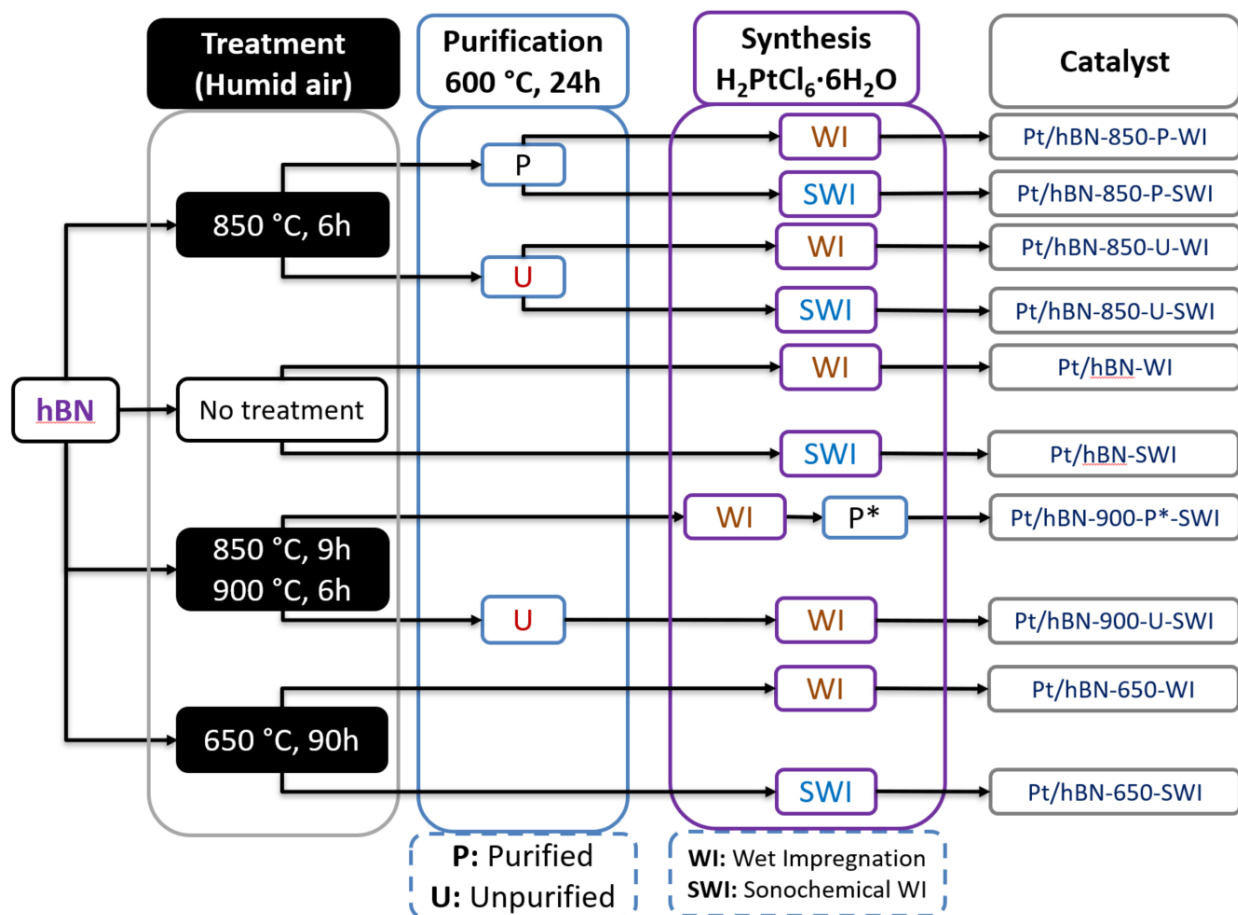


**Figure B 1** Pt catalysts synthesized during the exploration phase.

Figure B 2 shows the methane conversion during the POM reaction on different Pt catalysts. Figure B 3 and Figure B 4 show the CO and H<sub>2</sub> selectivity.

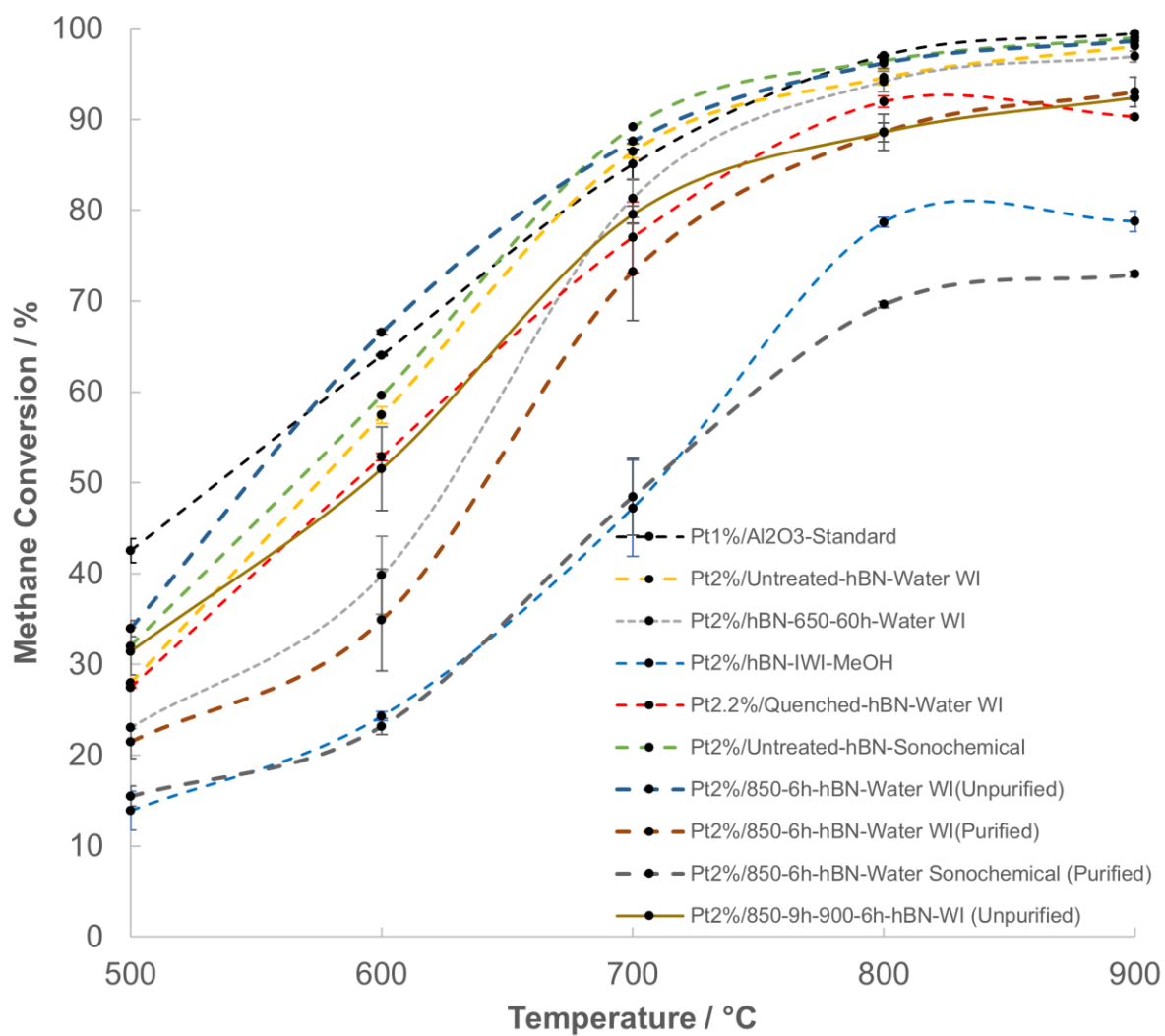


**Figure B 2** Methane conversion for the Partial Oxidation of Methane reaction on Pt catalysts.

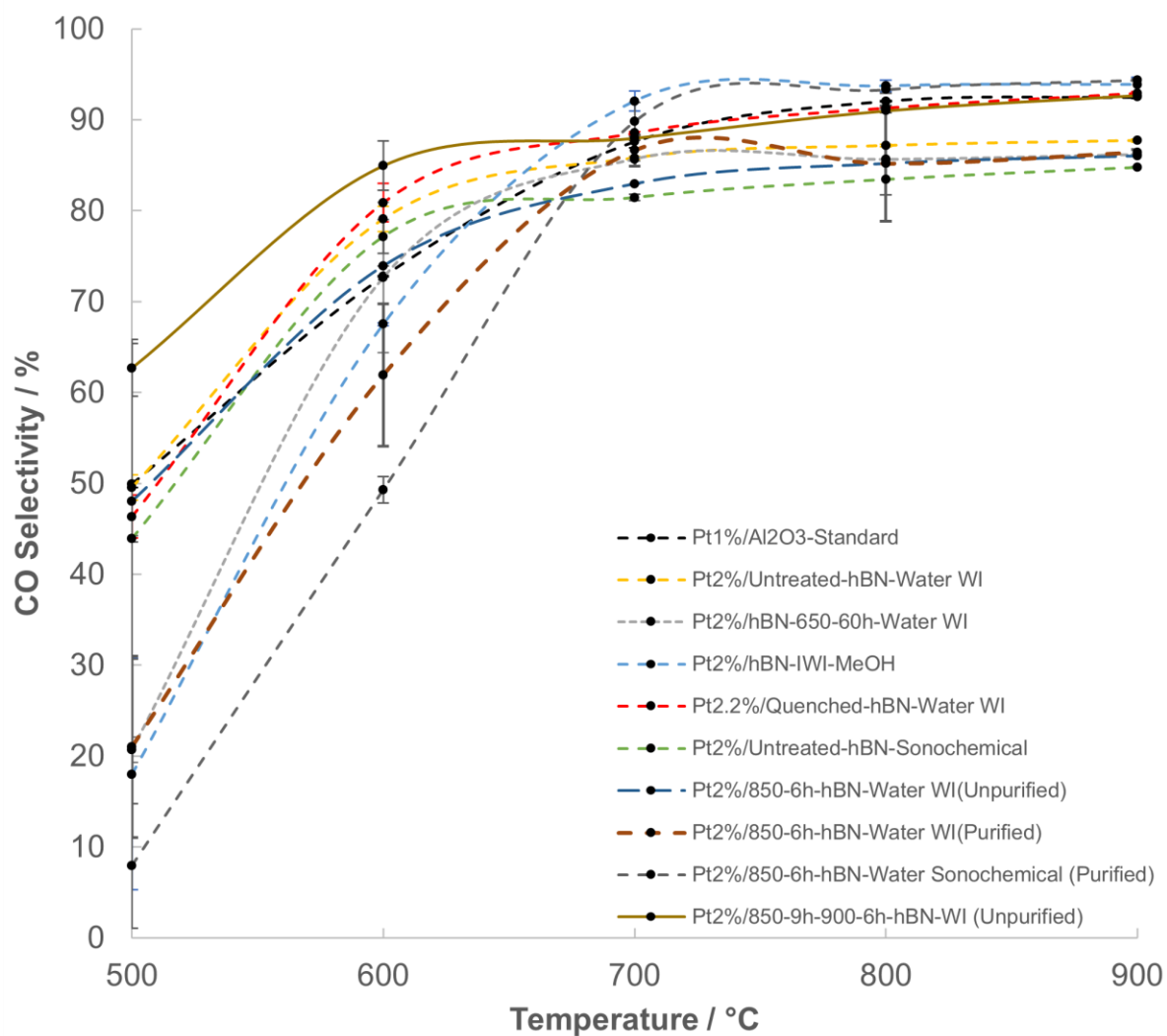


**Figure B 3** CO selectivity for the Partial Oxidation of Methane reaction on Pt catalysts.

### Preliminary insights

The catalysts showing the lower conversions were the ones synthesized using IWI or Sonochemical WI.

The removal of boric acid by a thermal treatment (in thermally treated hBN) before the catalyst synthesis produced catalysts that led to a lower methane conversion compared with the unpurified thermally treated hBN.

The thermal treatment at lower temperatures (650 °C) also produced a catalyst that led to a lower methane conversion compared to the treatments at 850 °C.

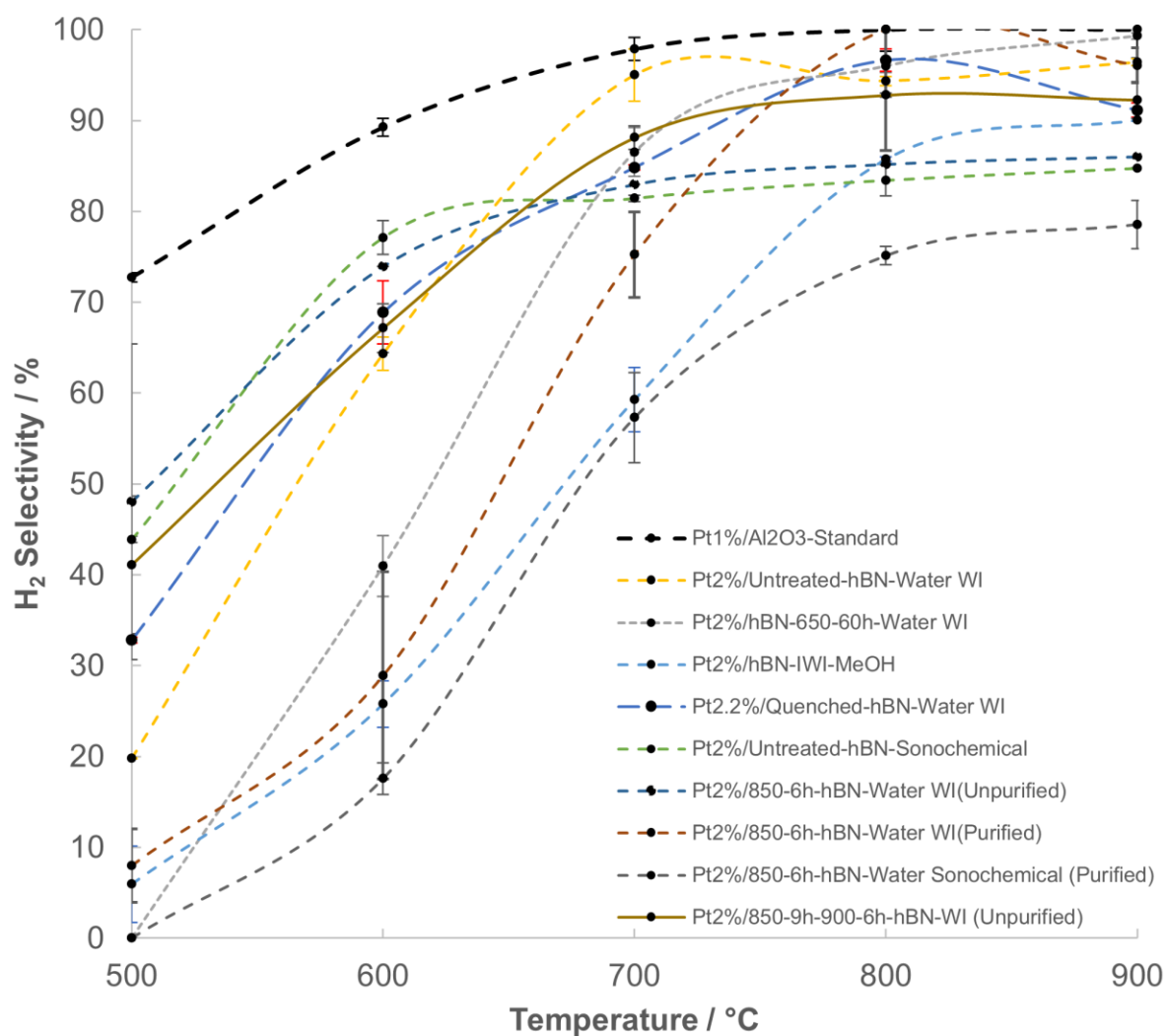


**Figure B 4** H<sub>2</sub> selectivity for the Partial Oxidation of Methane reaction on Pt catalysts.

After these first observation we proceed to explore if the lower conversion was related to a lower dispersion or to a lower catalytic activity comparing the TOF. The results are presented in a previous chapter.

## Appendix C - Oxidative Dehydrogenation (ODH) of ethane

During the preliminary explorations to determine the catalytic activity of thermally treated hBN, we used hBN pellets for the experiments. Before each experiment, pellets were prepared applying a 1000 psi pressure to a catalyst sample for 60 seconds. Then pellets were crushed and sieved to a size between 300  $\mu\text{m}$  and 500  $\mu\text{m}$ . The reason for using pellets was to prevent the catalyst bed to generate an excessive pressure drop that moved it out of place.

Figure Figure C 1 shows the ethane reaction rate on hBN materials:

- **hBN**: Untreated hBN. hBN-R and hBN-R2 are repetitions with pristine hBN.
- **hBN-850-6h**: hBN treated with humid air for 6 h. U means Unpurified, P means purified with humid air for 24 h at 600 °C to remove the boric acid.
- **hBNO**: Thermally treated hBN, sonicated and centrifuged.
- **hBN-Air-600-144h**: hBN thermally treated at 600 °C for 144 h.

Figure C 2 and Figure C 3 show the ethylene and CO production rate for the hBN materials. The main conclusion of this preliminary exploration was the variability of the samples, the variations between hBN materials are similar to the variations between experiments for a given material. We found the palletization to be the cause of this variability, hBN is hard to pelletize consistently. To solve the problem, we switch to powder samples and the repeatability improved. All the results presented in Chapter 5 are based



in powder samples. To prevent the excessive pressure drop we changed the amount of catalyst used from 0.2 g to 0.1 g. We also reduced the flow rate.

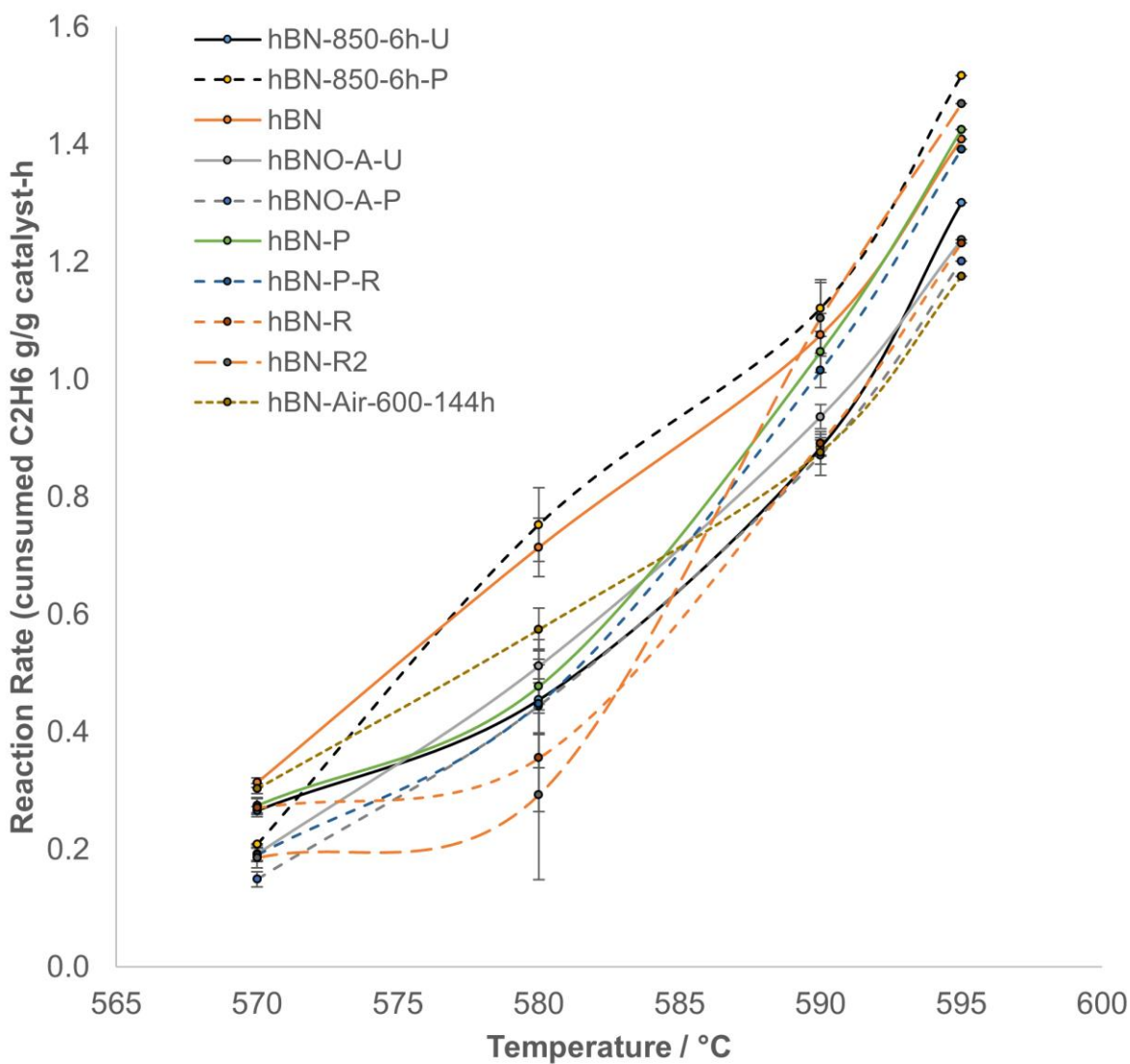


**Figure C 1** Ethane consumption for the ODH reaction on thermally treated hBN.

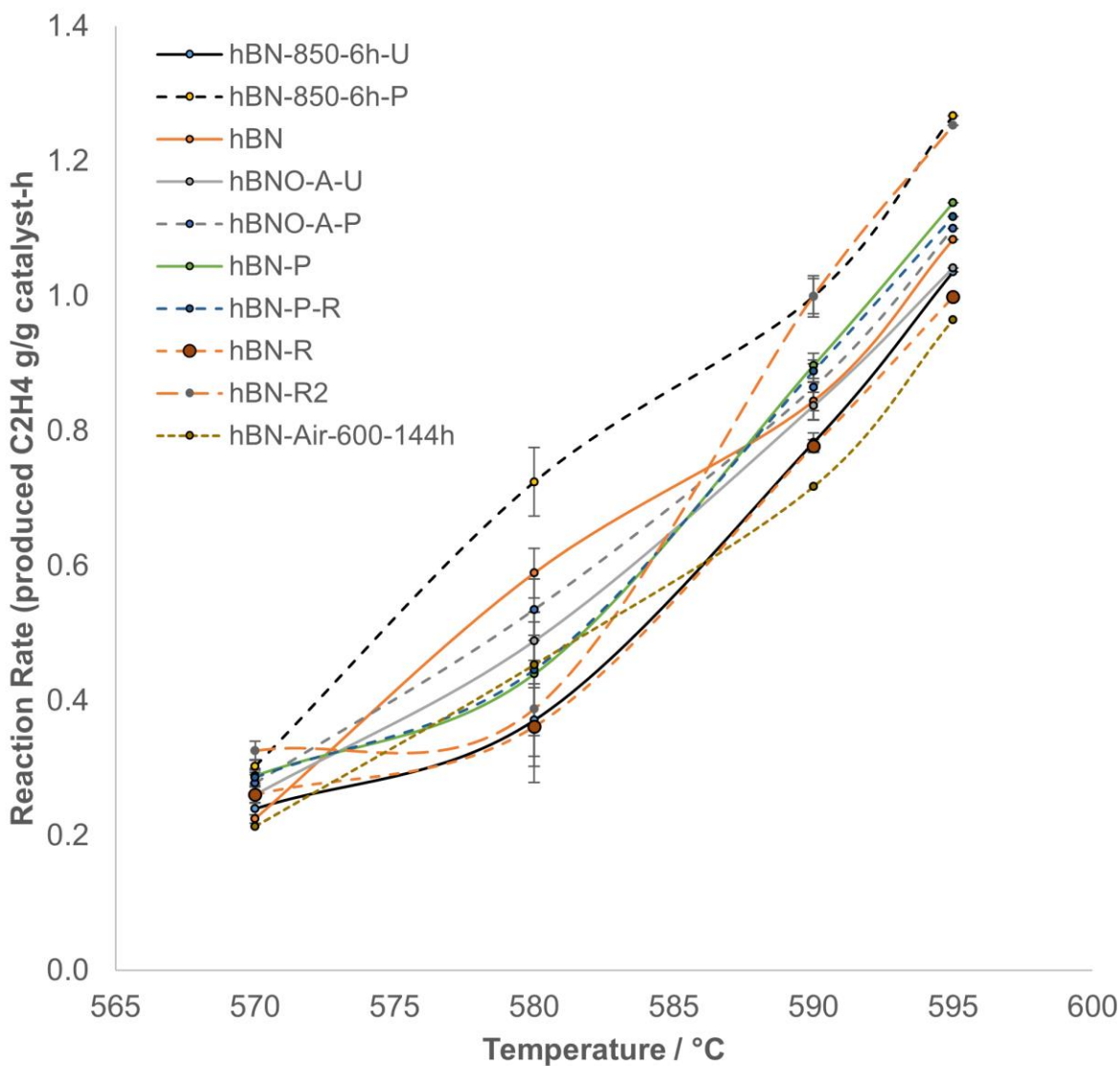


**Figure C 2** Ethylene production for the ODH reaction on thermally treated hBN.

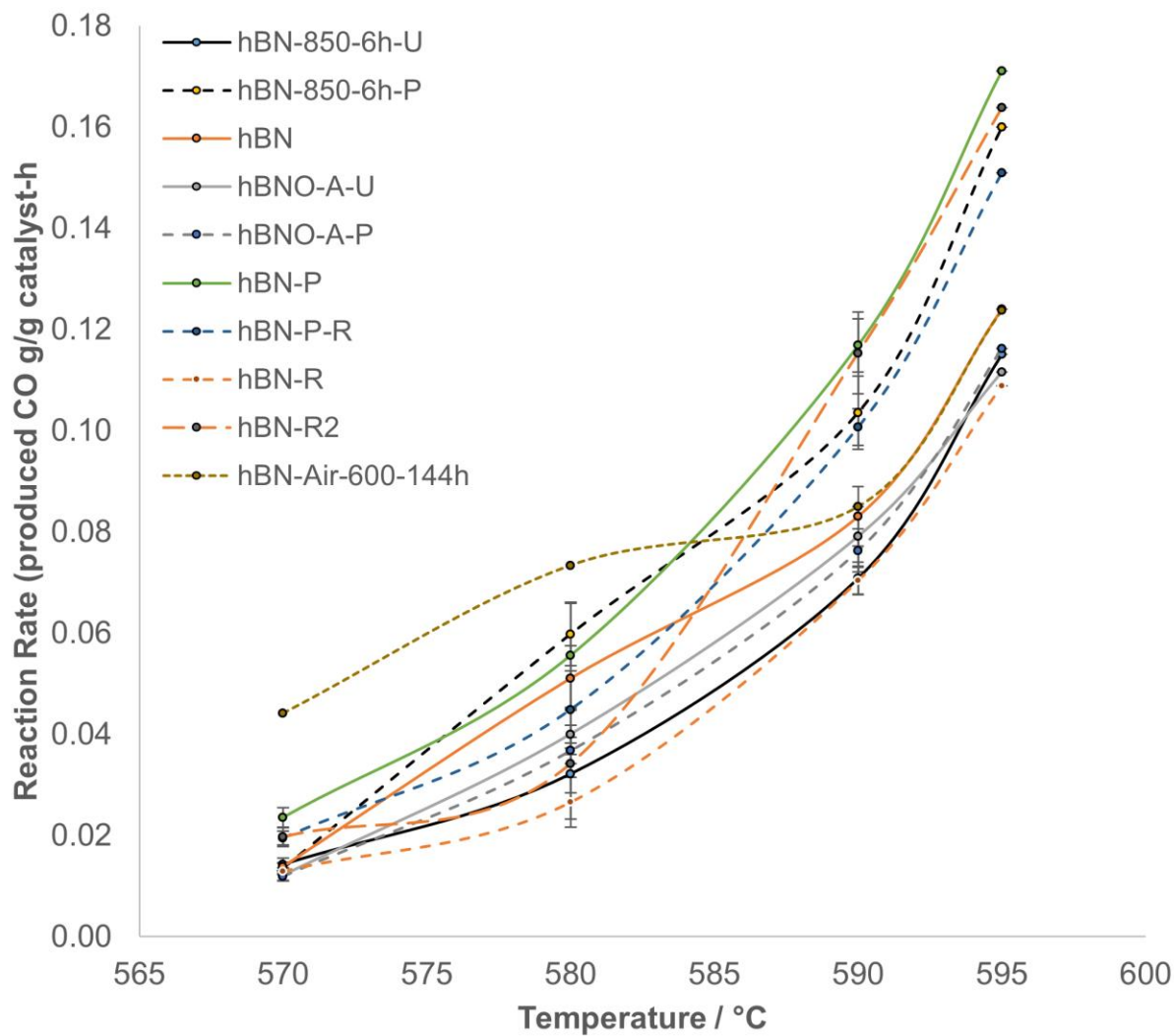


**Figure C 3** CO production for the ODH reaction on thermally treated hBN.